An H... controller for the floating platform diminishing the wave effects

Hogendoorn, Robert P.

Award date:
1993

EINDHOVEN UNIVERSITY OF TECHNOLOGY
DEPARTMENT OF ELECTRICAL ENGINEERING
Measurement and Control Section

An H_∞ Controller for the Floating Platform diminishing the Wave Effects.

by Robert P. Hogendoorn

M. Sc. thesis on Practical training period
carried out from Sept.'92 to June.'93
commissioned by :Prof.Dr.Ir. A.C.P.M. Backx
under supervision of :Dr.Ir. A.A.H. Damen
date :June 1993

Summary.

In this report, a continued development and testing of a controller for a floating platform is described. The platform is a laboratory process. The actual platform consists of three horizontal beams connected at angles of 120°. The end of every beam is resting on a float. The vertical distances between the beams and the floats can be controlled by three servo-motors. In the centre of the platform, a crane has been mounted. The platform is floating in a water tub of about 2 m diameter.
The crane is driven by a servo-motor and it rotates a load of 1 kg. Because of the rotating load, and the disturbances caused by the waves in the tub, the platform won't rest in the same position in the course of time. The goal of this research is to find a controller which is able to hold the platform in a strictly horizontal position.
For this control problem, several control theories have been applied. An H_∞ controller seems to give the best results. For the platform, an H_∞ controller had already been designed. The disturbances caused by the rotating load could be reduced to one sixth. By using stronger controllers, the waves caused by the movements of the floats are becoming to big, and unstable systems were the result. To arrive at to better results there are two possibilities:

1) Modelling the disturbing wave effects also.
2) Adding extra input signals to the controller by measuring the waves around the floats.

It is expected that the first option will give the best results. However, the controller can only be used in this tub and moreover, the waves are hard to model because of the reflections and changing delays caused by the drifting of the platform. Therefore, the second option has been investigated first. The disadvantage of this option can be found in the fact that the wave disturbances are being seen as independent disturbances. However, there is a feedback between the movements of a float and the magnitude of the wave disturbances. Therefore there is a possibility that the designed controller will lead to a unstable system.
Before the design of the controller was started, a simulation model of the platform in the tub was derived first. The waves are modelled by making use of measured step responses. The simulation model has been verified with measurements of the platform. After some modifications, the model was able to reproduce these measurements quite well.
After deriving the simulation model, the design of an H_∞ controller has been started. Since the wave disturbances can be measured well, these disturbances can be reduced by a feed-forward controller. However, the disturbances can't be ruled out completely because the ideal controller has to be a predictor in the discrete time implementation.
To improve the performance of this controller, the sample frequency of the platform model has been increased to 50 Hz. With this sampling frequency, satisfying controllers for both the crane- and wave disturbances can be derived. The end of a beam of the platform varies less than a millimetre. This means that the disturbances are reduces more than a hundred times.

CONTENTS

1: Introduction.

The Measurement and Control section of the Department of Electrical Engineering of the Eindhoven University of Technology finds study topics in the identification and measurement of processes. New strategies obtained from the theory, are tested in practice here on several laboratory processes.
A good example is the use of the H_∞ theory in control techniques. Examples of using this theory in practice can only be found in recent years. One of the laboratory processes on which this theory is tested, is the floating platform (see figure 2.1). The actual platform consists of three horizontal beams connected at angles of 120^0. Every end of a beam is resting on a float. However, the platform has one particularity. There is no fixed construction between the end of a beam and the float. The distance between a float and the end of a beam can be controlled by a servo-motor which is placed on the end of the beam. In the centre of the platform a rotatable crane has been mounted. With this crane it is possible to pick up and rotate a load.
The platform has been positioned in a water tub of about 2 m diameter. Due to the movements of the crane and the waves in the tub, the platform won't rest in a strictly horizontal position. The goal of this research is to find a controller which is able to hold the platform in a horizontal position, in spite of the disturbances caused by crane and waves.
Many controllers have already been investigated. However, a H_∞ controller gave the best performance. This controller exists of two parts, a feedforward and a feedback. The feedforward controller is used to deal with the high frequencies, the feedback controller for the lower (see [1]).
Up until now only the disturbances caused by the rotation of the crane have been modelled. Problems arise when the floats move too fast in the water. Due to this movement, the waves are becoming too big and can't be caught in the existing model. The whole platform is becoming instable then. However, by moving the floats much slower,it is impossible to rule out all the disturbances.
For a better result, it seems necessary to model the wave disturbances also, or to measure the height of the waves around the floats to get more input signals. With these extra input signals a new H_∞ controller will be designed.
To design a good controller, a simulation model is a good toolbox. Therefore the first action to be taken is designing a simulation model of the platform in combination with the waves in the tub.

2: Process description.

2.1: Introduction.

Designing a good controller is only possible when an adequate model of the process exists. The parameters and variables which are used in the model have to be defined first.

2.2: Definitions.

A model for the platform without wave disturbances has already been derived. (see [1] and [8]) The position of the platform is described in cartesian coordinates. The position is described by an average height, the rotation around the positive x-axis and negative y-axis. The gravity centre of the platform coincides with the origin. This is shown in figure 2.1.

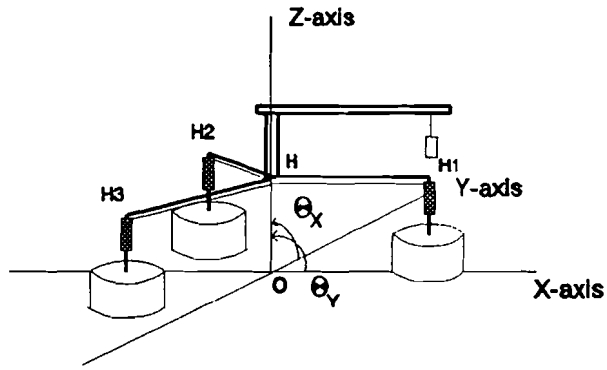

figure 2.1: schematic representation of the platform.

The crane on the platform needs some definitions too. The bracket of the crane makes a circular movement. At the end of the crane's arm, at a distance L, a load is positioned. At every moment of time, the position (angle of the arm) can be defined. At t=0 the angle Φ is supposed to be zero.

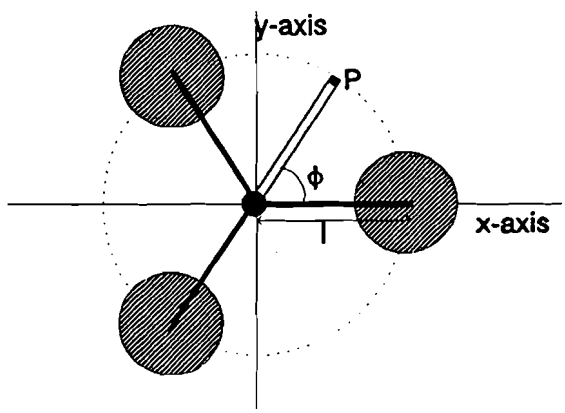

figure 2.2: crane definitions.

The three floats of the platform are identical. The parameters and variables used for the float are defined in figure 2.3.

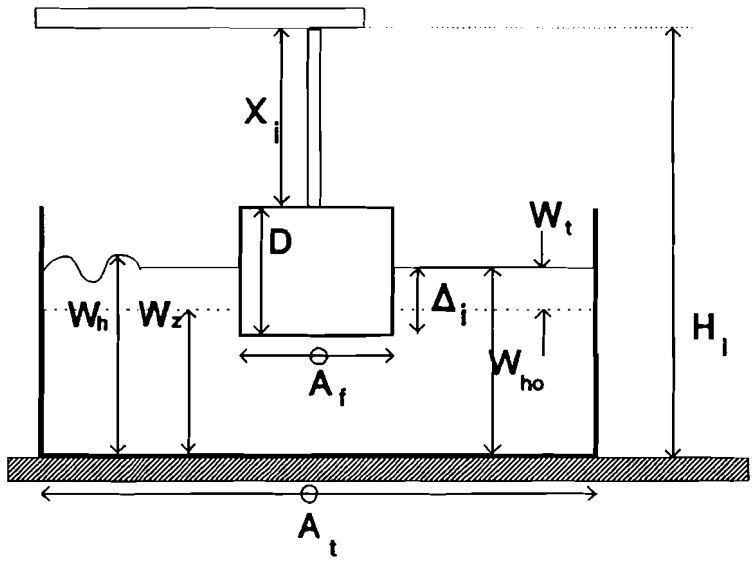

figure 2.3: float definitions.

The meaning of the abbreviations use in figure 2.1 to 2.3 are explained in the next table.

Table 2.1: definitions

symbol	unities	description
L	m	distance between centre and end of beam
M	kg	mass of the total platform
m	kg	mass of the load
g	m/s^2	gravity force
Φ	rad	angle between x-axis and the bracket
Θ_x	rad	rotation around the positive x-axis
Θ_y	rad	rotation around the negative y-axis
W_h	m	water height in regard to the ground
W_z	m	water height without a float
W_{h0}	m	water height in stationary circumstances
W_t	m	increase of water height caused by float
A_f	m^2	surface of the bottom of the float
A_t	m^2	surface of the tub
D	m	height of the float
Δ_i	m	depth of the float i in the water
H_a	m	height of centre in regard to the ground
H_i	m	height of beam i in regard to the ground
X_i	m	distance between float i and the platform
J_x	$kg(rad/s)^2$	inertia of the rotation around the positive x-axis
J_y	$kg(rad/s)^2$	inertia of the rotation around the negative y-axis

The variables mentioned above can be used to define different distances.

- A capital is used when a distance between two points is mentioned.
- Small letters are used when distances to the equilibrium point are mentioned
- The characters get a subscript 0 when the distances in the stationary situation are mentioned.

(example: The H is used for the distance with regard to the ground, h for distances to the equilibrium point, an H_0 for a distance in the stationary situation.)
When the distance for a certain float is meant, an i is added in the subscribt.

2.3: Transferfunctions of the platform.

The average height, and the rotation around the x- and y-axes (H_a, θ_x, θ_y) have been calculated form the heights of the end of the beams with regard to the ground (H_1 to H_3 in figure 2.1).
For these three qualities the first order approximations of formula 2.1 can be made.

$$\begin{aligned} H_1 &= H_a + \theta_y L \\ H_2 &= H_a - \frac{L}{2}\theta_y + \frac{L}{2}\sqrt{3}\theta_x \\ H_3 &= H_a - \frac{L}{2}\theta_y - \frac{L}{2}\sqrt{3}\theta_x \end{aligned} \qquad (2.1)$$

After some restructions follows:

$$\begin{aligned} \textit{average height} &: H_a = \frac{1}{3}(H_1+H_2+H_3) \\ \textit{rotation around y-axis} &: \theta_y = \frac{2}{3L}(H_1-\frac{1}{2}H_2-\frac{1}{2}H_3) \\ \textit{rotation around y-axis} &: \theta_x = \frac{\sqrt{3}}{3L}(H_2-H_3) \end{aligned} \qquad (2.2)$$

The influence of the load can be decomposed in three independent forces. One on the average height, one on the rotation around the positive x-axis, and one on the rotation around the negative y-axis. The changing influence on the x and y inertia have been neglected

$$\begin{aligned} F_a(t) &= -mg \\ F_y(t) &= -mg\cos\phi \\ F_x(t) &= -mg\sin\phi \end{aligned} \qquad (2.3)$$

Combination of 2.2. and 2.3 yields the next dynamic equations.

$$\begin{aligned} \textit{average height} &: M\ddot{H}_a = F_1(t)+F_2(t)+F_3(t)-F_z-F_a(t) \\ \textit{rotation around y-axis} &: J_y\ddot{\theta}_y = LF_1(t)+\frac{L}{2}F_2(t)-\frac{L}{2}F_3(t)-F_y(t) \\ \textit{rotation around x-axis} &: J_x\ddot{\theta}_x = \frac{L}{2}\sqrt{3}F_2(t)-\frac{L}{2}\sqrt{3}F_3(t)-F_x(t) \end{aligned} \qquad (2.4)$$

In equation 2.4 J_y and J_x are the inertia of the rotation around the x and y axis respectively.
The forces F_1 to F_3 are corresponding with the upward forces on every float. F_z is the gravitation force on the platform. Therefore $F_z = Mg$.

Filling up equation 2.2 and 2.3 in 2.4 gives:

$$\begin{aligned} \frac{1}{3}M(\ddot{H}_1+\ddot{H}_2+\ddot{H}_3) &= F_1(t)+F_2(t)+F_3(t)-F_z-F_a \\ J_y\frac{2}{3L}(\ddot{H}_1-\frac{1}{2}\ddot{H}_2-\frac{1}{2}\ddot{H}_3) &= L\left(F_1(t)-\frac{1}{2}F_2(t)-\frac{1}{2}F_3(t)-F_y(t)\right) \\ J_x\frac{\sqrt{3}}{3L}(\ddot{H}_2-\ddot{H}_3) &= L\frac{\sqrt{3}}{2}\left(F_2(t)-F_3(t)-\frac{2}{\sqrt{3}}F_x(t)\right) \end{aligned} \qquad (2.5)$$

In equilibrium, the upward forces on the floats will be equal to the gravitation forces on the platform. (In equilibrium there is no load on the crane). In this situation the next equation is in force:

$$F_{O1} + F_{O2} + F_{O3} = F_z = Mg \qquad (2.6)$$

When there is a distance to the equilibrium the platform will start moving. That's the reason for rewriting equation 2.5 in such a manner that distances to the equilibrium are mentioned. In the subjoined equations we made use of:

$$\begin{aligned} F_r &= (F-F_0) \\ h &= (H-H_0) \end{aligned} \qquad (2.7)$$

After Laplace transformation and filling up equation 2.7 in 2.5, the result will be as reproduced in 2.8.

$$\begin{aligned} \frac{1}{3}Ms^2(h_1(s)+h_2(s)+h_3(s)) &= F_{r1}(s)+F_{r2}(s)+F_{r3}(s)-F_a(s) \\ s^2\left(h_1(s)-\frac{1}{2}h_2(s)-h_3(s)\right) &= \frac{3L^2}{2J_y}\left(F_{r1}(s)-\frac{1}{2}F_{r2}(s)-\frac{1}{2}F_{r3}(s)-F_y(s)\right) \\ s^2(h_2(s)-h_3(s)) &= \frac{3L^2}{2J_x}\left(F_{r2}(s)-F_{r3}(s)-\frac{2}{\sqrt{3}}F_x(s)\right) \end{aligned} \qquad (2.8)$$

The disturbances, caused by the load of the crane, have a fixed shape. Therefore they can be seen as input signals.
The Laplace transformation of these forces are shown in equation 2.9.

$$
\begin{aligned}
F_a(s) &= -\frac{mg}{s} = D_a(s) \\
F_y(s) &= -\frac{mgs}{s^2+\omega_2} = D_y(s) \\
F_x(s) &= -\frac{mg\omega}{s^2+\omega^2} = D_x(s)
\end{aligned}
\qquad (2.9)
$$

The float in the water can be seen as a damped spring mass system. Distances to the equilibrium are indicated with a δ. For each float, the next equation is in force.

$$
F_{upward}(t) = K_s\delta(t) + D_s\dot{\delta}(t) \qquad (2.10)
$$

In equation 2.10 the D_s and K_s are indicating the damping and spring constant respectively. The next equations (2.11 to 2.16) are in force for every float. Therefore the subscribt i will be omitted.
The δ can be calculated as follows. (see figure 2.3 and table 2.1)

$$
H = X + (D-\Delta) + W_h \qquad (2.11)
$$

In equilibrium, the next equations are in force:

$$
\begin{aligned}
\frac{1}{3}Mg &= K\,\Delta_0 \\
H_0 &= X_0 + D - \frac{Mg}{3K} + W_{ho} \\
W_{ho} &= \Delta_0\frac{A_f}{A_t} + W_z
\end{aligned}
\qquad (2.12)
$$

By making use of 2.12, the next equations for the distances to the equilibrium can be derived.

$$
\begin{aligned}
\Delta - \Delta_0 &= (X-X_0) + (W_h-w_{ho}) - (H-H_0) \\
&\Updownarrow \\
\delta &= x + w_h - h
\end{aligned}
\qquad (2.13)
$$

For w_h of equation 2.13 can be written:

$$
w_h = W_h - W_{ho} = \delta\frac{A_f}{A_t} + waveheight \qquad (2.14)
$$

Filling up this equation into 2.13 gives the next result for the changes in Δ.

$$
\begin{aligned}
\delta &= x + w_h - h \\
\delta &= x + \delta\left(\frac{A_f}{A_t}\right) + wave\ height - h \\
\delta &= \frac{1}{1-\frac{A_f}{A_t}}(x + wave\ height - h)
\end{aligned}
\qquad (2.15)
$$

The height of the wave will be abbreviated to w_{wh}.
Equation 2.15 can be substituted in equation 2.10. After Laplace transformation, the next equation is found.

$$F_{upward}(s) = (K_s' + sD_s')\,((x(s) + w_{wh}(s) - h(s)) \qquad (2.16)$$

The height of the waves is meant to be measured on the platform itself. Since the platform floats in the tub freely, it is desirable that the height of the waves is derived without making a connection with the tub. The height of the waves can be calculated with the aid of equation 2.17. The variables used in this equation are defined in figure 2.4.

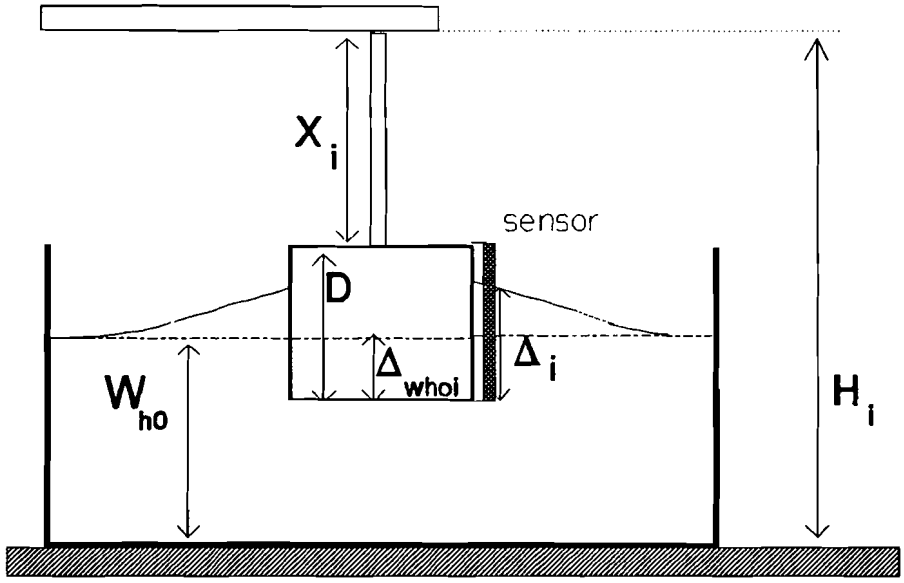

figure 2.4: Wave height measurement on the platform

The variable Δ_{whoi} used in figure 2.4, is defined as the depth of the float in regard with the average water level W_{ho}. In equation 2.17 w_{whi} will be defined as the average height of the wave around float i. The other variables are defined in table 2.1. The height of the wave can be calculated as follows:

$$\begin{aligned} \Delta_{whoi} &= X_i + D - (H_i - W_{ho}) \\ &\Updownarrow \\ w_{whi} &= \Delta_i - \Delta_{whoi} = \Delta_i - (X_i + D - (H_i - W_{ho})) \end{aligned} \qquad (2.17)$$

In equation 2.17, the D and W_{h0} are time invariant.

The upward force which has been found in equation 2.16, can be substituted in equation 2.8. After some restructions, two sets of equations can be derived. (2.19 and 2.20).

The first set describes the transfer of position x_i (see figure 2.3) and the wave heights w_{whi} (see equation 2.17) to the next three outputs: average height, rotation around the positive x- axis, and the rotation around the negative y-axis (see equation 2.2).
The second set describes the transfer function of the disturbances, caused by the crane, to the three outputs mentioned above.

The transfer function form distance x_i to the outputs will make use of the definitions given in equation 2.18.

$$\begin{aligned} x_a(s) &= x_1(s)+x_2(s)+x_3(s) & w_a(s) &= w_{wh1}(s)+w_{wh2}(s)+w_{wh3}(s) \\ x_y(s) &= x_1(s)-\tfrac{1}{2}x_2(s)-\tfrac{1}{2}x_3(s) & w_y(s) &= w_{wh1}(s)-\tfrac{1}{2}w_{wh2}(s)-\tfrac{1}{2}w_{wh3}(s) \\ x_x(s) &= x_2(s)-x_3(s) & w_x(s) &= w_{wh2}(s)-w_{wh3}(s) \end{aligned} \qquad (2.18)$$

The transfer function from distance x_i to the height can be described as follows.

$$3h_a = h_1(s)+h_2(s)+h_3(s) = \frac{\frac{3}{M}(sD'+K')}{s^2+\frac{3}{M}(sD'+K')}[x_a+w_a]$$

$$\frac{3L}{2}\Theta_y = h_1(s)-\frac{1}{2}h_2(s)-\frac{1}{2}h_3(s) = \frac{\frac{3L^2}{2J_y}(sD'+K')}{s^2+\frac{3L^2}{2J_y}(sD'+K')}[x_y+w_y] \qquad (2.19)$$

$$\frac{3L}{\sqrt{3}}\Theta_x = h_2(s)-h_3(s) = \frac{\frac{3L^2}{2J_x}(sD'+K')}{s^2+\frac{3L^2}{2J_x}(sD'+K')}[x_x+w_x]$$

The transfer function from the disturbances of the crane to the three outputs is given in equation 2.20.

$$3h_a = h_1(s)+h_2(s)+h_3 = \frac{\frac{3}{M}}{s^2+\frac{3}{M}(sD'+K')}D_a(s)$$

$$\frac{3L}{2}\Theta_y = h_1(s)-\frac{1}{2}h_2(s)-\frac{1}{2}h_3(s) = \frac{\frac{3L^2}{2J_y}}{s^2+\frac{3L^2}{2J_y}(sD'+K')}D_y(s) \qquad (2.20)$$

$$\frac{3L}{\sqrt{3}}\Theta_x = h_2(s)-h_3(s) = \frac{\frac{3L^2}{2J_x}\left(\frac{2}{\sqrt{3}}\right)}{s^2+\frac{3L^2}{2J_x}(sD'+K')}D_x(s)$$

The outputs of equation 2.20 are defined as the outputs of the three subprocesses of the platform. The output of these subprocesses will be indicated by y_i (i={a,y,x}). For this y_i, the next definitions are in force.

$$\begin{aligned} y_a &= h+h_2+h_3 = 3h_a \\ y_y &= h_1-\frac{1}{2}h_2-\frac{1}{2}h_3 = \frac{3L}{2}\Theta_y \\ y_x &= h_2-h_3 = \frac{3L}{\sqrt{3}}\Theta_x \end{aligned} \qquad (2.22)$$

When the wave disturbances are omitted, two transfer fuctions can be derived. The transfer function P_i will be defined as the transfer function of changes x_i to the output y_i (i={a,y,x}). The transfer function R_i will be defined as the transfer function of the disturbances caused by the crane to the output y_i. For P_i, R_i and y_i (i={a,y,x}) the next equations can be derived.

$$\begin{aligned} P_i(s) &= \frac{y_i(s)}{x_i(s)} = \frac{K_{Pi}(s+n_1)}{(s+p_1)(s+p_2)} \\ R_i(s) &= \frac{y_i(s)}{D_i(s)} = \frac{K_{Ri}}{(s+p_1)(s+p_2)} \\ y_i(s) &= P_i(s)x_i + R_i(s)D_i \end{aligned} \qquad (2.21)$$

The three actual outputs, average height, rotation around the positive x-axis, and rotation around the negative y-axis, can be derived by multiplying the outputs y_i with a certain constant. (see equation 2.2). In the next derivations this constant will be ignored. In spite of this, the outputs y_i will be noted as average height, rotation around the positive x-axis, and rotation around the negative y-axis. When the exact values of these variables are wanted, these constants have to be used of course.

The end of the beams of the platform are resting on vertical steel rods with racks. The distances X_i of the floats to the platform are controlled by servo-motors. It is assumed that the servosystems are exactly the same in bahavior. The transfer functions of these servo-motors are indicated by H_s.
The servo system is assumed to act like an ideal integrator. Therefore the tranfer function will be:

$$H_s(s) = \frac{K_{servo}}{s} \qquad with\ K_{servo}\ is\ a\ constant \qquad (2.23)$$

The input signals of these servo-motors are the voltages $V_i(s)$. The distances x_i are the output signals of these servo systems.
The input signals of equation 2.19 are a combination of the three distances x_i.

If we want to describe the platform by the three decoupled transfer functions mentioned above, the input signal of the servo system H_s has to be a combination of input voltages also.
For the three input voltages of the subprocesses, the next equations are in force.

$$\begin{aligned} V_a &= V_1 + V_2 + V_3 \\ V_y &= V_1 - \frac{1}{2}V_2 - \frac{1}{2}V_3 \\ V_x &= V_2 - V_3 \end{aligned} \qquad (2.22)$$

Each of the three subprocesses can be represented in a schematic way shown in figure 2.5.

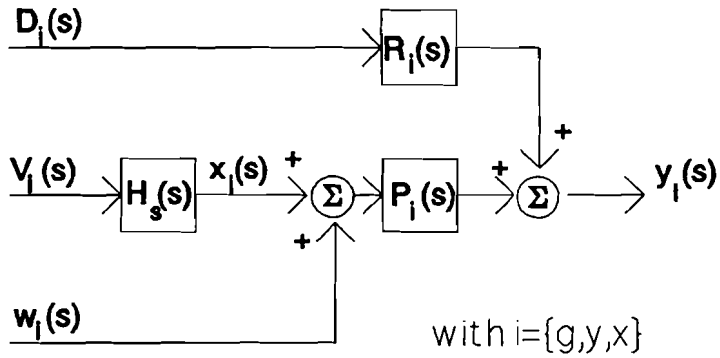

figure 2.5: block diagram subprocess with disturbance

The three subprocesses mentioned above, have been identified by J.P.H.M. Bouwels [1]. The poles and zeros of the processes are mentioned in appendix 1.

3.1: Introduction.

The equations of chapter 2 show that for good simulations, it is necessary to know the heights of the waves. The waves are caused by movements of the floats in the water. To arrive at satisfying simulations, the wave disturbances ghave to be modelled also. The tub in which the platform is positioned, is very small. Due to this fact, the waves caused by the movements of the floats, will reflect against the wall very soon. Because of these reflections, and the changing delays caused by the drifting of the platform, it will be hard to derive a Laplace transformation of the transfer of a float's movement to the height of the waves. A model which describes the height of the waves on every point in the tub, is not needed. Only the waves around the floats are of interest. Therefore the possibility of using measured responses for the calculation of the wave height will be investigated. If the wave process shows linearity, the height of the waves can be calculated easily by making use of superposition in the shape of a convolution sum.
To investigate the linearity of the wave process, some studies have to be made.

3.2: Linearity of the waves.

The linearity of the waves has been investigated with the help of a test array. The construction exists of a cross which is put over the tub (see figure 3.1).

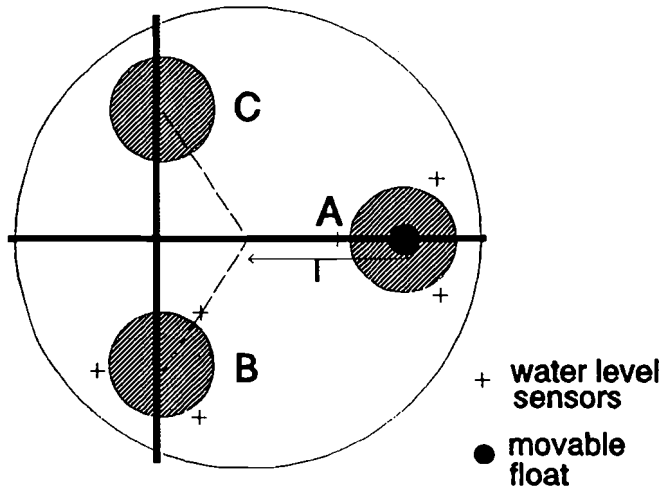

figure 3.1: test array wave responses

The floats of the platform are fixed on this cross. The distances between the floats are equal to the distances between the floats of the platform. However, one of the floats is movable in a vertical way. The distances of the floats to the edge of the tub are equal.

Around one of the fixed floats, and the movable float, water level sensors are placed. The water level is measured with regard to the ground. Because the distances of a float to the edge of the tub are equal, the response of the movable float on the fixed ones will be the same. Therefore there are sensors around one of the fixed floats only. The other float is not taken away because of the reflections it causes. The test array is shown in figure 3.1.

The effects of a movement of the float are measured by giving a punch ('impulse') by hand on the movable float. The wave pattern which come into existence are detected by the water level sensors and registered in a computer file.

At this moment, a modelling error has been introduced. The test array has two fixed floats (B and C in figure 3.1). The waves are unable to move these floats and therefore when a wave meets a float , reflections are the only possibility. In reality, the floats of the platform are not fixed, and a wave can make them move. This means that the float gets some energy of the waves, and the reflections will decrease. On the other hand, the response will last longer because the movements of the floats cause new waves. Because of this, the response will become smaller and will last longer. In the simulation model, all the floats are able to move, but the measured response with the fixed floats is used. For this reason, there will be too much energy in the simulated waves and therefore there is a possibility that the simulations will become instable.
Approximations of the energy transport of the waves to a float are hard to make. Making a correction for this error is only possible when a new platform is built and measurements can be done. For the time being, the measured response will be used. In case of instable simulations, the measured step response will be reduced until stable results are reached.

The responses are formatted by taking the average of the water level measured by the three sensors around a float.

The first measurements were meant to find the dominant frequencies and time constants of the waves. The frequencies of the waves are between 0.5 and 2 Hertz. Therefore, the next measurements have a sample time of 0.1 second.
The next step to be taken was changing the circumstances in order to find the factors which lead to different wave spectrums. From this measurements it is clear there are two factors of importance. The water level in the tub, and the position of the water level sensors. The frequencies of the waves on the edge of the tub are quite different in comparison with the waves in the middle. This is probably caused by the sloping walls of the tub. All the following measurements are done by a constant water level and fixed positions of the sensors.

The float is moved by hand. Therefore it will be difficult to move it in exactly the same

way twice. To be sure it is not of great influence on the measured data, two measurements are done and plotted in figure 3.2.

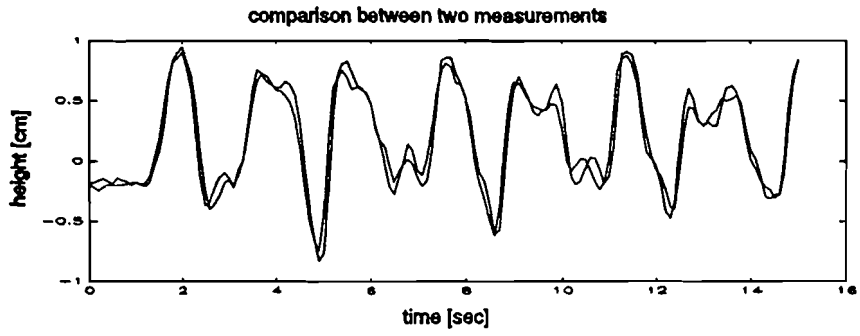

figure 3.2: comparison of two different measurements

In spite of moving the float by hand, it is seen that the plotted measurements in figure 3.2 are quite similar. Because of this, it is possible now to do more measurements in order to investigate the linearity of the wave process.
During the next test, the depth of the movement (impulse) of the float in the water is linearly enlarged step by step. The impulses are made in the same period of time. The results are shown in figure 3.3.

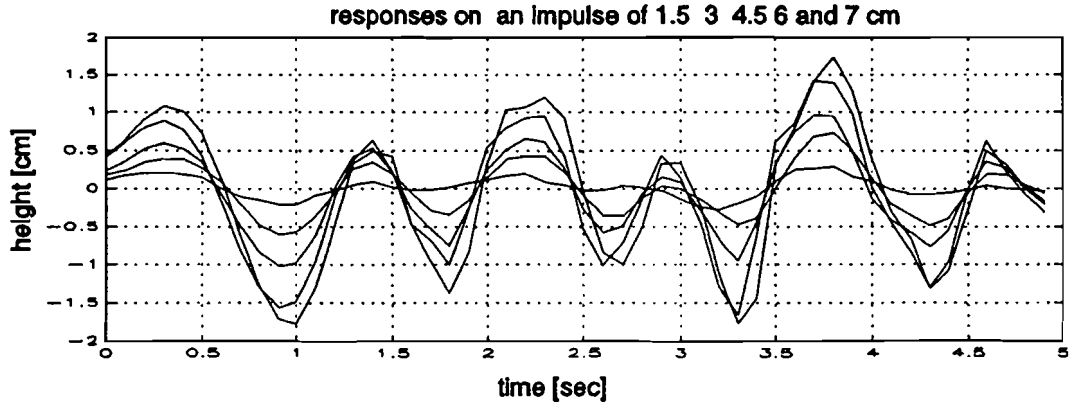

figure 3.3: different impulse responses

Figure 3.3 shows that there is a fairly linear relation between the size of the movement and the measured height of the waves. The differences are probably caused by the fact that the float is moved by hand.

If the waves can be seen as a linear process, an upward movement of the float has to show the inverted image of a downward movement. The two measurements are done. One of the measurements is inverted, and both are plotted in figure 3.4

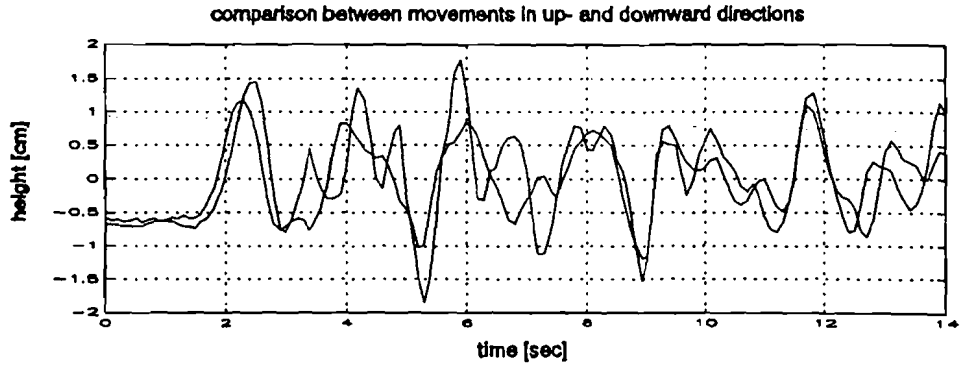

figure 3.4. responses of an up and downward movement.

In figure 3.4, it is seen that the images are not fitting very well. This had to be the case if the process is exactly linear. However, it is hard to move the float upward and downward in the same time and with the same velocity. Of course, if the movements are not exactly inverted, the response will not either.

From the measurements shown above, it can be concluded that the waves can fairly be seen as a linear process. However, there are some restrictions.
During the measurements, the water level in the tub, and the position of the water level sensors, might not be changed.
Because of the concluded linearity, the simulation model derived in the next sections will make use of superposition.

3.3: Modelling platform and waves.

To calculate the height of the waves, two impulse responses are needed. One has to describe the response of the movable float to the waves around this float, and a second one has to describe the response of the movable float to the height of the waves around a fixed one.

Of course, the measured responses will not fit exactly on the theoretical impulse responses. At least two reasons can be mentioned:

1) The impulse on the moveable float doesn't take place within one sample moment.
2) Due to the waves, the water level around the fixed float varies. This means that the Δ of this float varies (see figure 2.3). Variations of this Δ will be used for the calculation of the wave height. Therefore new waves will be calculated in spite of the fact that these waves are included in the measured responses also.

Initially, these effects will be neglected. The possibility of making a simulation model with these measured responses will be investigated first. Only when modelling with measured responses seems possible, the effects mentioned above will be investigated also.

As mentioned before, the waves are caused by movements of the float in the water. These movements are indicated by δ (see equation 2.15). To calculate the height of the wave disturbances, the δ has to be convoluted with the measured impulse responses. The convolution sum is shown in equation 3.1.

$$Y(n) = \sum_{k=-\infty}^{\infty} H(k)\, U(n-k) \qquad (3.1)$$

To calculate the wave height w_{wh} caused by the movement of one float, the U(n-k) has to be replaced by δ(n-k). For H(k) the measured responses have to be used. In this case the convolution sum becomes:

$$w_{wh}(n) = \sum_{k=0}^{M} H_{measured}(k)\, \delta\,(n-k)$$

The upper boundary M of k depends on the length of the measured responses and has to be derived first.

The measured responses around the moveable and fixed float are shown in figure 3.5.

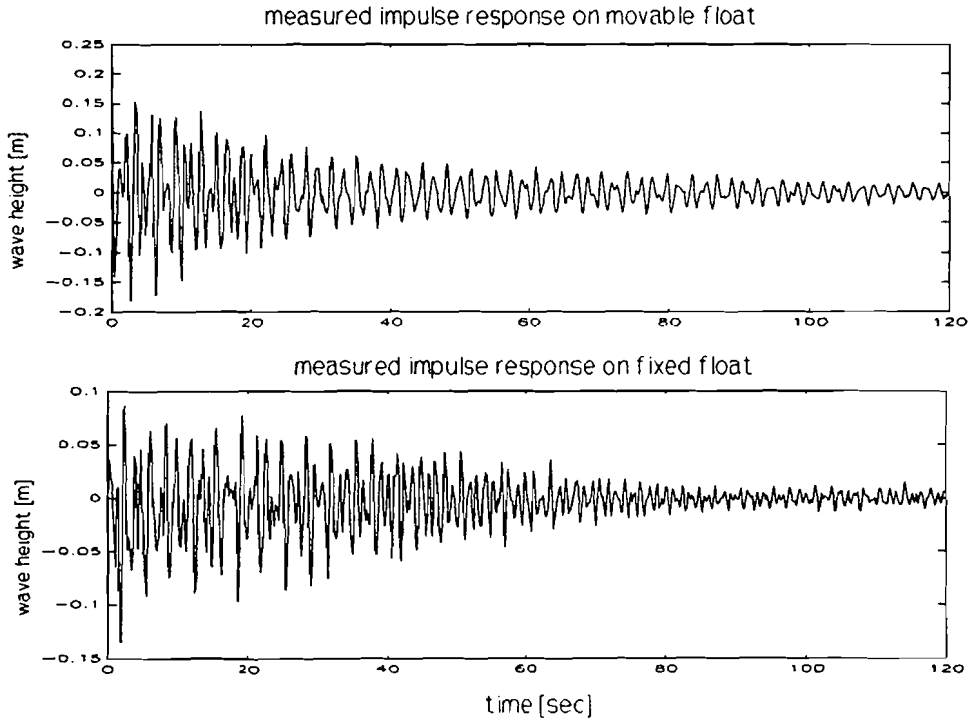

figure 3.5: measured impulse responses.

The output shown in figure 3.5, is scaled to the response on an impulse of 1 meter. For two reasons, only the first 2 minutes of the responses will be used.

1) The tail of the response contains measurement errors also. For this reason a longer lasting response will probably not give better simulation results.
2) The measured responses will be used in a convolution sum. Longer responses will cause longer calculation times also.

The responses shown in figure 3.5 are measured with a sampling frequency of 10 Hz. Therefore, the upper boundary M in equation 3.2 will be equal to 120/0.1=1200.

In figure 3.5 it attracts the attention that the response on the fixed float is about half of the response on the movable float. This effect is caused by the fact that the average of the three sensors is taken. Not all of the sensors around the fixed float are influenced by the waves in the same measure. After taking the average, a smaller response will be left.

The height of the waves around every float are caused by movements of the three floats. The wave height can be calculated with the matrix shown in equation 3.3. In this vector $\underline{\delta_i}$ ($i=\{1,2,3\}$) contains the last 1200 samples of δ_i; $\underline{m}$ and $\underline{f}$ contain the 1200 elements of the measured impulse responses. The first element of the column vector $\underline{\delta_i}$ contains the last sample. The first element of the row vectors $\underline{m}$ and $\underline{f}$ contains the first measured sample. Multiplying $\underline{\delta_i}$ by $\underline{m}$ or $\underline{f}$, gives the result of the pertinent convolution sum.

$$\begin{bmatrix} W_{wh1} \\ W_{wh2} \\ W_{wh3} \end{bmatrix} = \begin{bmatrix} \underline{m} & \underline{f} & \underline{f} \\ \underline{f} & \underline{m} & \underline{f} \\ \underline{f} & \underline{f} & \underline{m} \end{bmatrix} \cdot \begin{bmatrix} \underline{\delta_1} \\ \underline{\delta_2} \\ \underline{\delta_3} \end{bmatrix} \qquad (3.3)$$

with m = measured response on movable float

f = measured response on fixed float

The δ_i can be calculated with equation 3.4 (equation 3.4 is derived in chapter 2).

$$\delta_i = \frac{1}{1-\frac{A_f}{A_t}} (x_i + w_{whi} - h_i) \qquad (3.4)$$

As can be seen in equation 3.4, the δ_i is calculated by using x_i, w_{whi} and h_i ($i=\{1,2,3\}$ see figure 2.3). The transfer function of the platform derived in the chapter before, was divided in three independent sub-processes (average height, rotation around the positive x-axis, and rotation around the negative y-axis). The in- and output signals of these three processes are combinations of voltages V_i and heights h_i $\{i=\{1,2,3\}\}$.
The input of the three sub-processes can be calculated with the transformation matrix shown in equation 3.5.

$$\begin{bmatrix} V_a \\ V_x \\ V_y \end{bmatrix} = \begin{bmatrix} 1 & 1 & 1 \\ 1 & -\frac{1}{2} & -\frac{1}{2} \\ 0 & 1 & -1 \end{bmatrix} . \begin{bmatrix} V_1 \\ V_2 \\ V_3 \end{bmatrix} = F . \begin{bmatrix} V_1 \\ V_2 \\ V_3 \end{bmatrix} \qquad (3.5)$$

The actual heights h_i ($i=\{1,2,3\}$) of the platform can be calculated with the outputs y_i ($i=\{a,y,x\}$) of the three subprocesses. The transfer matrix is given in equation 3.6.

$$\begin{bmatrix} h_1 \\ h_2 \\ h_3 \end{bmatrix} = \frac{1}{6} \begin{bmatrix} 2 & 4 & 0 \\ 2 & -2 & 3 \\ 2 & -2 & -3 \end{bmatrix} . \begin{bmatrix} y_a \\ y_y \\ y_x \end{bmatrix} = F^{-1} \begin{bmatrix} y_a \\ y_y \\ y_x \end{bmatrix} \qquad (3.6)$$

The sampling frequency of the three subprocesses is 10 Hz [1]. The poles, zeros, and constants of each subprocess are tabled in appendix 1. The three subprocesses describe the transfer of combinations of servo input voltages, to combinations of platform heights. The output of a servo is the distance X_i in figure 2.3. In the chapter before it is concluded that the waves can be seen as disturbances on the distance X_i. Therefore the identified processes have to be divided in a servo part $H_s(z)$ and a part P(z) which describes the platform dynamics. The servo system will be seen as an ideal integrator.

The three identified transfer functions (average height, rotation around the negative y-axis and rotation around the positive x-axis) are of the same form, and can be written as follows:

$$G_i(z) = k_{pi} \frac{(z-z_{1i})\,(z-z_{2i})}{(z-1)\,(z-p_{1i})\,(z-p_{2i})} \qquad with\ i=\{a,y,x\} \qquad (3.7)$$

Dividing equation 3.7 into a servo part and a platform part gives:

$$\begin{aligned} G_i(z) &= H_s(z) \,.\, P(z) \\ G_i(z) &= K_{1i} \left(T \frac{1}{z-1} \right) . K_{2i} \left(\frac{(z-z_{1i})\,(z-z_{2i})}{(z-p_{1i})\,(z-p_{2i})} \right) \end{aligned} \qquad (3.8)$$

The problem is, how to calculate K_{1i} and K_{2i} ($i=\{a,y,x\}$). As mentioned in chapter two, the platform without the servo's can be seen as a damped spring mass system. If the mass of the platform is constant, the equilibrium stays on the same position.
If the distances X_i of the platform (see figure 2.3) are enlarged by a unity step, the transfer of P(z) will become equal to 1 if $t \to \infty$. A change in the height H_i ($i=\{1,2,3\}$ see figure 2.3) is caused by a change of the distance X_i ($i=\{1,2,3\}$) which can be caused only

by the servo system.

By making use of the theorem given in equation 3.9, the K_{1i} and K_{2i} (i={a,y,x}) of equation 3.8 can be calculated

$$f(\infty) = \lim_{z \to 1} (z-1)\, F(z) \qquad (3.9)$$

filling up F(z)=step(z).P(z):

$$1 = \lim_{z \to 1} z-1 \,.\, K_2 \,.\, \frac{z}{z-1} \,.\, \frac{(z-z_{1i})\,(z-z_{2i})}{(z-p_{1i})\,(z-p_{2i})}$$

$$1 = K_{2i} \,.\, \frac{(1-z_{1i})\,(1-z_{2i})}{(1-p_{1i})\,(1-p_{2i})} \qquad (3.10)$$

$$K_{2i} = \frac{1-(p_{1i}+p_{2i})+p_{1i}p_{2i}}{1-(z_{1i}+z_{2i})+z_{1i}z_{2i}}$$

With $K_{pi}=K_{1i}K_{2i}$ the K_{1i} (i={a,y,x)} can be written as:

$$K_{1i} = \frac{K_{pi}}{(T.K_{2i})} \qquad with\ T = 0.1\ sec \qquad (3.11)$$

For each of the subprocesses (average height, rotation around the negative y-axis and rotation around the positive x-axis), the K_{1i} and K_{2i} (i={a,y,x}) can be calculated. The calculated values are tabled in appendix 2.

Right now, the three subprocesses are divided in a part describing the servo system, and a part describing the dynamics of the platform. The input signals of the equation describing the platform dynamics, are combinations of the distances x_i (see equation 2.3). The servo transfer function found in equation 3.8, makes use of a combination of input voltages also. It describes the transfer of a combination of input voltages, to a combination of output distances x_i.
However, for the calculation of the depths δ_i (see 3.14) the variations of the distances X_i (i={1,2,3}) have to be known individually. Therefore the servo part has to be rewritten in such a way that the values of x_1, x_2 and x_3 can be derived.

The transfer function of a single servo can be written as:

$$H_s(z) = K_s . T . \frac{1}{z-1} \qquad (3.12)$$

The K_s can be derived easily if the equation of the average height is used.

$$\begin{aligned} x_a &= K_{1a}\int V_a\,dt = K_{1a}\int (V_1 + V_2 + V_3)\,dt = x_1 + x_2 + x_3 \\ x_1 &= K_s\int V_1 dt \end{aligned} \qquad (3.13)$$

Therefore the K_s is equal to K_a.

For each float, the value X can be written as:

$$\begin{aligned} x_1 &= \int K_{1a}V_1\,dt \\ x_2 &= \int K_{1a}V_2\,dt \\ x_3 &= \int K_{1a}V_3\,dt \end{aligned} \qquad (3.14)$$

Since the platform dynamics are given by the three subprocesses: average height, rotation around the negative y-axis and rotation around the positive x-axis, the x_1, x_2 and x_3 have to be transformed to x_a, x_y, and x_x. This can be done with the aid of equation 3.15

$$\begin{aligned} V_a &= V_1 + V_2 + V_3 \\ x_a &= K_{1a}\int (V_1 + V_2 + V_3)\,dt = K_{1a}(x_1 + x_2 + x_3) \end{aligned}$$

$$\begin{aligned} x_x &= K_{1x}\int (V_2 - V_3)\,dt \\ x_x &= K_x(x_2 - x_3) \qquad \text{with } K_x = \frac{K_{1x}}{K_{1a}} \end{aligned} \qquad (3.15)$$

$$\begin{aligned} x_y &= K_{1y}\int (V_1 - \tfrac{1}{2}V_2 - \tfrac{1}{2}V_3)\,dt \\ x_y &= K_y(x_1 - \tfrac{1}{2}x_2 - \tfrac{1}{2}x_3) \qquad \text{with } K_Y = \frac{K_{1y}}{K_{1a}} \end{aligned}$$

Hence:

$$\begin{bmatrix} x_a \\ x_y \\ x_y \end{bmatrix} = \begin{bmatrix} 1 & 0 & 0 \\ 0 & K_y & 0 \\ 0 & 0 & K_x \end{bmatrix} . F . \begin{bmatrix} x_1 \\ x_2 \\ x_3 \end{bmatrix} \qquad (3.16)$$

The matrix F in equation 3.16 is defined in equation 3.5.

Now the three sub-processes are transformed in such a way that the input variables for the calculation of δ_i (i={1,2,3}) can be derived. The derivation of δ_i is described in section 2.3. The δ_i can be calculated as follows:

$$\delta_i = \frac{1}{1-\frac{A_f}{A_t}} (x_i + w_{whi} - h_i) \qquad with\ i = \{1,2,3\} \tag{3.17}$$

Equation 3.17 can be used to derive a simulation model. The block diagram of the model is shown in figure 3.6. The disturbances caused by the crane, are not presented. They are inserted in the platform block.

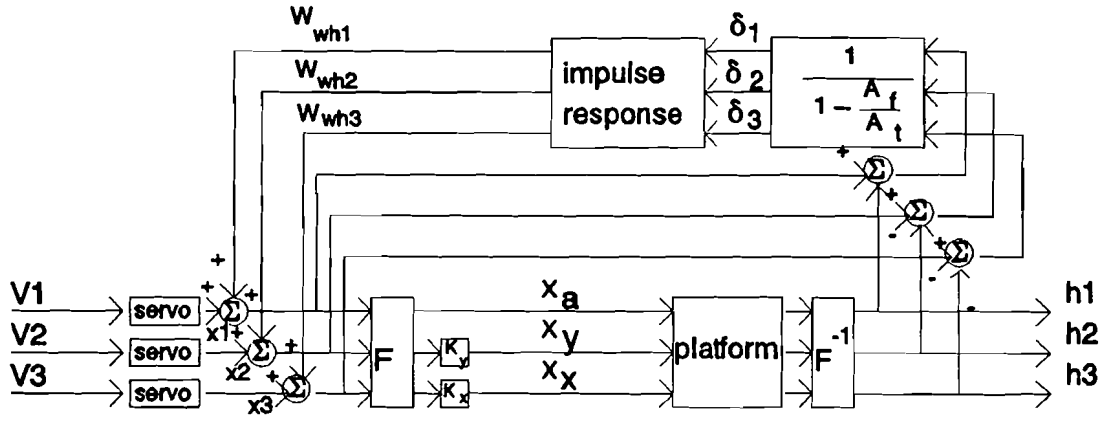

figure 3.6: Block diagram simulation model.

In figure 3.6, the block impulse response contains the matrix shown in equation 3.3. As can be seen in figure 3.6, the calculated height of the waves, W_{whi}, has to be used by the calculation of the δ_i. This means that there is a feed-back.

With the block diagram of 3.6, together with the identified poles, zeros, and constants given in appendix 1 and 2, the simulation model can be programmed in the Matlab toolbox SIMULINK [4].
The simulations done with the model of figure 3.6, are showing instability. The output is drifting away. If one of the floats is excited for a moment, the height of the waves increases in the course of time. This implies the energy of the waves is increasing also.
Since this isn't what is seen in reality, there must by an error in the simulation model.

However, an explanation for this instability can be derived easily. The simulation model makes use of a measured impulse response.
The measured impulse responses are cut off after 2 minutes. Consequently, the tail of this response is omitted.

The transfer of the float's movement to the height of the waves has a differentiative character. Fast movements cause bigger waves than slower ones. There is a possibility, the differential character of the wave process can't be found in this incomplete response. As a consequence $H(0) \neq 0$, and a constant will be left and fed back to the input. New waves are caused, and as a result, the process is becoming instable.

By differentiating the input of the convolution sum (δ_i) first, the constant feedback is removed and the simulation model can be stabilized. In this case, the convolution sum has to be calculated with a step response instead of an impulse response.
With the adjustment mentioned above, the block diagram of figure 3.5 becomes as shown in figure 3.7.

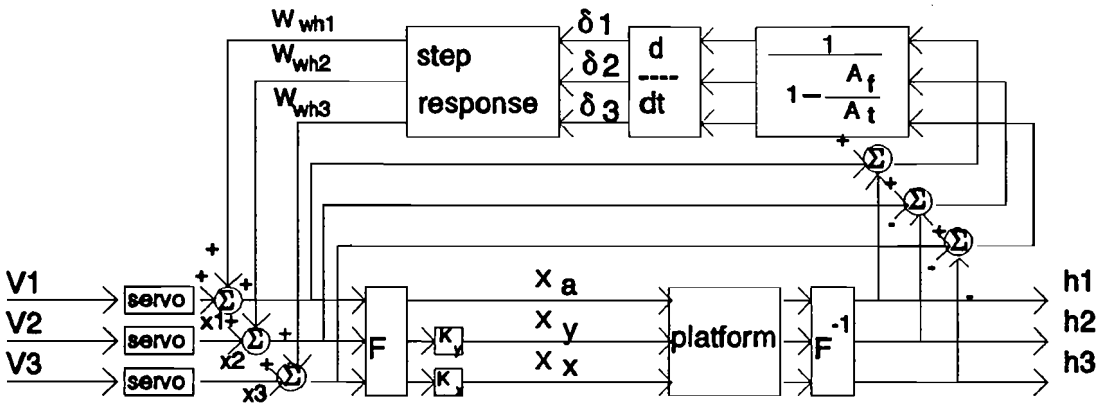

figure 3.7: block diagram simulation model.

Instead of the impulse responses, the step responses are measured now. The block step response in figure 3.7 contains the matrix of equation 3.3. However, the measured impulse responses $\underline{m}$ and $\underline{f}$ of equation 3.3 have to be replaced by measured step responses. The simulation program is adjusted as mentioned in figure 3.7. After starting up the simulation, the outputsignal showed instability again.
The reason for this instability can be found in the fact that the step responses contain measurement errors also. Especially when the responses become small, these errors become noticeable. Because of these errors, new waves come into existence, and instability will be the result.

Stability can be reached in two different ways.

1) Reducing the measured step responses.
2) By placing a lower bound on the input signal of the convolution sum.

The first option doesn't give good results. The measured responses have to be reduced

more than 50% to come to stable results. As a consequence the simulations with these responses do not show much resemblance with reality. However, the second option shows better results.
Signals smaller than a certain bound will be made zero. Adding this bound to the simulation model, the wave disturbances show the desired damped response. A good boundary for acceptable simulation results is 0.0025 m/sec. Of course it depends of the magnitude of the float's movement. (See appendix 4 and 5).

3.4: Adjustments of the measured step responses.

In the previous section, a simulation model is derived. This model makes use of measured step responses. The output of the model is stable but, as mentioned before, there are some measurement and model errors which can probably not be neglected.

One of the errors arises by the measurement of the step response. The movement of the float lasts more then a sample moment (=0.1 sec). This means that it isn't a perfect step, and the response will be smaller than expected. To investigate the influence of this impure step response, an approximation of the transfer function of the float's movement to the wave height will be derived.
The wave process has a differentiative character. A fast movement of the float will cause bigger waves than a slower one. In the S-plane this means there is a zero in the origin. The transfer of a movement of the float to the wave height can be approximated by a sine wave with a certain damping factor.
The frequency of the sine wave is 1 Hz, and the time constant is about 30 seconds. The simplified transfer function is given in equation 3.18.

$$H(S) = K\frac{S}{S^2 + AS + B} \qquad (3.18)$$

The pole-zero plot of this process is shown in figure 3.8.

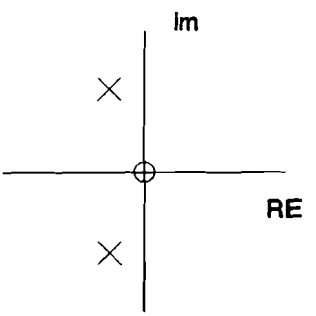

Figure 3.8: pole-zero plot wave process

To analyze the effects, some simulations will be done with the transfer function mentioned in equation 3.18. The first picture of figure 3.9 shows the input signals. The picture underneath shows the responses of the input signals.

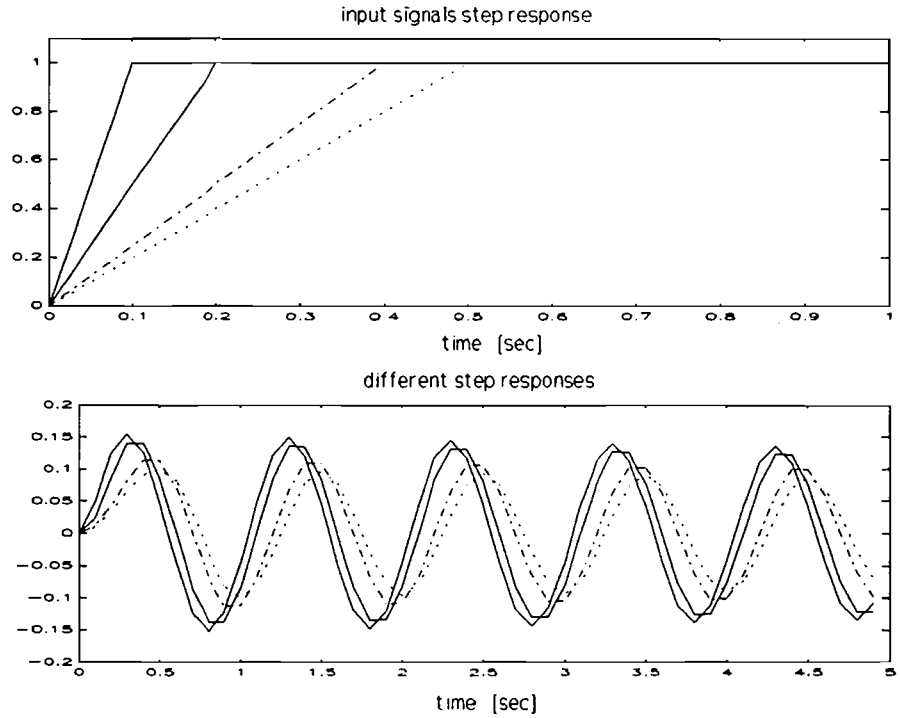

figure 3.9: responses of different input signals.

As can be seen in figure 3.9, the response becomes smaller when the steepness of the input signal decreases. Besides, a little phase shift is appearing also. The measured responses used in the convolution sum are derived by a float's movement of 5 cm. The period of time in which the float is moved 5 cm, isn't exactly known. An estimation of 0.25 seconds is used.
In figure 3.9 it can be seen that the response has to be multiplied by about a factor 1.2 to reach the value of the ideal step response. Therefore, in the following simulations, the measured step responses are multiplied by a factor 1.2. The phase shift is not corrected.

3.5: Testing the simulation model.

The simulation model, derived in the sections before, gives the opportunity to investigate the behaviour of the platform under the influence of the waves. To trace the similarity between the simulations and reality, some tests have to be done. Unfortunately the platform described and tested by J.P.H.M. Bouwels [1], has been broken down. Therefore, the measurements described in his report [1] have to be sufficient. The measurements mentioned on page 33 to 37 of his report are repeated with the simulation model. The results are presented in the next figures.

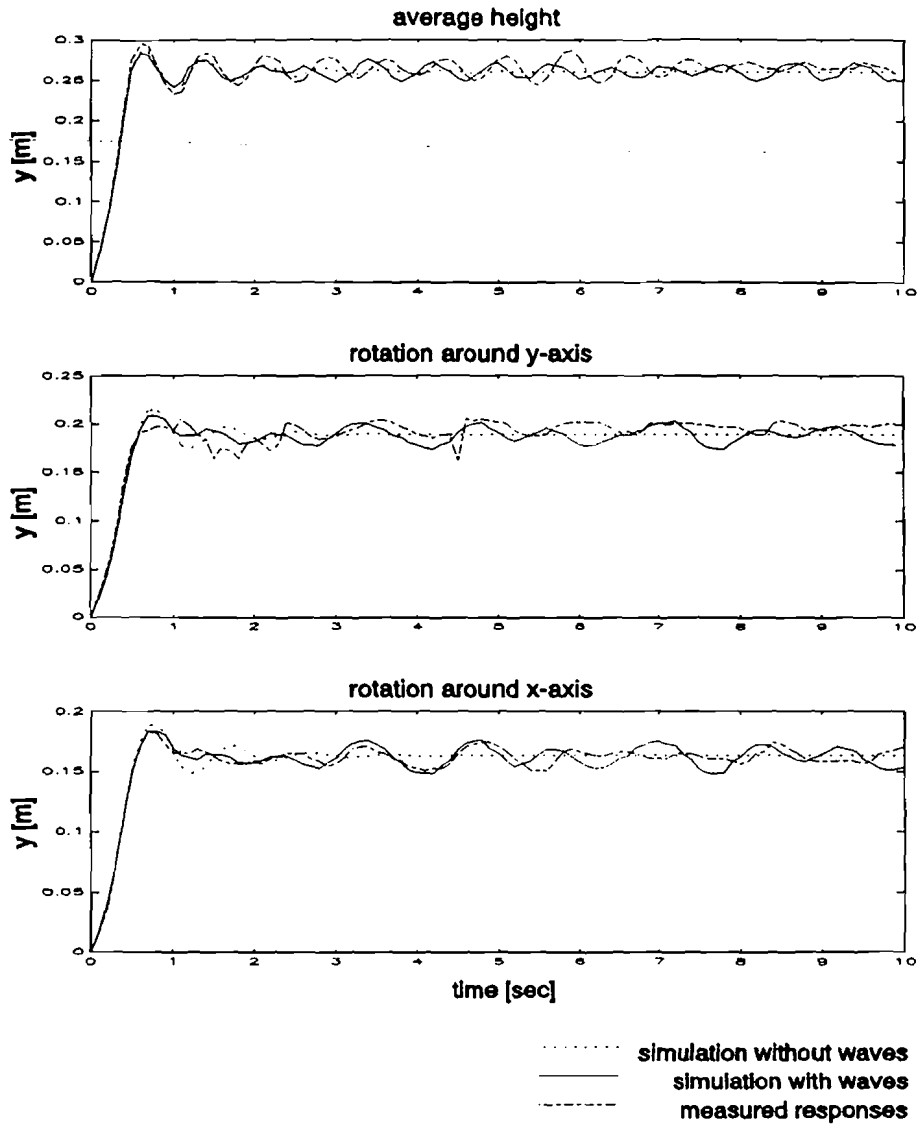

figure 3.10: measurements by a step on the distance X.

When the simulations are compared with the measurements done by J.P.H.M. Bouwels, two facts attract attention:

- In the simulations, the shape of the variations of the average height are different.
- In the simulations the rotation around the positive x-axis and negative y-axis show a less capricious course.

Possible explanations:

The simulations and the responses measured in reality, will never fit exactly because of two reasons.
The step responses used in the simulation model are not the exact step responses (see section 3.4) and the measures of the platform used by J.P.H.M. Bouwels don't agree with the measures of the test array used to come to the simulation model. The distance between the floats of the test array is larger than the distance between the floats of the platform used in [1]. So the disturbances on the average height will be different also.

The measurements of the height of the platform described in [1] are done by making connections to the edge of the tub. Therefore, the platform could not move freely. This probably is the reason for the capricious course of the rotation around the x -and y-axis found by J.P.H.M. Bouwels. It is not expected that these measurements could be reproduced. It is more likely that the course of the rotation around the x- and y-axis agrees with the course found by the simulation model. It attracts the attention that the measured and simulated courses are of the same size.

The second set of measurements used to test the simulation model makes use of the crane on the platform. During the measurements, a 1 kg load is picked up by the crane. The crane rotates at a frequency of 0.04 Hz. The distances X of the floats will be constant during the measurements.
To test the response on the average height, the load is picked up after 10 seconds. After 40 seconds the load is put down. To test the response of the rotation around the x- and y-axis, the load is picked up at t=0 and never put down during the measurement. Unfortunately the data of this measurement could not be found and the plots shown in [1] had to be copied. The simulations and measured responses are plotted side by side. On the left side the simulations, on the right side the measurements done by J.P.H.M. Bouwels [1]. The results are shown in figure 3.11, 3.12 and 3.13.

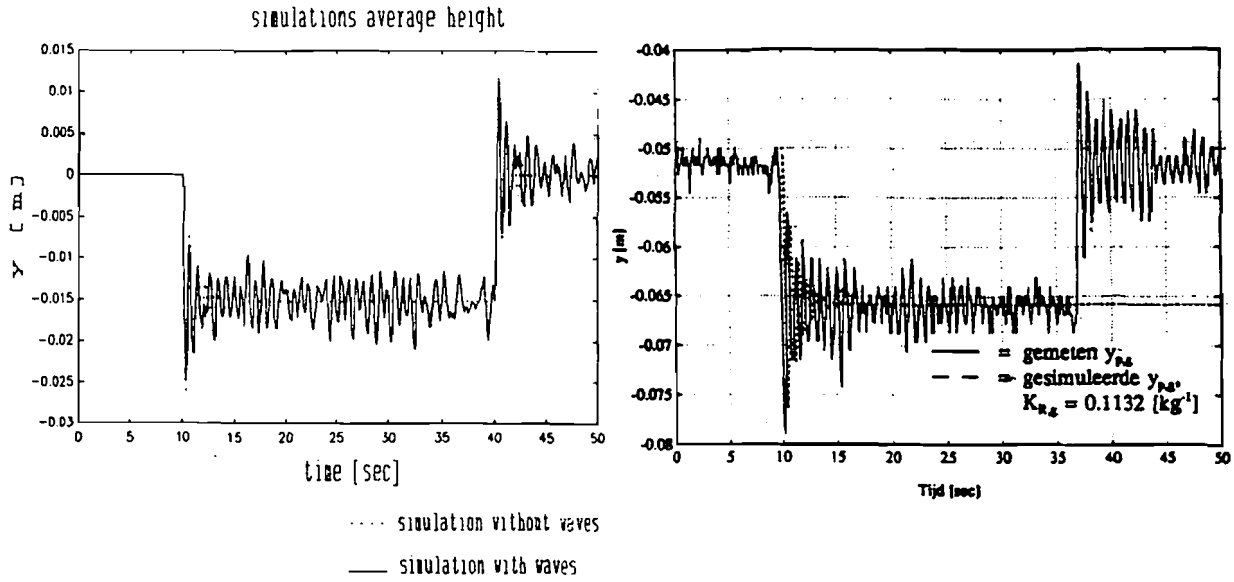

figure 3.11:test results average height

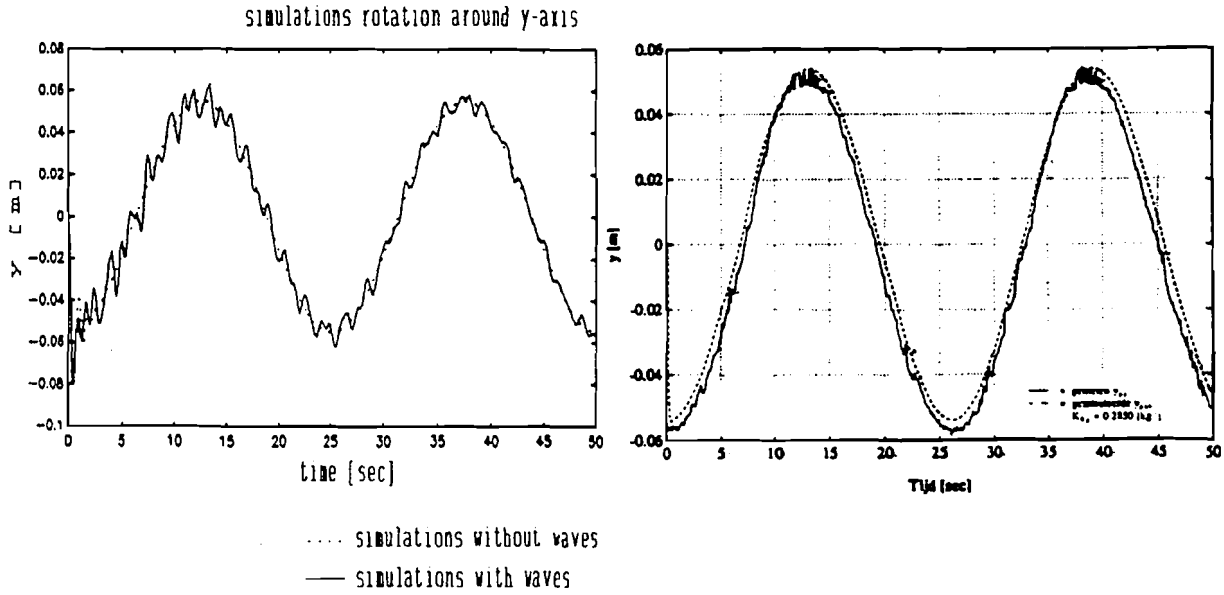

figure 3.12: test results rotation around the negative y-axis

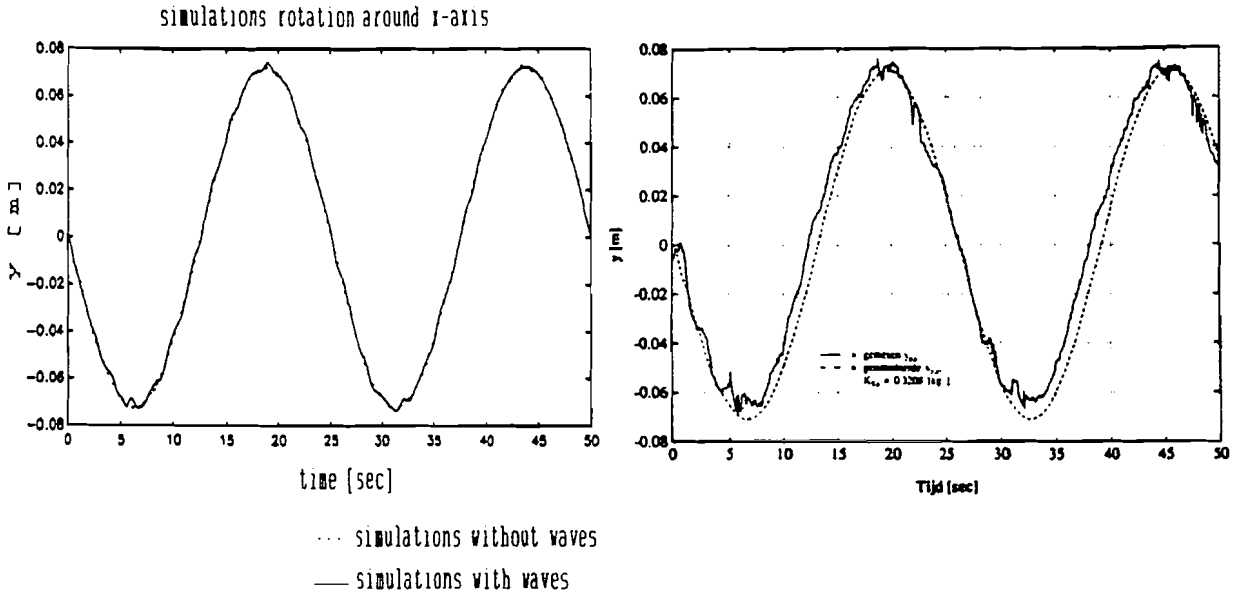

figure 3.13: test results rotation around the positive x-axis

If the simulated results are compared with the measured results, it can be concluded that the plots of the average height and the rotation around the negative y-axis agree a lot. Only the rotation around the positive x-axis shows some differences. The influence of the waves seems to be zero in the simulation results. The explanation below will give a solution. The waves which come into existence by the rotation of the crane are very small. One has to remember that the crane is rotating with a very low frequency and the floats are moving very slowly. The disturbances of the waves which can be seen in figure 3.12 are caused by picking up the load at t=0. Of course this takes place with a much higher frequency. However, at t=0 the angle Φ (see figure 2.2) is still equal to zero.
Picking up the load causes a movement of one float only. The response of this movement causes wave disturbances that are equal for both the other floats. Therefore there will almost be no rotation around the positive x-axis, and the disturbances can't be seen in the left plot of figure 3.13.

By changing the starting point of the crane, the symmetry will be disturbed and the influence of the waves will be seen.
However, the plot of the measured rotation around the x-axis mentioned in [1], shows disturbing influences of the waves. These are caused by the fact that the platform is able to move a little bit. There is a great possibility the platform wasn't exactly positioned in the middle during the measurements. In this case there will be no symmetry either.

To investigate the usefulness of the simulation, one more test can be done. In the report of J.P.H.M. Bouwels [1], two different H_∞ controllers are designed. First a strong controller was designed. In theory, this controller was able to rule out all the disturbances caused by the crane. However, in practice the caused waves became to big and the platform showed instability. Therefore a second controller was designed. The performance was not as good as the first one, but in practice, it was able to gave some stable responses.

Both controllers consist of a feed back and a feed forward part. The controller can be inserted in the simulation model. A general view is given in figure 3.14.

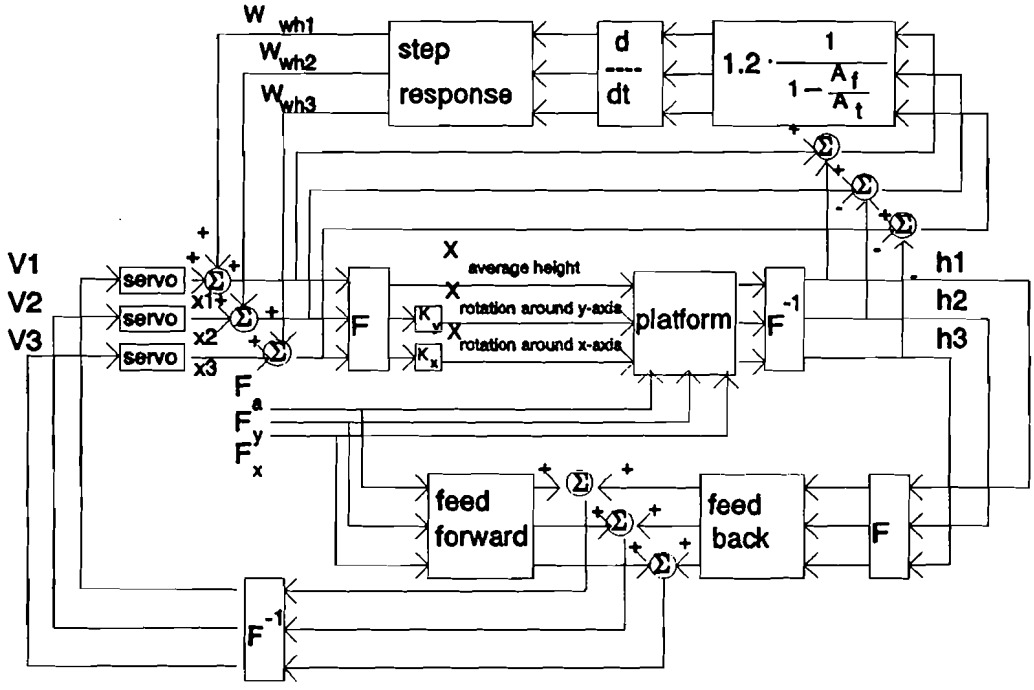

figure 3.14: block diagram simulation model with a controller

The poles, zeros and constants of both controllers are mentioned in appendix 3. The factor 1.2 in the diagram of figure 3.14 is derived in section 3.4.
The simulations results are shown in figure 3.15 and 3.16. The plots of figure 3.15 show the results when the influence of the waves is omitted. Figure 3.16 shows the results when the disturbances of the waves are allowed.

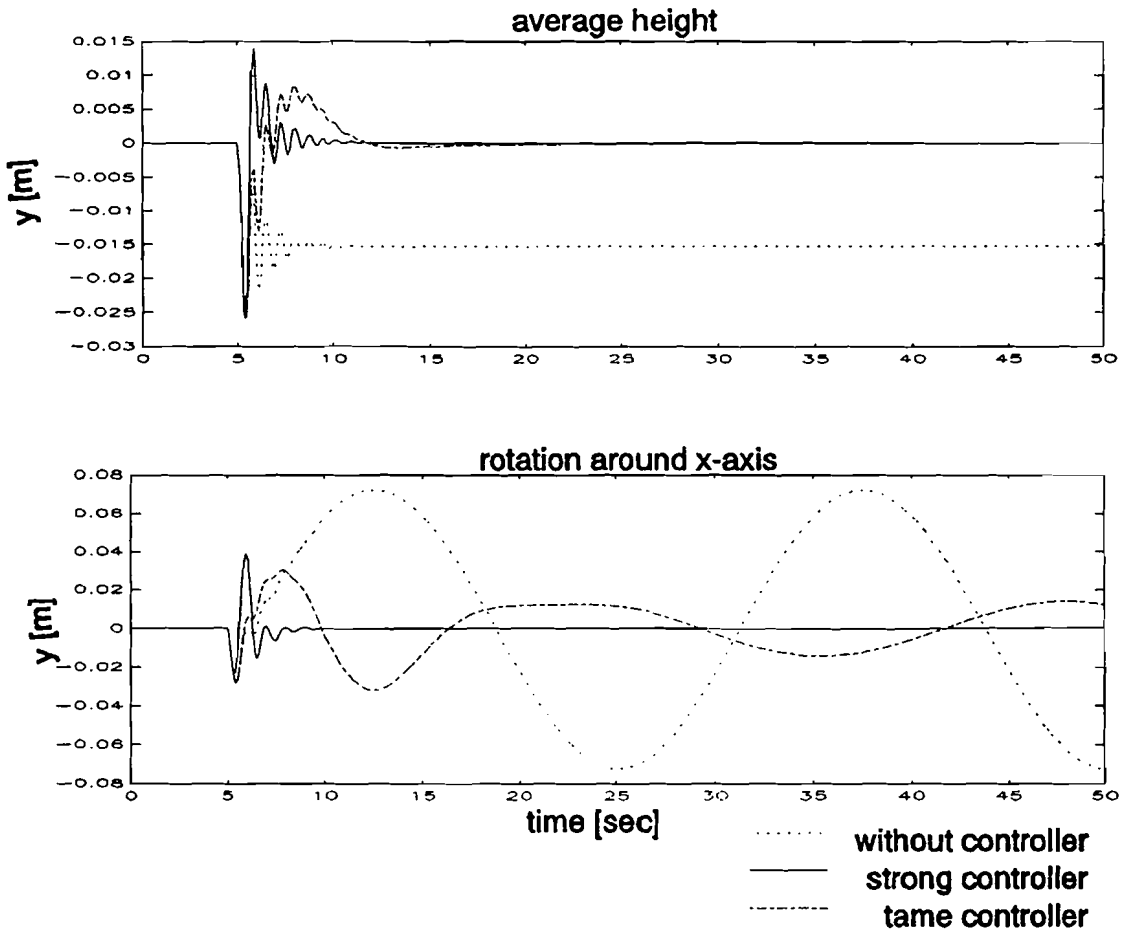

figure 3.15: simulations without wave disturbances

Under the influence of the waves the results plotted in figure 3.16 can be derived.

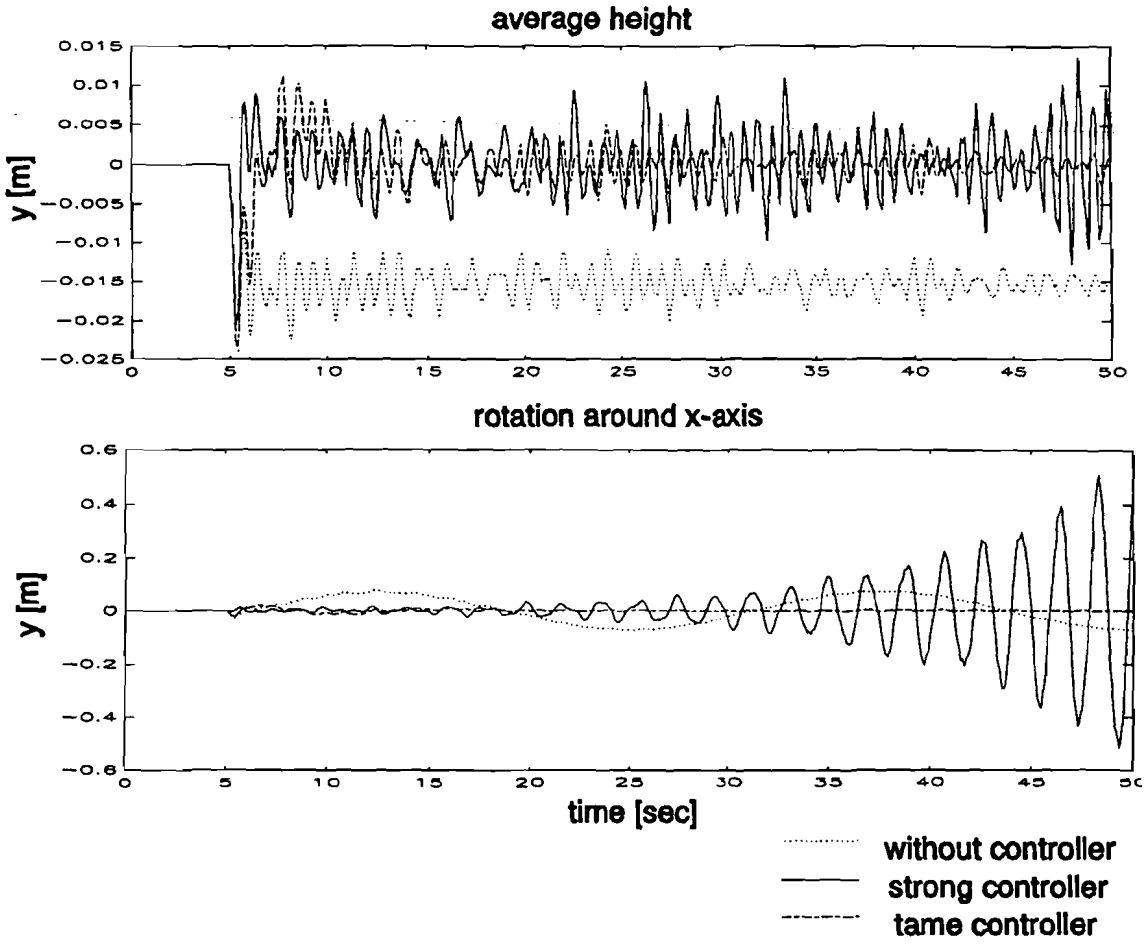

figure 3.16: simulations with wave disturbances.

As was found in reality, the simulations also show instability when the strong controller is used.

3.6: A short survey

Three kind of tests are done to investigate the usefulness of the simulation model. All of the tests show results that agree a lot with the results found in [1]. For this reason, all the controllers which will be designed will be tested on this simulation model first. In appendix 4, a manual of the simulation model is given.

4.1: Introduction.

To solve the control problem of the platform, many control theories have been investigated. Up until now the H_∞ theory seems to give the best results. For this reason the research shall continue in this direction. First, a short summary of the H_∞ will be given. A more detailed survey is given in [2]. The controllers are designed by using the Matlab toolbox MHC written by H. Falkus

4.2: The standard H_∞ problem.

Many control problems can be converted to an equivalent problem in which the H_∞ criterion will have the same form. A block diagram of this standard problem is given in figure 4.1.

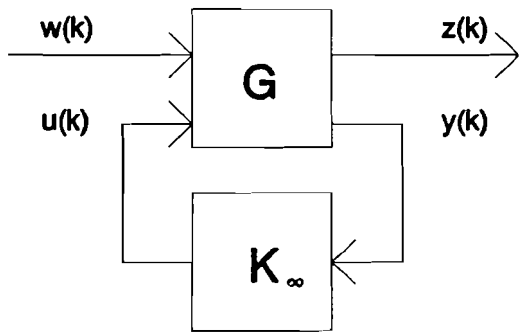

figure 4.1: Block diagram standard problem.

The augmented Plant G (process with weighting and shaping filters) is controlled by a H_∞ controller which is indicated by K_∞. The shaping filters of the augmented plant are used to model the spectrum of the disturbances. The weighting filters are used to emphasize the desired performance of the controlled plant. The definition of the input signals w and u, and the output signals y and z is given in table 4.1.

table 4.1:input and output signals of the standard problem

$w(k)\epsilon\mathbf{R}^{m1}$	exogenous input	input of disturbances
$u(k)\epsilon\mathbf{R}^{m2}$	control input	output controller
$z(k)\epsilon\mathbf{R}^{p1}$	output to be controlled	output signals to be minimized
$y(k)\epsilon\mathbf{R}^{p2}$	measured output	measured output process

A solution of this standard form is given by Glover and Doyle [5]. The controller is designed for a MIMO (Multiple Input Multiple Output) system with a transfer function G. The transfer matrix G can be subdivided into four sub-matrices with in- and outputs as given in table 4.1.

$$G = \begin{bmatrix} G_{11} & G_{12} \\ G_{21} & G_{22} \end{bmatrix} \tag{4.1}$$

The equations for the augmented plant are:

$$\begin{aligned} z(k) &= G_{11}(z)\, w(k) + G_{12}(z)\, u(k) \\ y(k) &= G_{21}(z)\, w(k) + G_{22}(z)\, u(k) \\ u(k) &= K_{\infty}(z)\, y(k) \end{aligned} \tag{4.2}$$

For the equations shown below, the index (k) will be omitted.
By solving equation 4.2, a transfer from w to z can be derived.

$$z = M_k w = \left[G_{11} + G_{12}K_{\infty}(I - G_{22}K_{\infty})^{-1}G_{21}\right]w \tag{4.3}$$

M_k is the closed loop transfer function of the exogenous input w to the controlled output z. The intention of the H_∞ theory, is to minimize the H_∞-norm of this transfer matrix M_k for all stabilizing controllers K_∞. This gives the next criterion.

$$\alpha \equiv \inf_{K_{\infty}} \left[\sup_{w \in L_2} \frac{||z||_2}{||w||_2} \right] = \inf_{K_{\infty}} ||M_k||_{\infty} \tag{4.4}$$

The H_∞-norm of M_k is defined as follows

$$||M_k||_{\infty} \equiv \sup_{\omega \in R} (\sigma_{\max}(M_k)) \tag{4.5}$$

In words: Search for the largest singular value of the transfer matrix M_k : σ_{max} (M_k) for every ω.

The standard problem is defined as follows:
Search for a controller K_∞ which is minimizing the H_∞-norm of the transfer matrix M_k of w to z, in such a way that the controller K_∞ is stabilizing the transfer G:

$$\alpha \equiv \inf_{K_{stabilizing}} ||G_{11} + G_{12}K_{\infty}(I - G_{22}K_{\infty})^{-1}G_{21}||_{\infty} \tag{4.6}$$

The solution of this standard problem is given by K. Glover and J.C. Doyle [5]. To arrive at the solution, the state-space description of the augmented plant has to be used. In this case, the controller is found by solving two Riccati equations. The solutions of these equations are of the same order as the augmented plant. At first, the state-space description of the augmented plant will be given.

$$\begin{aligned} x(k+1) &= Ax(k) + B_1 w(k) + B_2 u(k) \\ z(k) &= C_1 x(k) + D_{11} w(k) + D_{12} u(k) \\ y(k) &= C_2 x(k) + D_{21} w(k) + D_{22} u(k) \end{aligned} \qquad (4.7)$$

The transfer function G(z) of the augmented plant can be written as follows:

$$G(z) = \begin{bmatrix} G_{11} & G_{12} \\ G_{21} & G_{22} \end{bmatrix} = \begin{bmatrix} D_{11} & D_{12} \\ D_{21} & D_{22} \end{bmatrix} + \begin{bmatrix} C_1 \\ C_2 \end{bmatrix} (zI - A)^{-1} \begin{bmatrix} B_1 & B_2 \end{bmatrix} \qquad (4.8)$$

For matters of simplicity, the state-space description will be written in the following way.

$$\begin{bmatrix} A & B_1 & B_2 \\ C_1 & D_{11} & D_{12} \\ C_2 & D_{21} & D_{22} \end{bmatrix} \equiv \begin{bmatrix} A & B \\ C & D \end{bmatrix} \qquad (4.9)$$

The two Riccati equations can be solved if the state-space matrices fulfil the next requirements [2]

1) (A,B_2) has to be stabilizable and (A,C_2) has to be detectable. Only in this case a controller K_∞ can exist. If the system matrix A has instable poles, these poles have to be stabilized first.
2) $\text{rank}(D_{12})=m_2$, $\text{rank}(D_{21})=p_2$. (see also table 4.1). This is sufficient to ensure that the controllers are proper. Otherwise the controllers might become improper which makes truncation at high frequencies necessary to obtain sub-optimal physically realizable proper controllers.
3) There are allowed no zeros on the unit circle, otherwise loss of column and row rank will appear.
4) $p_1 \geq m_2$ and $m_1 \geq p_2$. Otherwise the describtoin of the plant can't be unique

If a controller exists, the method of Glover and Doyle derives a controller K_∞ with the next H_∞-norm of $M_k(G,K_\infty)$:

$$\| M_k(G, K_\infty) \|_\infty < \gamma \qquad (4.10)$$

In this case γ is the H_∞-norm of the closed loop transfer matrix $M_k(G,K_\infty)$. The optimal solution is defined as $\alpha=\min(\gamma)$.

5: Designing the augmented plant of the platform.

5.1: introduction.

With the theory mentioned in chapter 4, a controller for the platform can be designed. For the platform, two signals have to be controlled. The variations in the distance H_i (see figure 2.3) have to be minimized, and the input voltage V_i ($i=\{1,2,3\}$) of the servos is constrained. For low frequencies, the performance has to be as good as possible. For the higher frequencies, the servo voltage has to be low in order to avoid actuator saturation. These requirements will be transformed to requirements on the three identified subprocesses (average height, rotation around the negative y-axis and rotation around the positive x-axis). The required performance is modelled by using weighting filters on the input voltage V and the output y of the three subprocesses.
The variations in H_i (see figure 2.3) are caused by three kind of disturbances. Crane disturbances , wave disturbances, and model errors. For all of these disturbances, shaping filters have to be designed. First a diagram of the control strategy has to be derived.

5.2: Designing a control diagram.

In chapter two, the disturbances of the waves have been modelled. In this chapter it was seen that the waves can be regarded as disturbances on the distance X_i (see figure 2.3, equation 2.18, and 2.19). In chapter 3, it was seen that the waves can be measured quite well. Therefore a good approximation of the disturbances is available. Just like the crane disturbances, good results are expected by using a feed forward controller. The influence of the disturbances can be ruled out by measuring the height of the wave (the disturbance on the distance X_i) and adding the height with a negative sign to the distance X_i. As a result, the variations of H_i (see figure 2.3) will be very small. The remaining variations are caused by measurement errors only.
However, there is one problem. The distance X_i can be varied only by using the servo system. Therefore the measured wave height has to be differentiated before to remove the influence of the servo's integration. At this moment, two different control strategies can be derived.

1) The waves are seen as independent disturbances. The existing connection between the moving of the float and the wave height is not modelled.
2) There is a feedback (H_w) between the moving of a float and the waves arising in the modelling of the complete system.

The block schemes of both models are given in figure 5.1 and 5.2.

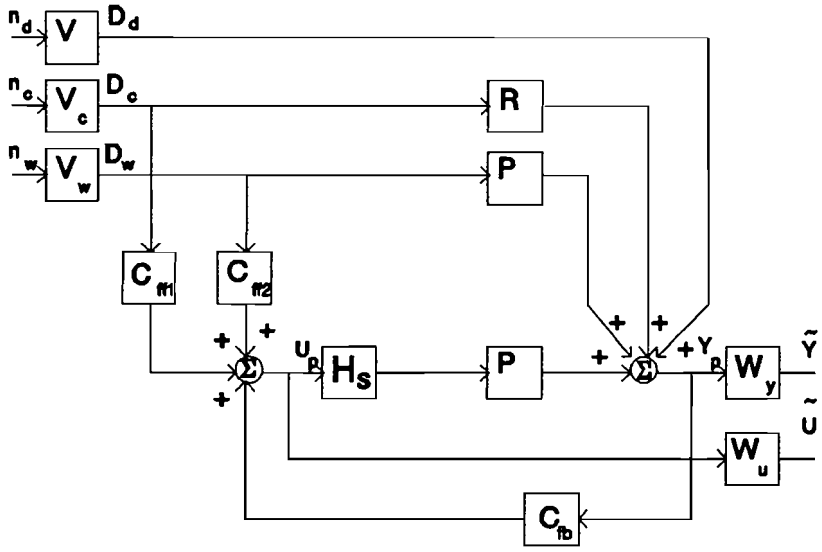

figure 5.1: Model without feed back

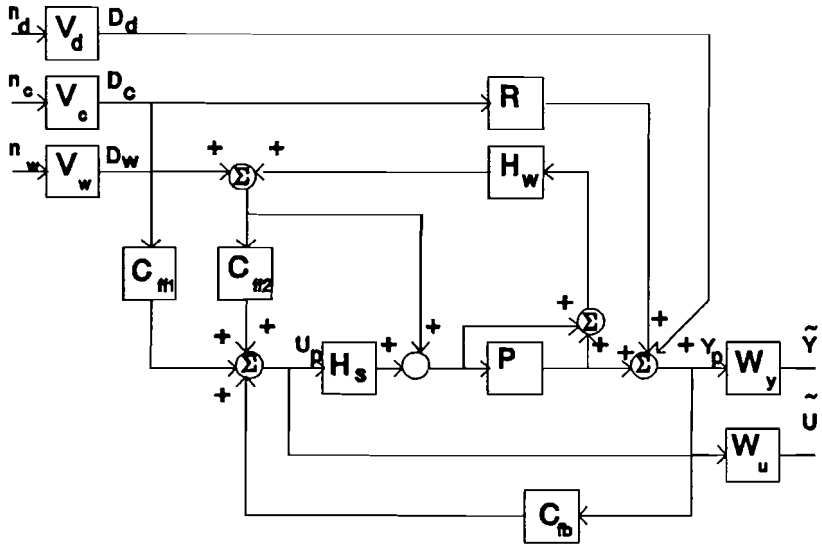

figure 5.2: Model with a feedback

The transfer functions seen in figure 5.1 and 5.2 are explained in table 5.1 on the next page. In figure 5.1, the shaping filter V_w is used to model the spectrum of the wave disturbances. In figure 5.2 this filter is used to account for the modeling errors in the wave transfer function H_w. There is a possibility that the model of figure 5.1 leads to an unstable controller. In this model, the waves are seen as independent disturbances. However, there is a feedback between the movements of the floats and the height of the wave disturbance. In the model of figure 5.1, these disturbances can't be controlled directly. In other words, there is a possibility the height of the waves increases to a unacceptable level.

On the other side, the second option (figure 5.2) results in a very complicated model. For this reason the first controller designs will be done by making use of figure 5.1. If the result is not satisfying, the second model, figure 5.2, will be investigated.

table 5.1: explanations abbreviations of figure 5.1 and 5.2

P=P(z)	Platform dynamics
R=R(z)	Crane disturbance dynamics
$V_w=V_w(z)2$	Shaping filter wave disturbances
$V_c=V_c(z)$	Shaping filter crane disturbances
$V_d=V_d(z)$	Shaping filter other disturbances
$H_s=H_s(z)$	Servo dynamics
$C_{ff1}=C_{ff1}(z)$	Feed forward controller crane
$C_{ff2}=C_{ff2}(z)$	Feed forward controller waves
$C_{fb}=C_{fb}(z)$	Feed back controller
$W_y=W_y(z)$	Weighting filter output y
$W_u=W_u(z)$	Weighting filter servo input u
$H_w=H_w(z)$	Transfer function of waves to the float

5.3: Deriving the G matrix of the augmented plant.

In chapter 4 the augmented plant was represented by a matrix G with input signals w and u, and output signals z and y. For the configuration of figure 5.1 this matrix can be derived also.

For the D_d, D_c and D_w of figure 5.1, the next statements are in force.

$$\begin{aligned} D_d &= V_d n_d \quad n_d \in L_2 \ \|n_d\|_2 \le 1 \\ D_c &= V_c n_c \quad n_c \in L_2 \ \|n_c\|_2 \le 1 \\ D_w &= V_w n_w \quad n_w \in L_2 \ \|n_w\|_2 \le 1 \end{aligned} \qquad (5.1)$$

For z, y, w and u the following matrices can be derived:

$$z=\begin{bmatrix}\tilde{Y}\\ \tilde{U}\end{bmatrix} \qquad y=\begin{bmatrix}Y_p\\ D_c\\ D_w\end{bmatrix} \qquad w=\begin{bmatrix}n_d\\ n_c\\ n_w\end{bmatrix} \qquad u=U_p \tag{5.2}$$

It follows that: $p_1=1$ $p_2=3$ $m_1=3$ $m_2=1$ (see also table 4.1).
With the aid of figure 5.1, equation 5.2 can be worked out.

$$y=\begin{bmatrix}Y_p\\ D_c\\ D_w\end{bmatrix}=\begin{bmatrix}H_s P U_p + P V_w n_w + R V_c n_c + V_d n_d\\ V_c n_c\\ V_w n_w\end{bmatrix} \tag{5.3}$$

$$z=\begin{bmatrix}\tilde{Y}\\ \tilde{U}\end{bmatrix}=\begin{bmatrix}W_y Y_p\\ W_u U_p\end{bmatrix}=\begin{bmatrix}W_y H_s P U_p + W_y P V_w n_w + W_y R V_c n_c + W_y V_d n_d\\ W_u P_u\end{bmatrix} \tag{5.4}$$

Rewriting the matrices in a form as mentioned in chapter 4:

$$\begin{bmatrix}z\\ y\end{bmatrix}=\left[\begin{array}{c}\tilde{Y}\\ \tilde{U}\\ \hline Y_p\\ D_c\\ D_w\end{array}\right]=\left[\begin{array}{ccc|c} W_y V_d & W_y R V_c & W_y P V_w & W_y P H_s\\ 0 & 0 & 0 & W_u\\ \hline V_d & R V_c & P V_w & P H_s\\ 0 & V_c & 0 & 0\\ 0 & 0 & V_w & 0\end{array}\right]=\left[\begin{array}{c}n_d\\ n_c\\ n_w\\ \hline U_p\end{array}\right] \tag{5.5}$$

$$=\left[\begin{array}{c|c}G_{11} & G_{12}\\ \hline G_{21} & G_{22}\end{array}\right]\begin{bmatrix}W\\ U\end{bmatrix}=G\begin{bmatrix}W\\ u\end{bmatrix}$$

For the controller the next equation can be derived.

$$U=U_p=\begin{bmatrix}C_{fb} & C_{ff1} & C_{ff2}\end{bmatrix}\begin{bmatrix}Y_p\\ D_c\\ D_w\end{bmatrix}=K_m Y \tag{5.6}$$

The closed-loop transfer function of w to z can be described as follows (see chapter 4 and appendix 6).

$$
\begin{aligned}
\|M_k\|_\infty &= \|G_{11} + G_{12}K_\infty (I - G_{22}K_\infty)^{-1} G_{21}\|_\infty \\
&= \frac{1}{I - PHC_{fb}} \left\| \begin{matrix} W_y V_d & W_y (PH_s C_{ff1} + R)\, V_c & W_y (PH_s C_{ff2} + P)\, V_w \\ W_u C_{fb} V_d & W_u (C_{fb} R + C_{ff1})\, V_c & W_u (C_{fb} P + C_{ff2})\, V_w \end{matrix} \right\|_\infty \qquad (5.7) \\
&= \left\| \begin{matrix} M_{11} & M_{12} & M_{13} \\ M_{21} & M_{22} & M_{23} \end{matrix} \right\|_\infty
\end{aligned}
$$

As can be seen in equation 5.7, there are six criterions the H_∞ controller has to minimize. The meaning of these criteria are mentioned in table 5.2

table 5.2: criterions H_∞ controller

Criterion	description	weighting filter	transfer function
$M_{11}=Y_p/n_d$	sensitivity	$W_y V_m / \gamma$	$(1-PHC_{fb})^{-1}$
$M_{12}=Y_p/n_c$	crane disturbance reduction	$W_y V_c / \gamma$	$(1-PHC_{fb})^{-1}(R+PC_{ff1})$
$M_{13}=Y_p/n_w$	wave disturbance reduction	$W_y V_w / \gamma$	$(1-PHC_{fb})^{-1}(P+PC_{ff2})$
$M_{21}=U_p/n_d$	control sensitivity	$W_u V_m / \gamma$	$C_{fb}(1-PHC_{fb})^{-1}$
$M_{22}=U_p/n_c$	actuator saturation caused by crane	$W_u V_c / \gamma$	$(1-PHC_{fb})^{-1}(C_{fb}R+C_{ff1})$
$M_{23}=U_p/n_w$	actuator saturation caused by waves	$W_u V_w / \gamma$	$(1-PHC_{fb})^{-1}(C_{fb}P+C_{ff2})$

The γ is defined as the upper bound of the H_∞ norm. If the H_∞ norm is scaled to 1, γ becomes a scale factor in the weighting functions (see table 5.1). The transfer function of a criterion will be smaller than $\gamma / V_i W_j$ ($i=\{d,c,w\}$ and $j=\{u,y\}$). The designing of the shaping and weighting filters are based on $\gamma < 1$. The designed controller K_∞ in figure 4.1 has to fulfil this requirement.

5.4: State-space description augmented plant.

For the solution of the H_∞ problem described in [6], the augmented plant of figure 5.1 has to be described in a state-space form. A solution can be found when the four requirements mentioned in chapter four, are fulfilled.

For the state-space descriptions of the augmented plant of figure 5.1, the transfer of HP is indicated by P_1. The transfer of P is indicated by P_2. The state-space equations are given in equation 5.8.

$$
\begin{aligned}
P_1(k) \quad & X_{p1}(K+1) = A_{p1}X_{p1}(k) + B_{p1}U_p(k) \\
P_2(k) \quad & X_{p2}(k+1) = A_{p2}X_{p2}(k) + B_{p2}D_w(k) \\
& \quad = A_{p2}X_{p2}(k) + B_{p2}(C_wX_w(k) + D_wn_w(k)) \\
R(k) \quad & X_R(k+1) = A_RX_R(k) + B_RD_c(k) \\
V_m(k) \quad & X_m(k+1) = A_dX_d(k) + B_dn_d(k) \\
V_c(k) \quad & X_c(k+1) = A_cX_c(k) + B_cn_c(k) \\
V_w(k) \quad & X_w(k+1) = A_wX_w(k) + B_wn_w(k) \\
& Y_p(k) = C_{p1}X_{p1}(k) + C_{p2}X_{p2}(k) + C_dX_d(k) + C_RX_R(k) + \\
& \quad D_{p1}U(k) + D_{p2}W(K) + D_RC(k) + D_dn_d(k) \\
& D_w(k) = C_wX_w(k) + D_wn_w(k) \\
& D_c(k) = C_cX_c(k) + D_cn_c(k) \\
W_y(k) \quad & X_y(k+1) = A_yX_y(k) + B_yY_p(k) \\
W_u(k) \quad & X_u(k+1) = A_uX_u(k) + B_uU_p(k) \\
& \tilde{Y}(k) = C_yX_y(k) + D_yY_p(k) \\
& \tilde{U}(k) = C_uX_u(k) + D_uU_p(k)
\end{aligned}
\qquad (5.8)
$$

With the set equations of 5.8, and the input, output and state vectors, the next matrices can be derived.

$$
input: \begin{bmatrix} w \\ u \end{bmatrix} = \begin{bmatrix} n_d \\ n_c \\ n_w \\ \\ U_p \end{bmatrix} \quad output: \begin{bmatrix} z \\ y \end{bmatrix} = \begin{bmatrix} \tilde{y} \\ \tilde{u} \\ \\ y_p \\ D_c \\ D_w \end{bmatrix} \quad states: x = \begin{bmatrix} \underline{x}_{p1} \\ \underline{x}_{p2} \\ \underline{x}_r \\ \underline{x}_d \\ \underline{x}_c \\ \underline{x}_w \\ \underline{x}_y \\ \underline{x}_u \end{bmatrix} \qquad (5.9)
$$

The state space matrix of the platform can be derived in a form as described in chapter 4. The complete matrix is derived in appendix 7. With the reductions mentioned in appendix 7, the state-space matrix of 5.11 can be derived.

$$\left[\begin{array}{c|cc} A & B_1 & B_2 \\ \hline C_1 & D_{11} & D_{12} \\ C_2 & D_{21} & D_{22} \end{array}\right] = \tag{5.10}$$

$$\left[\begin{array}{ccccc|ccc|c} A_{p1} & B_r C_c & B_{p2} C_w & 0 & 0 & B_d & B_r D_c & B_{p2} D_w & B_{p1} \\ 0 & A_c & 0 & 0 & 0 & 0 & B_c & 0 & 0 \\ 0 & 0 & A_w & 0 & 0 & 0 & 0 & B_w & 0 \\ B_y C_{p1} & 0 & B_y D_{p2} C_w & A_y & 0 & D_y D_D & 0 & B_y D_{p2} D_w & 0 \\ 0 & 0 & 0 & 0 & A_u & 0 & 0 & 0 & B_u \\ \hline D_y C_{p1} & 0 & D_y D_{p2} C_w & C_y & 0 & D_y D_m & 0 & D_y D_{p2} D_w & 0 \\ 0 & 0 & 0 & 0 & C_u & 0 & 0 & 0 & D_u \\ \hline C_{p1} & 0 & D_{p2} C_w & 0 & 0 & D_D & 0 & D_{p2} D_w & 0 \\ 0 & C_c & 0 & 0 & 0 & 0 & D_c & 0 & 0 \\ 0 & 0 & C_w & 0 & 0 & 0 & 0 & D_w & 0 \end{array}\right] \tag{5.11}$$

To arrive at a solution of the H_∞ problem, this state-space matrix of the platform has to fulfil the four requirements mentioned in chapter 4. For the state-space matrix of the augmented these requirements are checked one by one.

1) (A,B_2) has to be stabilizable and (A,C_2) has to be detectable. This can not be seen easily, but it will be checked by MHC.
2) For proper controllers, the matrices D_{12} and D_{21} have to fulfil two criterions:
   1) The rank of matrix D_{12} has to be equal to m2.
   2) The rank of matrix D_{21} has to be equal to q2.

   For the state-space matrix 5.11 it is easily seen that $m_1=3$, $m_2=1$, $q_1=2$, and $q_2=3$. To fulfil the criterions mentioned above, the matrices D_u, D_m, D_c, and D_w may not equal to zero. This means that the weighting- and shaping filters V_m, V_c, V_w and W_u have to be bi-proper.
3) To prevent that the augmented plant has zeros on the unity circle, the shaping and weighting filters may have no zeros on unity circle.
4) $p_1=3$, $p_2=1$, $q_1=2$, $q_2=3$. therefore $q_1 \geq p_2$ and $p_1 \geq q_2$.

Under the restrictions mentioned above, the augmented plant fulfils the requirements mentioned in chapter 4. An H_∞ controller can be designed now.

5.5: Designing the shaping and weighting filters.

In the previous section, it has been derived that the shaping filters have to fulfil three requirements.

1) The filters have to be stable
2) The filters may have no zeros on the unit circle.
3) The filters have to be bi-proper.

The disturbances of the augmented plant (w, see figure 4.1) are represented by n_d, n_c , and n_w. For these n_i ($i=\{d,c,w\}$), the next equation is in force.

$$||n_i||_2 \leq 1 \quad with \quad i=\{d,c,w\} \tag{5.12}$$

If a solution with $\gamma \leq 1$ for the H_∞ problem can be derived, the statement for z (see table 4.1) in figure 5.3 is in force.

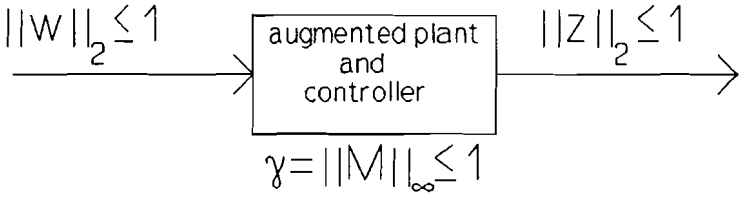

figure 5.3: magnitude of z for an solution with $\gamma=1$

Because of the fact that the disturbances on the platform don't have the same magnitude, the disturbances n_i ($i=\{d,c,w\}$) have to be scaled by shaping filters. However, there is one problem. The magnitude of the disturbances, and the required output accuracy (necessary for the designing of the weighting filters) have not been derived yet. Therefore only the shape of the shaping and weighting filters will be discussed in this section. The magnitude will be represented by δ_i ($i=\{d,c,w\}$) The δ_i will be derived in chapter 7.

5.5.1 Designing an disturbance shaping filter V_d.

Besides the disturbances caused by the waves and the crane, there are more disturbances which seize on the platform. For example the drift of the servos, offset and disturbances due to a limitted model set. These disturbances will be represented by the disturbance shaping filter V_d. A good shape of this filter can be found by the Kalman gain K_g which is used in the state-space observer. The optimal Kalman gain K_g turns the innovation ϵ to be a white noise sequence. The state-space observer is shown in figure 5.4.

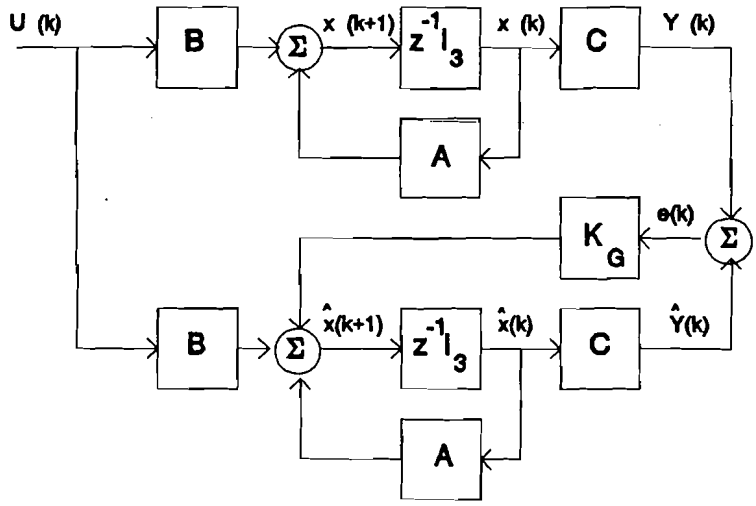

figure 5.4: state-space observer

For the output Y the transfer function 5.13 can be derived.

$$\begin{aligned} \epsilon(k) &= Y(k) - \hat{Y}(k) \\ Y(k) &= \hat{Y}(k) + \epsilon(k) \\ Y(k) &= C(zI-A)^{-1}B.U(k) + \epsilon(k) + C(zI-A)^{-1}K_g\epsilon(k) \\ Y(k) &= \frac{|zI-A-K_gC|}{|zI-A|}\epsilon(k) + C(zI-A)^{-1}Bu(k) \end{aligned} \qquad (5.13)$$

The disturbances are given by the first term of equation 5.13.
Therefore the filter V_d can be chosen as:

$$V_d = \delta_d \frac{|zI-A+K_gC|}{|zI-A|} \qquad (5.14)$$

As can be seen in equatiob 3.14, V_d contains a pole in $z=1$ so that the filtered disturbance represents the drift in the servo in a natural way so that n_d takes the form of the innovations ϵ. Equation 5.13 can then be illustrated as shown in figure 5.5. P_1 is the transfer function of the platform including the servo.

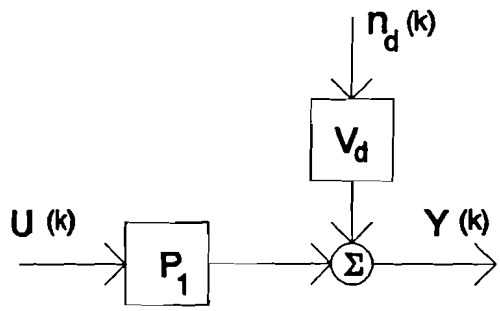

figure 5.5: shaping filter disturbances

The Kalman gains K_g have already been derived in [1], they are given in table 5.3

table 5.3: Kalman gains

$K_{g,a}$	$K_{g,y}$	$K_{g,x}$
1.090	1.002	1.349
2.600	3.200	3.272
2.617	1.526	1.661

The disturbance filter V_d can be used to represent the model errors as well. The robustness for modelling errors can be interpreted as follows. Since the servo's pole $z=1$ is part of the platform's transfer function, modelling errors can be best accounted for by using stable factor perturbation. In this case the nominal process P is divided in a stable part P_{stable} , and an unstable part $P_{unstable}$ by a left coprime factorization [5].

$$P = P_{unstable} P_{stable} = M^{-1} N \tag{5.15}$$

The modelling errors are represented by Δ_M and Δ_N. These Δ_M and Δ_N are the stable modelling errors of $(M^{-1})^{-1}$ (which is stable) and N.

$$\begin{aligned} (\tilde{P}_{unstable})^{-1} &= M + \Delta_M \\ \tilde{P}_{stable} &= N + \Delta_N \end{aligned} \tag{5.16}$$

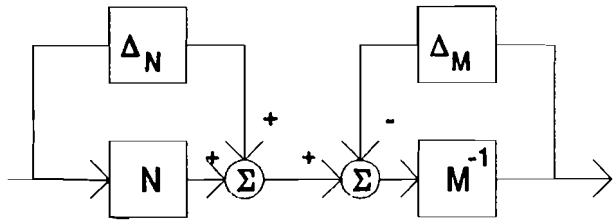

figure 5.6: Factor Perturbation.

The transfer of the process with modelling errors becomes:

$$\tilde{P} = \tilde{P}_{unstable} \cdot \tilde{P}_{stable} = (M + \Delta_M)^{-1} (N + \Delta_N) \tag{5.17}$$

According to MacFarlane [7], stability is guaranteed if C_{fb} stabilizes the nominal plant and:

$$\left\| \begin{matrix} W_m (I - P_1 C_{fb})^{-1} M^{-1} \\ W_n C_{fb} (I - P_1 C_{fb})^{-1} M^{-1} \end{matrix} \right\|_\infty \leq \epsilon \quad while \; \| \Delta_M \, W_M^{-1} \quad \Delta_N \, W_N^{-1} \|_\infty < \epsilon^{-1} \tag{5.18}$$

Since V_v contains the poles of the transfer P_1 including the servo's pole $z=1$, V_m can be used for M^{-1} (see also [6]). In this case, $N=V_m^{-1} P_1$ is defined implicitly. The condition given in equation 5.17 is then incorporated in G_{11} and G_{21} for $W_m=W_y$ and $W_N=W_u$ and ϵ bounded by γ.

The poles and zeros of the disturbance shaping filters are given in table 5.4.

table 5.4: poles and zeros model error transfer function

	poles	zeros
average height	0.6036+0.6960*i 0.6036-0.6960*i 1	0.4762+0.7591*i 0.4762-0.7591*i -0.0951
rotation around the y-axis	0.6624+0.5654*i 0.6624-0.5654*i 1	0.5025+0.6456*i 0.5024-0.6456*i -0.0023
rotation around the x-axis	0.7022+0.5392*i 0.7022-0.5392*i 1	0.5727+0.5725*i 0.5727-0.5725*i -0.4172

The transfer functions of the filters are given in equation 5.19. $V_{d,a}$,$V_{d,y}$ and $V_{v,x}$ are the filters for the average height, the rotation around the negative y-axis and the rotation around the positive x-axis respectively.

$$V_{d,a}=\delta_{d,a}\frac{(z+0.0951)(z-0.4762-0.7591.i)(z-0.4762+0.7591.i)}{(z-1)(z-0.6036-0.6960.i)(z-0.6036+0.6960.i)}$$
$$V_{d,y}=\delta_{d,y}\frac{(z+0.0023)(z-0.5025-0.6456.i)(z-0.5025+0.6456.i)}{(z-1)(z-0.6624-0.5654.i)(z-0.6624+0.5654.i)} \quad (5.19)$$
$$V_{d,x}=\delta_{d,x}\frac{(z+0.4172)(z-0.5727-0.5725.i)(z-0.5727+0.5725.i)}{(z-1)(z-0.7022-0.5392.i)(z-0.7022+0.5392.i)}$$

Equation 5.19 shows that the filters are bi-proper. So, they are fulfilling requirement 3 of section 5.5. The shapes of the modelling error filters are determined by equation 5.19. The magnitude depends on $\delta_{d,i}$ $\{i=\{a,y,x\}\}$. This $\delta_{d,i}$ will be derived later.

5.5.2: Designing the crane disturbance shaping filter V_c

The crane disturbance filters has to fulfil the three requirements mentioned in 5.5 also. The disturbances caused by the rotation of the crane are predefined. The crane rotates with a constant frequency, and the load is 1 kg. The effects of the crane disturbances on the three subprocesses are derived in chapter 1.

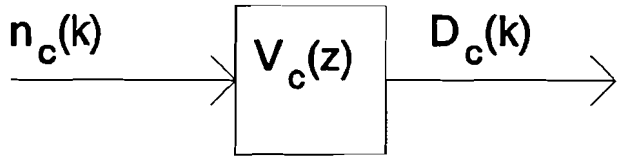

figure 5.7: shaping filter crane disturbance

The ideal shaping filters will be the Z-transformed of these disturbances. They are mentioned in equation 5.20.

$$\begin{aligned} c_g(k) &= -mg\epsilon(k) && \rightarrow C_g(z) = -mg\frac{z}{z-1} \\ c_Y(k) &= -mg\cos(\omega_o kT_s) && \rightarrow C_y(z) = -mg\frac{z(z-\cos(\omega_o T_s))}{z^2-2z\cos(\omega_o T_s)+1} \\ c_x(k) &= -mg\sin(\omega_o kT_s) && \rightarrow C_x(z) = -mg\frac{z\sin(\omega_o T_s)}{z^2-2z\cos(\omega_o T_s)+1} \end{aligned} \qquad (5.20)$$

The ω is the angular frequency of the rotating crane.

The filters $V_{c,a}$ $V_{c,y}$ and $V_{c,x}$ don't fulfil the two requirements mentioned above. All the shaping filters are unstable and the filter $V_{c,x}$ is not bi-proper. For this reason, the filters have to be modified.
The filter $V_{c,g}$ can be stabilized by shifting the pole into the unity circle. As a consequence the shape of the filter will change. For low frequencies the bode diagram will be horizontal instead of a slope of -20 dB/dec. The pole of the filter $V_{c,a}$ is shifted to 0.99.
Besides instability, the ideal filters $V_{c,y}$ and $V_{c,x}$ have a disadvantage. These filters are suitable for only a specific crane frequency and load. The controllers designed with filters which have this kind of shape, will show less reduction for crane frequencies which are a little different. Therefore a modified shape of these filters is desired.
Stability is reached by damping of the poles of $V_{c,y}$ and $V_{c,x}$. The poles are damped by a factor $e^{-\xi Ts}$. Because of this damping factor, the peaks in the bode plot become finite and occupy a larger frequency area. A damping factor of $\xi=0.0025$ is enough for a toleration of about 10% on the frequency the crane is rotating with.
The filter $V_{c,x}$ can be made bi-proper by placing an additional zero. Of course this zero may not change the shape of the filter essentially. By simulations, it is found that a zero $z=0.2$ fulfils this requirement.

With the damping factor, and the necessary changes in the filters $V_{c,a}$ and $V_{c,x}$ mentioned before, the shaping filters V_c become:

$$V_{c,a} = -mg\,\delta_{c,a}\frac{z}{z-p} = -9.81\,\delta_{c,a}\,\frac{z}{z-0.99}$$

$$V_{c,y} = -mg\,\delta_{c,y}\,\frac{z(z-0.9997)}{z^2 - 2ze^{-\xi T_s}\cos(\omega_o T_s) + e^{-2\xi T_s}}$$

$$= -9.81\,\delta_{c,y}\,\frac{z(z-0.9997)}{(z-0.9972-0.0251.i)(z-0.9972+0.0251i)} \qquad (5.21)$$

$$V_{c,x} = -mgk\delta_{c,x}\frac{z\sin(\omega_o T_s)(z-0.2)}{z^2 - 2ze^{-\xi T_s}\cos(\omega_o T_s) + e^{-2\xi T_s}}$$

$$= -0.3104\,\delta_{c,x}\,\frac{z(z-0.2)}{(z-0.9972-0.0251*i)(z-0.9972+0.0251i)}$$

The k in the shaping filter $V_{c,x}$ is used to make the magnitude of $V_{c,x}(z)$ equal to the magnitude of $C_x(z)$ mentioned in equation 5.20.
The filters of equation 5.21 are shown in figure 5.8

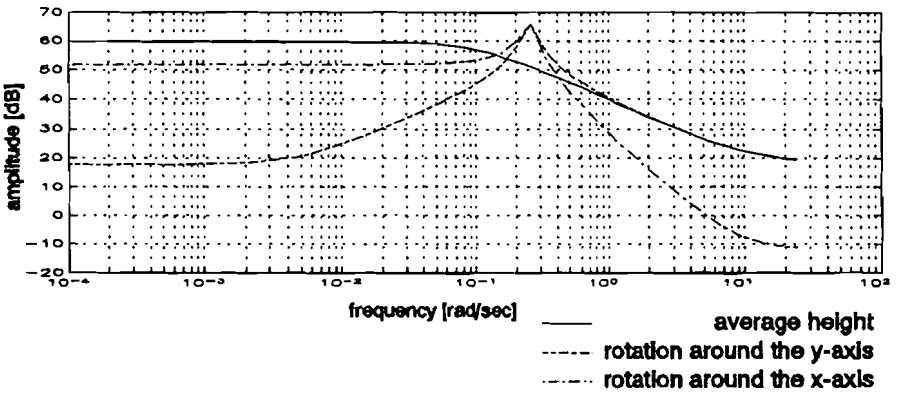

figure 5.8: crane disturbance shaping filters.

5.5.3: Designing the wave disturbance shaping filter V_w.

The wave disturbance shaping filter has to fulfil the 2 requirements mentioned in 5.4.2 also.
By using Fast Fourier Transformation on the measured step responses, it is possible to determine the dominant frequencies of the waves. The spectrum of the waves is given in figure 5.9.

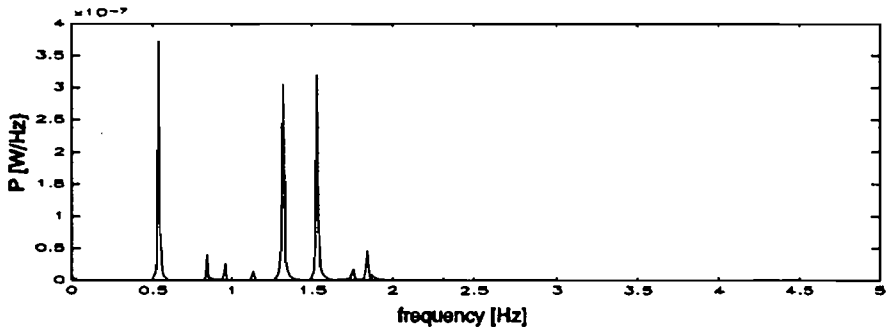

figure 5.9: Spectrum of the wave disturbances.

It can be seen that the frequencies of the waves are between the 0.5 and 2 Hz. Therefore the magnitude of the shaping filter has to have its maximum for these frequencies.
A useful shaping filter is given in equation 5.22

$$V_w = \delta_w \frac{(z+28.95)(z-0.9876)}{(z-0.3679)(z-0.3679)} \qquad (5.22)$$

The plot of the transfer function V_w is given in figure 5.10

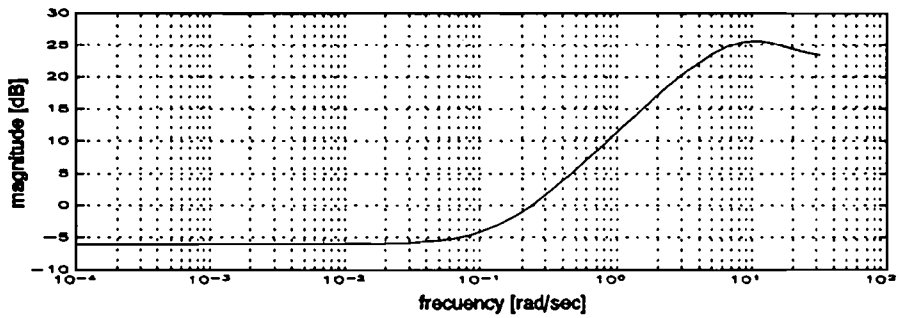

figure 5.10: Wave disturbance shaping filter

With the exception of the gains, all the shaping filters are designed now. Besides the shaping filters there are two weighting filters which have to be designed also.

5.5.4: Designing the weighting filters.

Both the weighting filters have to be stable. Only the weighting filter W_u has to be bi-proper.
The weighting filter W_u is used to avoid saturation of the servo amplifier. Because this saturation is mainly caused by high frequent peaks in the control signal, W_u has to be a high-pass filter.

The weighting filter W_y is used to emphasize a desired performance of the augmented plant including the controller. The performance has to be good for low frequencies. Therefore, the weighting filter W_y has to be a low-pass filter.
Initially, the order of these filters is chosen as low as possible. Only if the results are not satisfying, the order can be increased. Transfer functions of the weighting filter are given in equation 5.23.

$$W_y = \delta_y \frac{1}{z-0.6} \qquad W_u = \delta_u \frac{z-1}{z-0.2} \tag{5.23}$$

The shape of the transfer functions is plotted in figure 5.11.

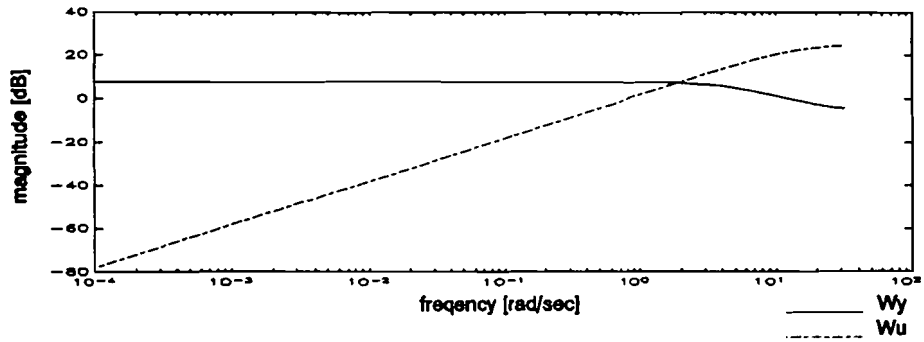

figure 5.11: weighting filter W_u and W_y

With the exception of the gains, all the shaping and weighting filters are designed now. With this augmented plant a H_∞ controller will be designed. Of course, the magnitude of the filters have to change to come to a acceptable result. The designing of the controller is described in chapter 6.

6.1: Introduction.

In chapter 5, a complete augmented plant for the platform has been derived. The augmented plant can be imported in MATLAB easily by using the toolbox MHC written by H.M. Falkus. With this toolbox a controller is calculated by using the state space solution given by Glover and Doyle [5].
By changing the magnitude of the weighting and shaping filters described in 5, the solution with $\gamma=1$ can be found. For all of the three subprocesses (average height, rotation around the negative y-axis and rotation around the positive x-axis), a set of controllers (two feedforward and one feedback) has to be designed. The controllers for the average height will be designed first.

6.2: Calculating a controller.

The augmented plant described in the previous chapter, is imported in the Matlab toolbox MHC. Unfortunately a satisfying controller couldn't be designed. In spite of changing the magnitudes of the shaping and weighting filters, there was hardly any suppression of the disturbances caused by the waves.
To investigate the reason of this disappointing result, the model is simplified. The new augmented plant only contains the feedforward controller used to reduce disturbances caused by the waves. A diagram is shown in figure 6.1.

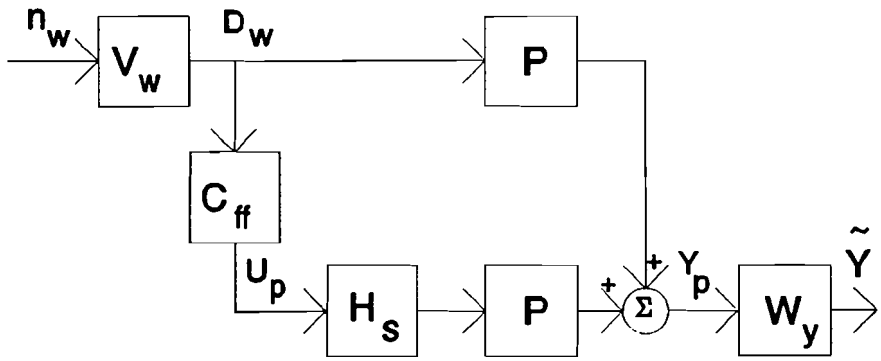

figure 6.1: Simplified model controller design

The augmented plant of figure 6.1 is not stable because of the servo system's pole in H_s. Designing a controller for this model is done by moving the unstable pole into the unit disc. The transfer of this servo system is given in equation 6.1:

$$H_s = 55.69\times10^{-3}\frac{1}{z-0.999} \qquad (6.1)$$

The ideal controller for this model is clear. The controller has to be the negative inverse of the servo transfer function. In this case the disturbances will be ruled out completely. Therefore, with the exception of the low frequencies (because of the shifted pole), the feedforward controller has to have the shape of a differentiator.

With the Matlab Toolbox MHC a controller for the augmented plant shown in figure 6.1 can be calculated. The first controller designs are done with the filters $V_w=W_y=1$, and a sampling frequency of 10 Hz.

With the calculated controller, a the transfer of D_w to Y_p can be derived. The transfer is given in figure 6.2.

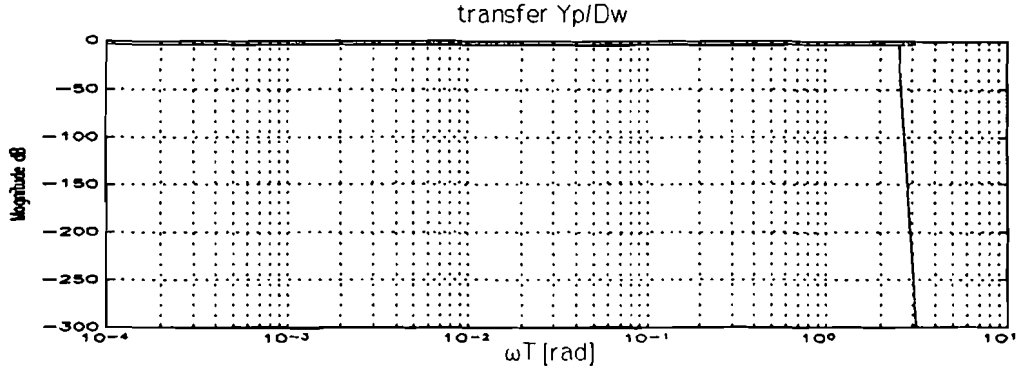

figure 6.2: Closed loop transfer.

In figure 6.2, both the transfer functions Y_p/D_w and the inverse weighting filter γ/V_wW_y are plotted. Since the augmented plant of figure 6.1 is a SISO (single input single output) process, these transfer functions will be equal. As a consequence, the dashed plotted transfer of γ/V_wW_y can't be seen.

For this augmented plant the calculated γ becomes:$\gamma=0.7$. This means that the suppression of the wave disturbances is equal to $V_wW_y/0.7\approx 1.5$. A bode-plot of the designed controller is given in figure 6.3.

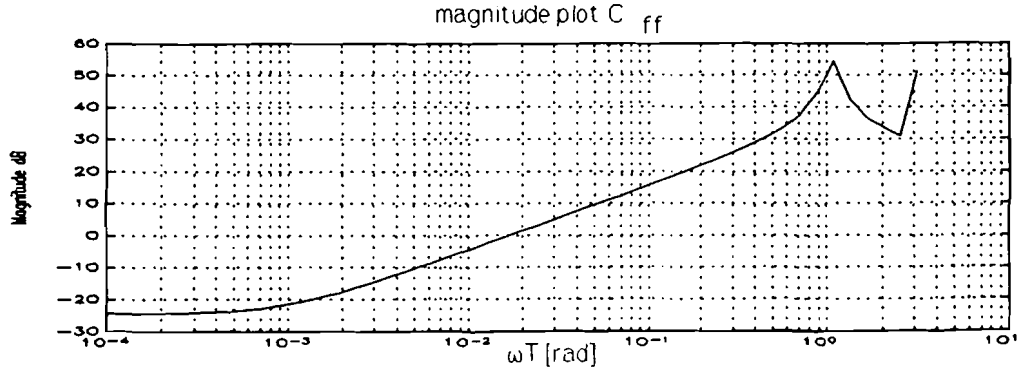

figure 6.3: Designed controller

The bode-plot of the ideal controller has to show a straight line with a slope of 20 dB/decade. With exception of the bend caused by the shifted pole of the servo, for low frequencies the designed controller agrees with a straight line. However, for high frequencies the bode-plot of the controller shows some strange oscillations. Unfortunately, the waves have a frequency of about 1 Hz ($\omega T=0.62$).
As can be seen in figure 6.3, the controller doesn't show the ideal straight line here, and therefore, it can not be expected that the performance will be good for this frequency.

The performance of the controller has to be much better for frequencies of about 1 Hz. Therefore the next step to be taken is clear. The shaping filter has to emphasize this frequencies much more. The shaping and weighting filters are replaced by the filters of figure 5.9 and 5.10 (since the U_p is not weighted, only W_y is used). The shaping filter V_w emphasizes the frequencies of about 1 Hz. The low-pass filter W_y had to be used, otherwise a controller could not be calculated. The magnitude of these weighting filters is changed until $\gamma \approx 1$. The final filters are given in equation 6.2

$$V_w(z) = 0.5\frac{(z+28.95)(z-0.9867)}{(z-0.3679)(z-0.3976)} \qquad W_y(z) = \frac{0.1}{(z-0.5059)} \qquad (6.2)$$

A controller with this set of filters has been calculated. The closed loop transfer, derived with this controller, is given in figure 6.4.

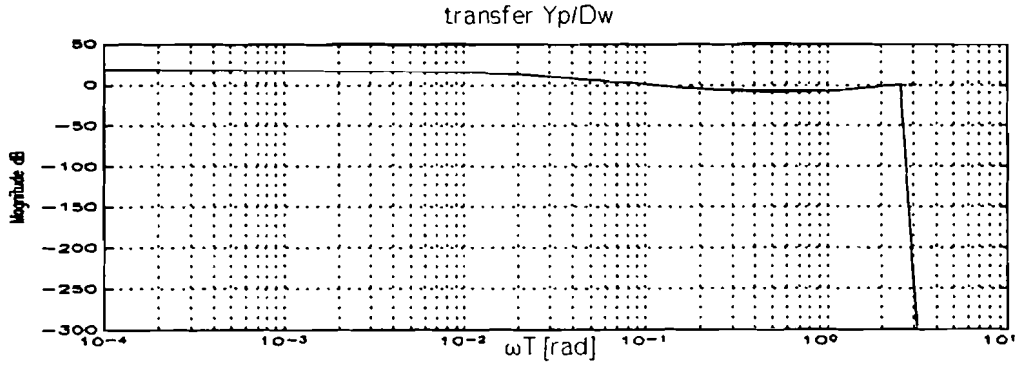

figure 6.4: bode-plot closed loop transfer with shaping filter

As can be seen in figure 6.4, the results are not much better. For frequencies of about 1 Hz, the suppression of the wave disturbances is low, and for low frequencies, the disturbances are even amplified. The bode-plot of the controller is given in figure 6.5.

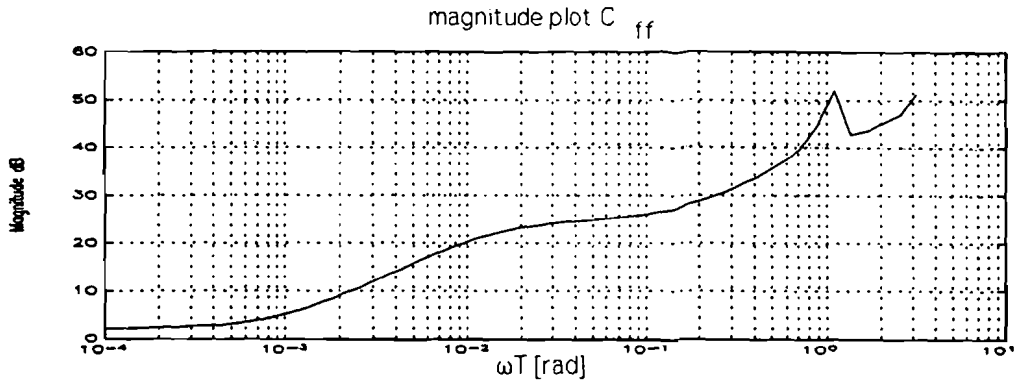

figure 6.5: Bode-plot controller designed with shaping filter.

In figure 6.5, an oscillation for high frequencies is shown again. It can be concluded that the addition of a shaping filter does not give a better result. Therefore the reason for the oscillations in the bode-plots of the controllers has been investigated.

First, the controller has been designed in the s-domain. The poles, zeros and constants of the platform in the s-domain, mentioned in [1], are given in appendix 8. The design is started with $V_w=W_y=1$. After the calculation of the controller, the transfer Y_p/D_w can be drived. The bode-plots of the transfer Y_p/D_w is given in figure 6.6.

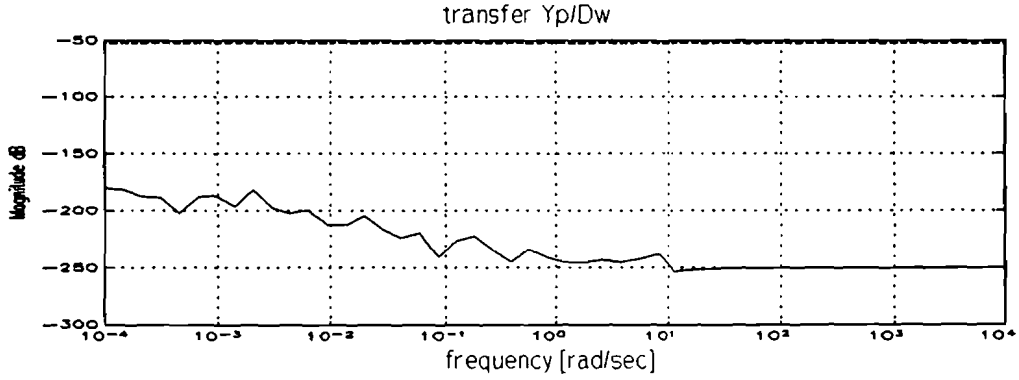

figure 6.6: closed loop transfer continuous time

For this augmented plant the calculated γ becomes very small ($\approx 10^{-3}$). This means that the disturbance reduction will be at least a factor 1000 for every frequency. As can be seen in figure 6.6, the transfer function Y_p/D_w (continuous line) and the transfer of the inverse weighting filter γ/V_wW_y (dashed line) don't coincide. This is probably caused by the fact that the γ becomes very small and numeric errors occur.

The magnitude plot of the calculated controller is given in figure 6.7.

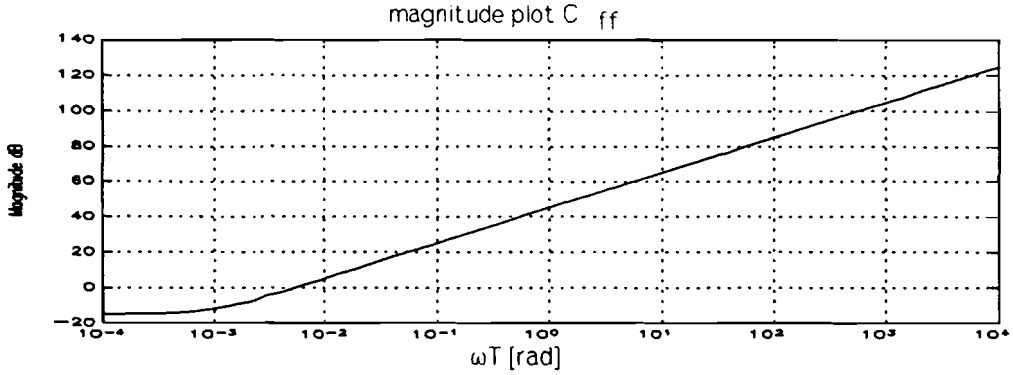

figure 6.7: bode plot controller continues time

With the exception of the bend caused by the shifted pole, the bode-plot of the calculated controller given in figure 6.7 shows the desired straight line.
It can be concluded that the oscillations in the bode-plots of figure 6.3 and 6.5 are caused by the fact that the controller has been calculated in the z-domain.
The result is clear, but what is the origin of the problem?

6.3: Solution of the oscillation problem.

In first instance it was taught that the problems were caused by the fact that the order of the designed controller has to be equal to the order of the augmented plant (see chapter 4). This means that, in the case $V_w=W_y=1$, the designed controller is of third order. The controller we are looking for, the ideal differentiator, is of first order. This means that there are two poles left. It was taught that the influence of these poles would be the origin of the bad performance of the controller

However, the bad performance of the controller was caused by some other problems.
If V_w and W_y are both equal to 1, the weighting on every frequency is the same. Therefore, it is expected that the two remaining poles (see the beginning of section 6.3) will be placed in the origin of the unit disc. In this case the influence of these poles will be equal for all frequencies. The transfer of the calculated controller of figure 6.3 is given in equation 6.3.

$$C_{ff}(z) = -10.9\frac{(z-0.999)(z+8.9497)(z-0.2812)}{(z-0.4631+0.8230i)(z-0.4631-0.8230i)(z+0.7799)} \qquad (6.3)$$

As can be seen in equation 6.3, there are no poles in the origin. This can be explained by redrawing the diagram of the augmented plant of figure 6.1.

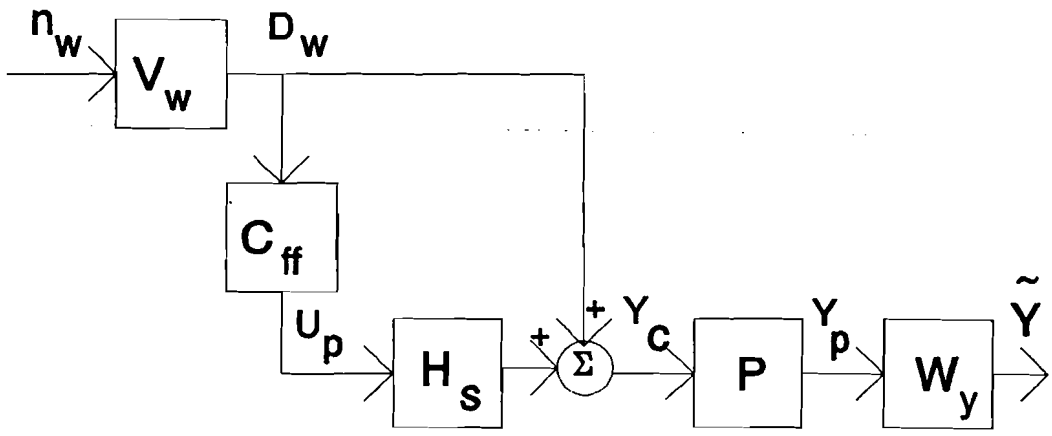

figure 6.8: second diagram of the augmented plant

In figure 6.8, it can be seen that, even when V_w and W_y are equal to 1, the output Y_c is weighed by the process P. The transfer of the process P is given in figure 6.9.

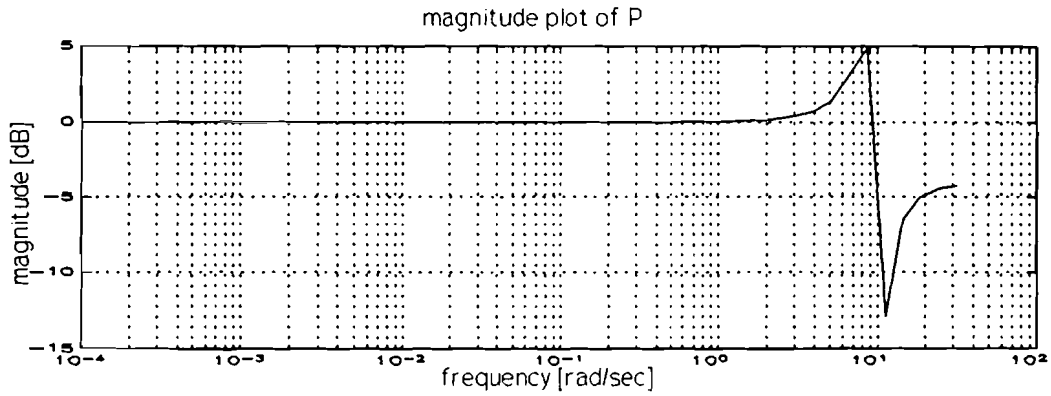

figure 6.9: bode-plot transfer function P

As can be seen in plot 6.9, the weighting of P is not equal for every frequency. Therefore the poles of the controller will be removed from the origin of the unit disc where they were expected when the weighting would be equal to 1. Plot 6.9 also explaines the oscillation seen in the bode-plot of the controller (figure 6.3). Because of the fact that the output Y_c (see figure 6.8) is weighed by the process P, the disturbance reduction has to be more for the frequencies the transfer of P shows a peak. To obtain this reduction, the calculated controller shows a peak for these frequencies also.

A explanation for the shape of the bode-plot of the controller of figure 6.3 has been found, but a solution for the fact that the disturbance reduction in the S-domain is much more than in the reduction in the z-domain is still not derived.

For this problem a explanation can be found also.
As mentioned in the beginning of section 6.3, the ideal controller has to be the negative inverse of the servo's transfer function. For both the s -and z-domain, the transfer functions of the servo systems are given in equation 6.4.

$$H_s(z) = 55.69\times10^{-3}\frac{1}{z-0.999} \qquad H_s(s) = 0.5569\times\frac{1}{s+0.001} \quad (6.4)$$

In the s-domain. the inverse transfer function can be inverted without any problem. In the z-domain the inverse can be derived also. However, when this function is transformed to the time-domain, the reason for the bad performance of the controller becomes clear. The transformed function is given in equation 6.5

$$C_{ff}(k): \quad y(k) = \frac{1}{55.69\times10^{-3}}\,(u(k+1) - 0.999\,u(k)) \qquad (6.5)$$

As can be seen in equation 6.5. the inverse of the servo system's transfer function makes use of the input u(k+1). This input can not be known at t=kT and therefore a prediction has to be made. The designed controller will predict this u(k+1) as good as possible, but since a perfect prediction is not possible, the disturbances can not be ruled out completely.
A solution for this problem could not be found, but by increasing the sampling frequency, it is expected that the prediction becomes more accurate. It is not clear how much the sampling frequency has to be increased to come to satisfying results. As a start, the frequency of the augmented plant shown in figure 6.1 will be increased to 50 Hz. The identified poles zeros and constants (mentioned in [1]) of the platform have a sampling frequency of 10 Hz. Therefore, they will be converted to a frequency of 50 Hz. These poles, zeros and constants are mentioned in appendix 9 and 10.

6.4: controller design by a sampling frequency of 50 Hz.

To verify the explanations mentioned above, the controller designs with the augmented plant of figure 6.1 are repeated with a sampling frequency of 50 Hz. The first verifications are done with $V_w=W_y=1$.

The controller has been calculated. Unfortunately the calculated γ is 0.68 again. The transfer of D_w to Y_p (see figure 6.1) is given in figure 6.10.

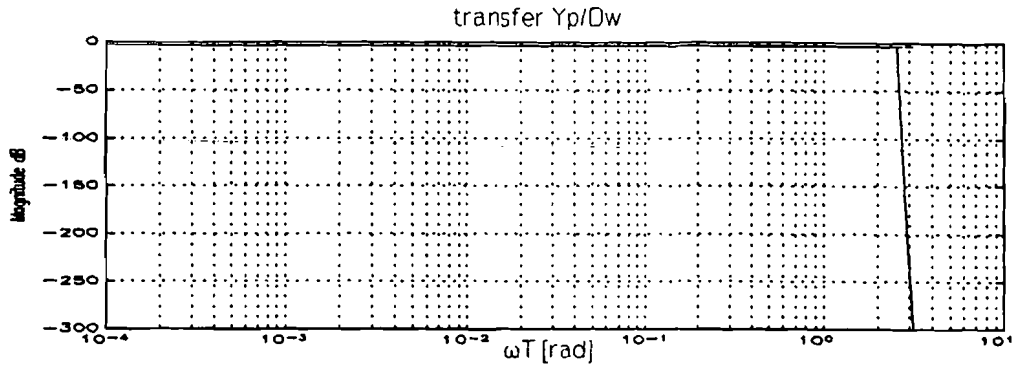

figure 6.8: closed loop transfer by 50 Hz.

As can be seen in figure 6.10, the suppression of the disturbances is not better than the suppression shown in figure 6.2.
The controller which has been calculated, is shown in figure 6.11.

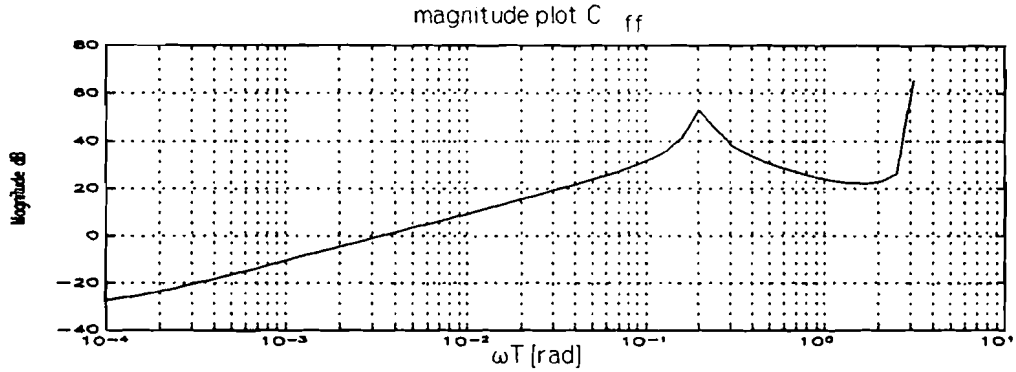

figure 6.11: bode-plot controller by 50 Hz

The bode plot of the controller is even worse than the plot of the 10 Hz controller. However, this plot shows that the given explanation for the peaks in the controller diagram must be right. For this controller there are some peaks at 1 Hz ($\omega T=0.13$) also.

To come to a better disturbance reduction, it seems that the heightening of the sample frequency is not the solution. Fortunately, better results can be derived when the weighting and shaping filters are replaced by the filters mentioned in figure 5.9 and 5.10. Of course, the sample frequency of these filters has to be increased to 50 Hz also.

The magnitude of these filters is changed until $\gamma=1$. The final shaping and weighting filters are given in equation 6.6.

$$V_w(k) = 0.77\frac{(z+12.13)(z-0.9975)}{(z-0.8187)(z-0.8187)} \qquad W_y = \frac{0.15}{1-0.9} \qquad (6.1)$$

The closed-loop transfer function becomes as shown in figure 6.12

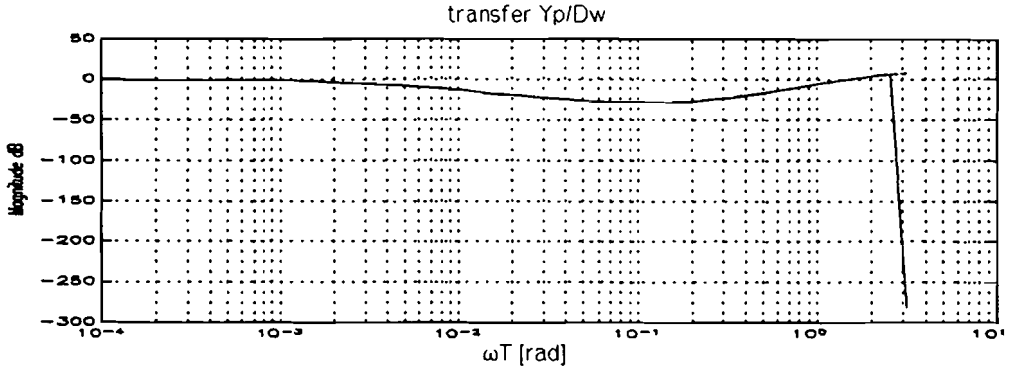

figure 6.12: closed-loop transfer with shaping filter

In figure 6.12, it can be seen that the disturbance reduction is much better. For a frequency of 1 Hz ($\omega T=0.13$), the reduction is about 30 dB. For the lower frequencies the reduction becomes less, but there is no amplification. The controller design is given in figure 6.13.

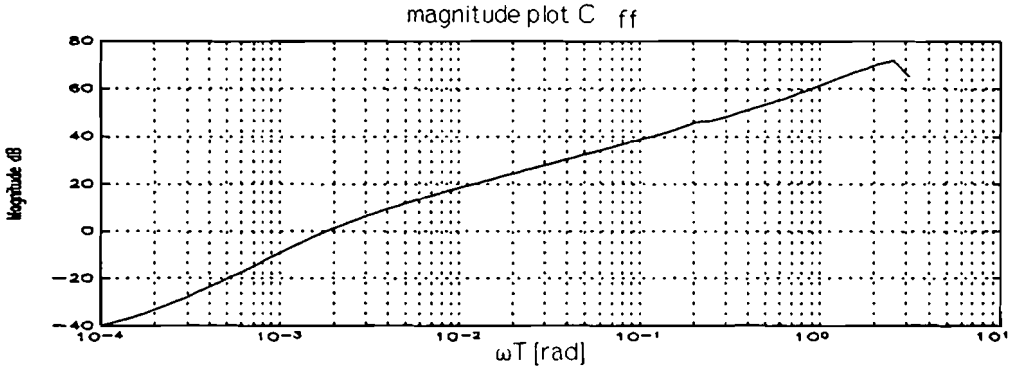

figure 6.13: bode-plot controller designed with shaping filter

The peaks in the bode-plot of the controller have become very small. For frequencies of about 1 Hz ($\omega T=0.13$), the bode-plot almost shows the ideal straight line. Therefore it can be expected that for the augmented plant described in chapter five, better results can be reached by increasing the sample frequency to 50 Hz. In the case the wave disturbance reduction will still be to small, there are two possibilities:

1) Increasing of the sampling frequency
2) Increasing the order of the shaping filter. With a higher order filter, it must be possible to make the prediction, mentioned in 6.3, more accurate.

The controller for the augmented plant of chapter five is derived in chapter 7.

7: Modifying the shaping and weighting filters.

7.1: Introduction

The designing of an H_∞controller is an iterative procedure. First the magnitude of the shaping and weighting filters has to be changed until the $\gamma \approx 1$ is reached. If a design with $\gamma = 1$ is found, the 6 transfer functions of the disturbances to the output signals have to checked on fulfilling the desired performance. If this is not true, the shape of the filters has to be changed and the procedure has be restarted.
The simulations are done with the aid of the Matlab Toolbox MHC written By H.M. Falkus. As mentioned in chapter 5, there are six transfer functions which have to be minimized. After calculating a controller by using MHC, the six closed loop transfer functions excluding the weighting and shaping functions are derived. The amplitude diagram of the bode-plots can be plotted. In these diagrams, the inverse transfer of the composed weighting filters is plotted also. For the ideal controller, the transfer of the composed weighting filter and the closed loop transfer functions have to coincide as much as possible. In this case the transfer function is optimized, and no more improvements can be reached.
For the augmented plant of chapter 5, there are six transfer functions to be checked. If for every design, these transfer functions have to be shown, the remainder of this report will contain bode-plots only. For this reason, the change in the filters will be discussed and only in a selection the simulations and the bode plots will be shown.

7.2: Imposed requirements of the controller.

Before the design of a controller can be started, one has to know what is required. Therefore, to get started, it is assumed that the variations in the distance H_i (see figure 2.3) have to be smaller than 1 mm. At the same time, the input voltage of the servo motor has to smaller than 5 Volt. To find out whether these requirements can be fulfilled, some researches have to be done. In the case there is no controller fulfilling these requirements, the demands will be lightened. Because of the fact that the magnitude of the disturbances caused by the rotation of the crane are known, the required reduction can be calculated. The disturbing force of the load is 10 N. The variation in the distance H has to be smaller than 1 mm. Therefore, the reduction factor of the transfer function of the crane disturbance to the output H has to be a factor $10N/0.001m = 10.000 = 80$ dB. At the same time, the transfer function of the crane disturbances to the servo must have a reduction factor of $10N/5V = 2 \approx 6$ dB.
The magnitude of the wave disturbances isn't predefined. The height of the waves depends of the magnitude of the movements of the float in the water. By taking the saturation point of the servo motor, an approximation of the necessary reduction can be

got, and the maximum magnitude of the disturbances can be determined.
If the servo motor reaches saturation, the wave disturbances can't be ruled out and the performance of the platform becomes bad.
Therefore, the design of the controller has to avoid that the saturation point can be reached. It is assumed that the waves have a frequency of about1 Hz. The maximum speed of the servo is:

$$v_{max} = K_{1a} V_{servo\ max} = 5 * 5.5.10^{-3} = 0.275 m/sec \qquad (7.1)$$

The K_{1a} has been derived in chapter 3. The maximum amplitude (A) of the wave disturbances (W_{wh}) can be derived by calculating the velocity of the waves at a certain point. The amplitude is derived in equation 7.2.

$$\begin{aligned} W_{wh} &= A\sin(4\pi t) \\ \dot{W}_{wh} &= A4\pi\cos(4\pi t) \\ &\Updownarrow \\ A4\pi &< v_{max} = 0.275 \\ A &< 0.022 m \end{aligned} \qquad (7.2)$$

In the following derivation, it is assumed that the amplitude of the wave disturbances will be smaller than 2.2 cm.
With this assumption, the necessary disturbance reduction can be calculated. If the wave disturbances have to be smaller than 1mm, the transfer function of the wave disturbances to the height H_i must have a damping factor of 0.022m/0.001m=22≈25dB. At the same time, the transfer function of the wave disturbances to the servo voltage may show a amplification of 5V/0.022m=225≈50 dB at most.

Finally the two transfer functions of the disturbances and modelling error to the height H and the input voltage of the servo U have to be derived. An estimation of the magnitude of these disturbances is hard to derive. In first instance, the modelling errors are assumed to be very small. A controller which fulfils the requirements of the crane and wave disturbances will be designed first. If a controller is found, the magnitude of the modelling error will be increased to the maximum possible level. In this way, a bound for the modelling error can be derived. Afterwards, the size of this band can be investigated.

The requirements mentioned above, are applied to variations in the height H_i (see figure 2.3) and the servo input voltage U. The controllers will be designed for the three subprocesses average height, rotation around the negative y-axis, and rotation around the positive x-axis. Properly speaking, the requirements mentioned above have to be transformed to these three subprocesses. However, it is difficult to derive the magnitude

of the tolerated errors for these three subprocesses.
Therefore, the requirements of 1 mm and 5 Volt will be applied to these three subprocesses also. In this case, it has to be verified afterwards that the servo voltage stays below the 5 Volt if the inputs U of the subprocesses are transformed to the servo voltages.

7.3: Adjustments to the simulation model.

To investigated the performance of the platform under the influence of the waves, the designed controller has to be analyzed. This will be done by making use of the simulation model mentioned in chapter 3. As mentioned in chapter 6, the wave disturbances will be suppressed by a second feed forward controller. This controller has to be added to the existing simulation model of figure 3.14. For the three subprocesses (average height and rotation around the negative y-axis and rotation around the positive x-axis), the waves are seen as independent disturbances. Therefore the wave disturbances on every float have to be transformed to disturbances on these three subprocesses. After this transformation, the designed feed forward controller can be placed. The block diagram of the simulation model is becoming very complex. Therefore some blocks will be taken together. The purport of the blocks will be clear with the aid of figure 3.14. In appendix 4, the simulink model is declared also.

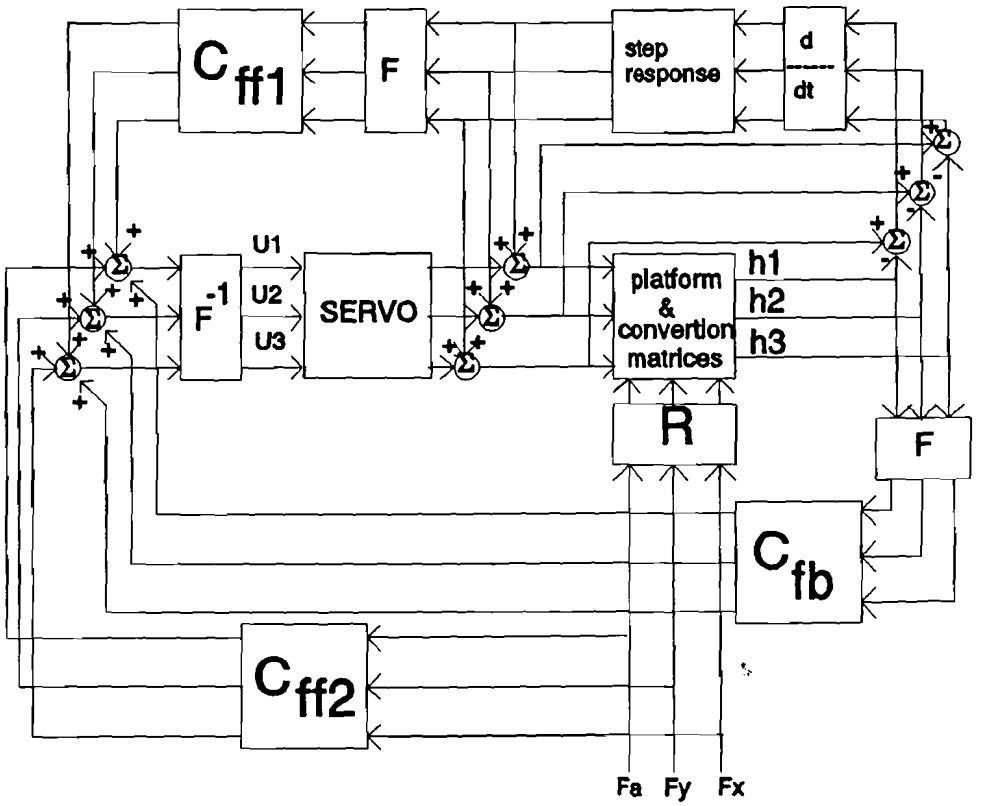

figure 7.1: simulation model with second feed forward

7.4: Designing a controller for the average height Y_a.

The controller design has been started with the weighting and shaping filters described in chapter 5. The magnitude of the shaping and weighting filters is changed until γ=0.99 was be reached. The transfer of the crane disturbances to these outputs are given in figure 7.2.

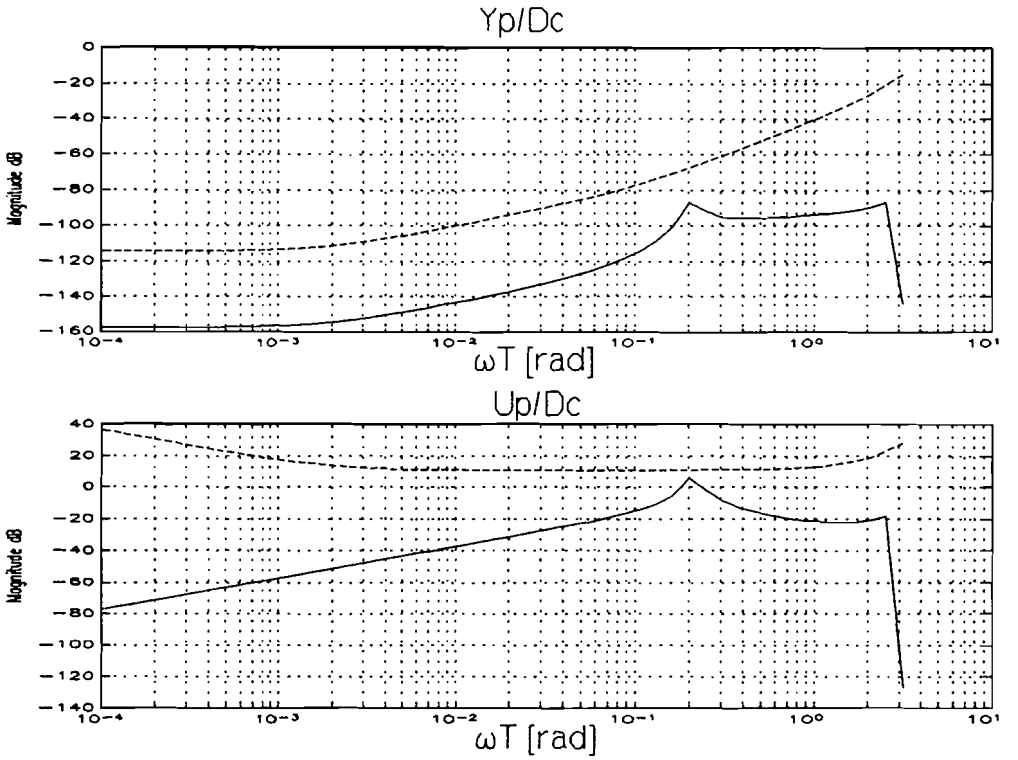

figure 7.2: transfer functions crane disturbances.

As can be seen in figure 7.2. The reduction of the crane disturbances to the output Y_a is more than 80 dB for every frequency. The damping of these disturbances to the servo voltage U_a is more than 6 dB for frequencies smaller than about 1 Hz. (ωT=0.13 in figure 7.2) For higher frequencies the servo will become saturated. The crane disturbances on the average height will have the shape of a step. Since a step function contains many frequencies, there is a possibility that the damping to the servo voltage U will be too less for these step disturbances. It has to be verified with the simulation model afterward, if the servo becomes saturated. The shape of the transfer function has to be modified. In this case the order of the filters has to be increased.

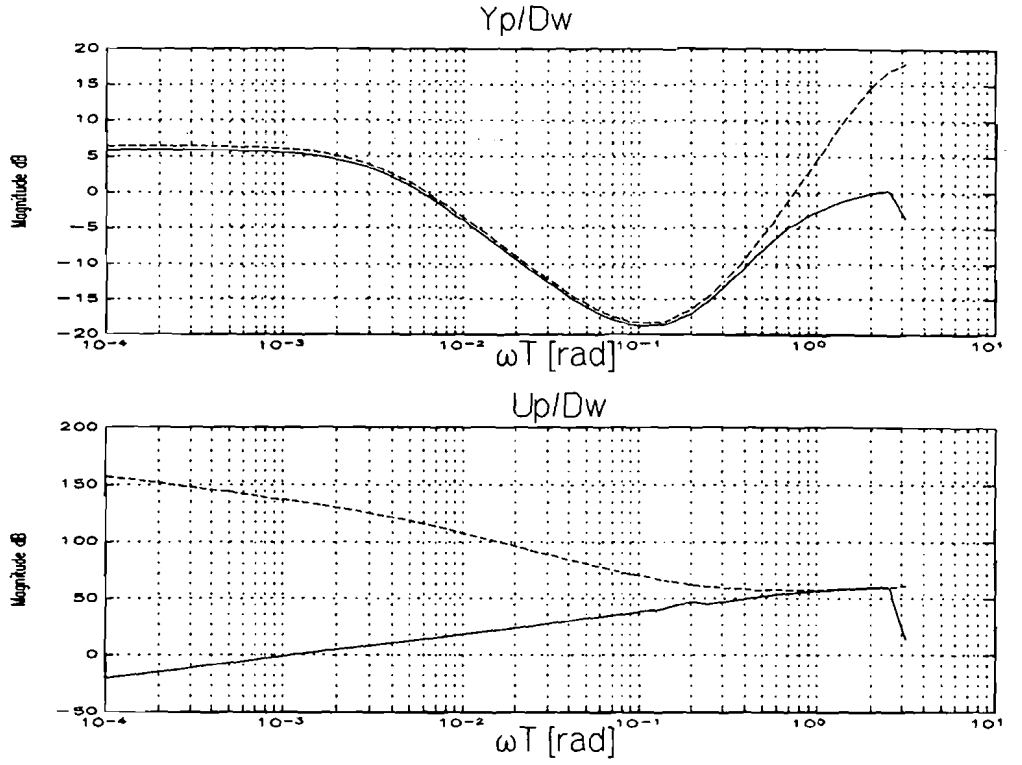

figure 7.3: transfer functions wave disturbances.

In figure 7.3 it can be seen that the maximum reduction of the wave disturbances is almost 20 dB. As a consequence, the requirement of 25 dB can not be reached. To arrive at better results, the order of the wave disturbance shaping filter will be increased to 3. For high frequencies there are no wave disturbances. For these frequencies the slope of the filter will become -40 dB/dec. For the lower frequencies, the shape of the filter will be the same. A plot of the filter is given in figure 7.4.

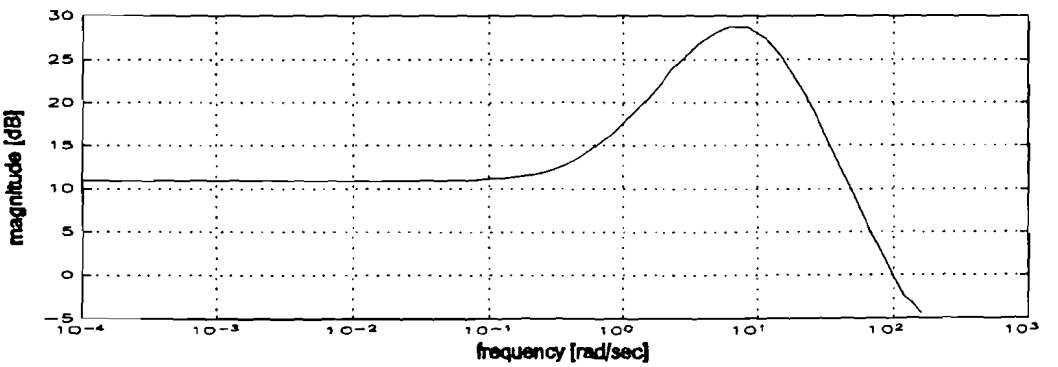

figure 7.4: third order shaping filter wave disturbances.

With these filters better results can be reached. The wave disturbances reduction becomes larger than 25 dB. The amplification of these disturbances to the servo input stays below 50 dB for frequencies smaller than 2 Hz (see appendix 11).

The controller for the crane disturbances already fulfils the requirements, therefore the shaping filter of the crane disturbances are not changed.
Finally, the magnitude of the shaping filter of the modelling error is increased to the maximum level which could be reached.
The requirements mentioned in section 7.1, are fulfilled and an acceptable controller for the average height is present.
The amplitude diagrams of the bode-plots of the six transfer functions are shown in appendix 11. Besides the plots of the closed loop transfer functions, the bode-plots of the three controllers are shown also. As expected, the feed forward controllers are active for the higher frequencies and feed back controller takes charges of the lower. The transfer functions of the filters used to come to these results, are mentioned in appendix 12.

7.5: Designing a controller for the rotation around the x-and y-axis.

Because of the fact that the transfer functions of the rotation around the negative y-axis and positive x-axis are almost equal. The design of the controllers will be described in parallel. For the designing of these controllers, the redesigned shaping filter for the wave disturbances of section 7.4 is used. For the crane disturbances, the filters described in chapter five will be taken. For these controllers, the requirements of a maximum variation of 1mm of the output Y, and a maximum of 5 volt for the input U are in force also. With the crane disturbance shaping filters mentioned in chapter 5, the controllers for the rotation around the negative y-axis and positive x-axis can be derived. The magnitude of the filters is changed until the $\gamma \approx 1$. The derived transfer functions are shown in figure 7.5 and 7.6.

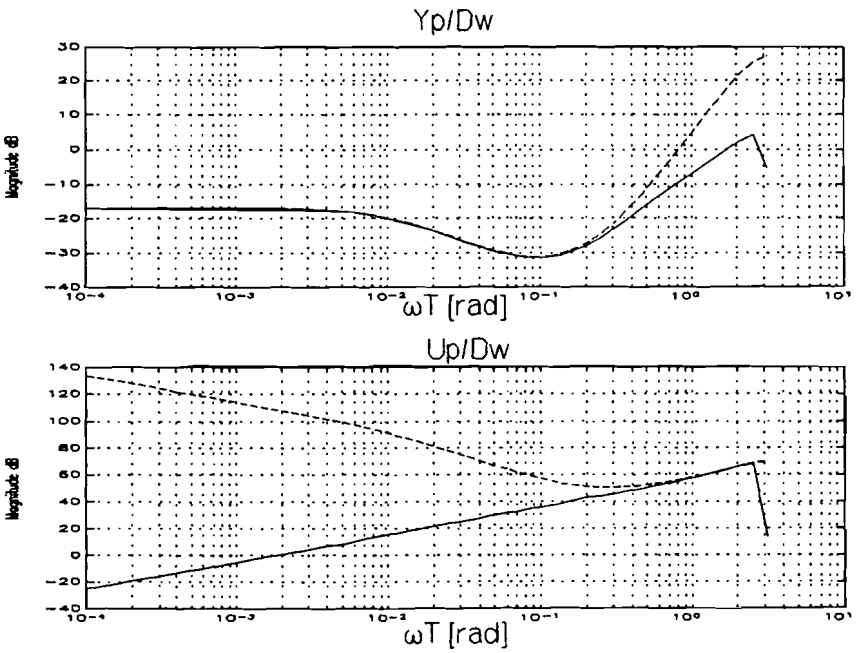

figure 7.5: closed loop transfer functions wave disturbances.

As can be seen in figure 7.5, the closed loop transfers of the wave disturbances fulfil the requirements mentioned in section 7.2.

The transfer functions of the crane disturbances are shown in figure 7.6.

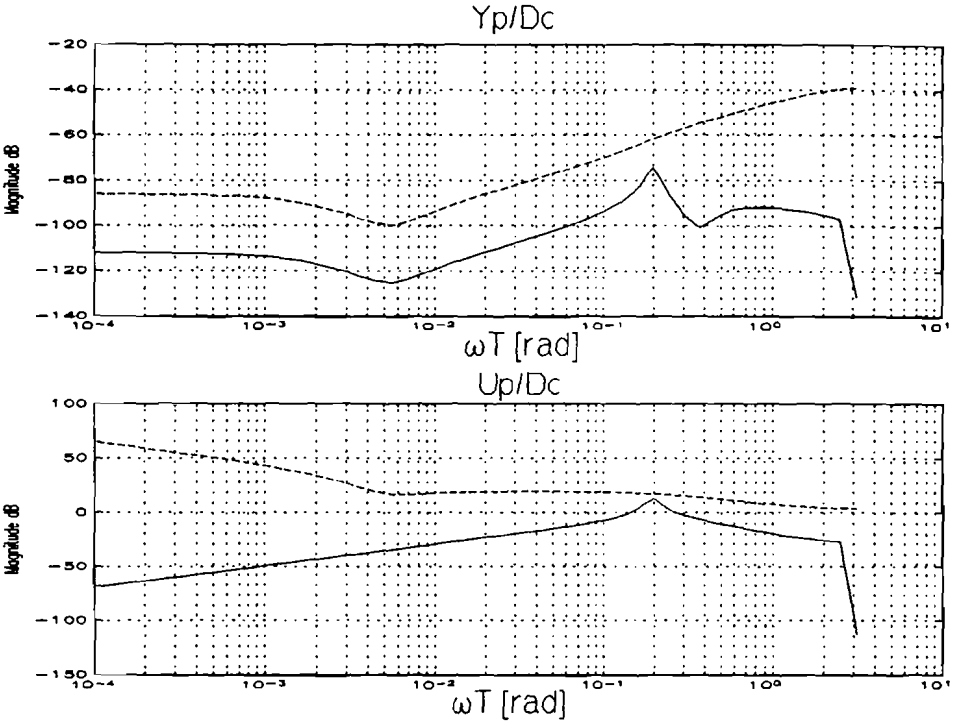

figure 7.6: closed loop transfer functions crane disturbances

As can be seen in figure 7.6, the reduction of the crane disturbances to the output Y is more than 80 dB for every frequency. For the frequency the crane is rotating with (0.04 Hz, $\omega T=5.10^{-3}$ in figure 7.6) the damping is even more than 130 dB. For this frequency, the reduction of the disturbances to the output U is more than the required 6 dB. Only at the moment the load has been picked up, the crane disturbances will have the shape of a step like the disturbances on the average height. Therefore, there is a possibility that the damping to the servo voltage U will be too less for these step disturbances. It has to be verified with the simulation model afterwards.

It can be concluded that the designed controller for the rotation around the negative y-axis fulfils the requirements mentioned in section 7.2 also. However, it is desirable that the performance will be modified a little. This can be explained with the aid of figure 7.7

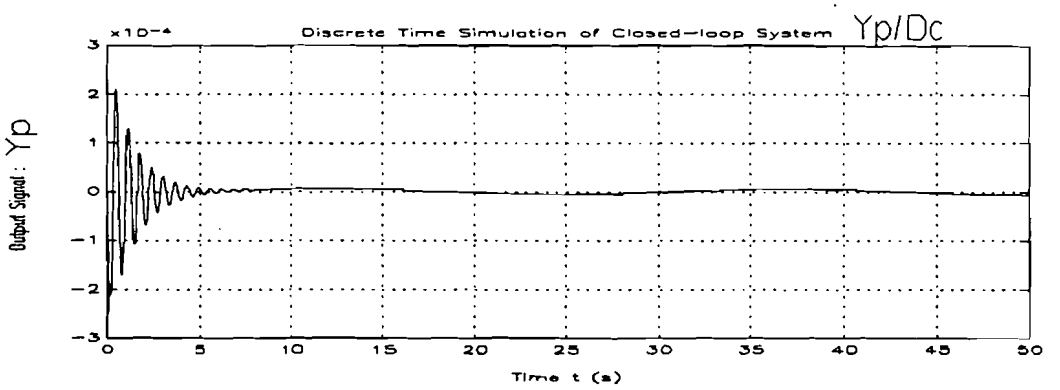

figure 7.7: time simulation crane disturbances on Y_y.

In figure 7.7 the time simulation of the crane disturbances to the output y_y has been plotted. As can be seen in this plot, the disturbances on Y are very small when the steady-state is reached. However, when the load is picked up, the output y_y shows some oscillations. which are large in comparison with the variations in the steady state. To prevent that waves caused by the reaction of the controller will become to big, it is desirable that the oscillations are reduced much more. Therefore the shaping filter of the crane disturbances for the rotation around the negative y- and positive x-axis will be modified. The weighting on the frequency the platform is oscillating with, will be increased. As a consequence, the disturbance reduction on the frequency the crane is rotating with, will become less. For the rotation around the y -and x-axis, the shaping filter of figure 7.8 will be used.

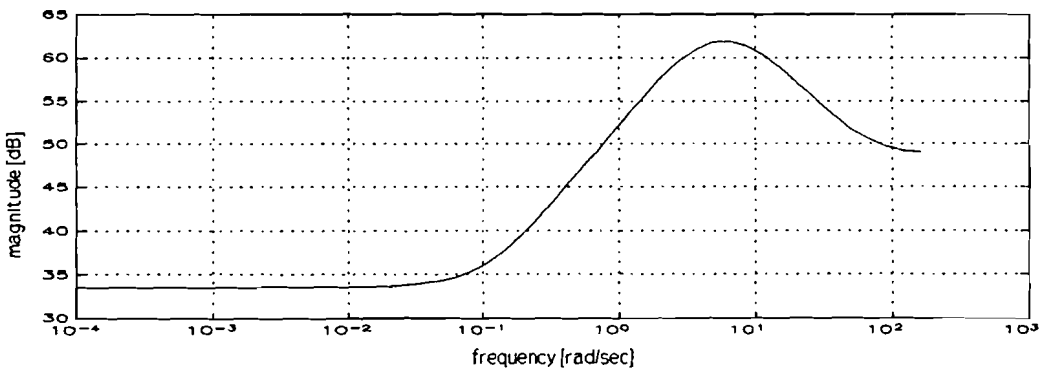

figure 7.8: redesigned shaping filter crane disturbances

With the shaping filter of figure 7.8, a new controller is designed. As always, the magnitude of the shaping filters is changed until the $\gamma \approx 1$. The closed loop transfer functions are plotted in figure 7.9. As expected, the disturbance reduction for the frequency the crane is rotating with (0.04 Hz, $\omega T=5.10^{-3}$) has become less, but is still larger than the required 80 dB. For the frequencies of about 1 Hz ($\omega T=0.13$) the reduction has become much more.

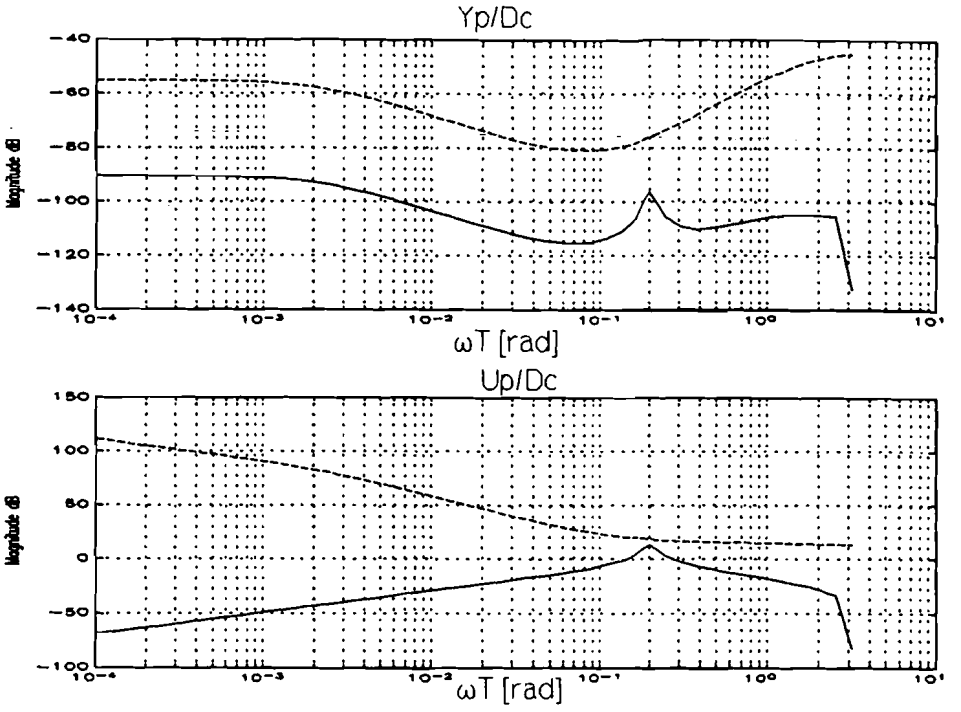

figure 7.9: closed loop transfer functions crane disturbances

When a time simulation is done with this controller, the following result can be derived.

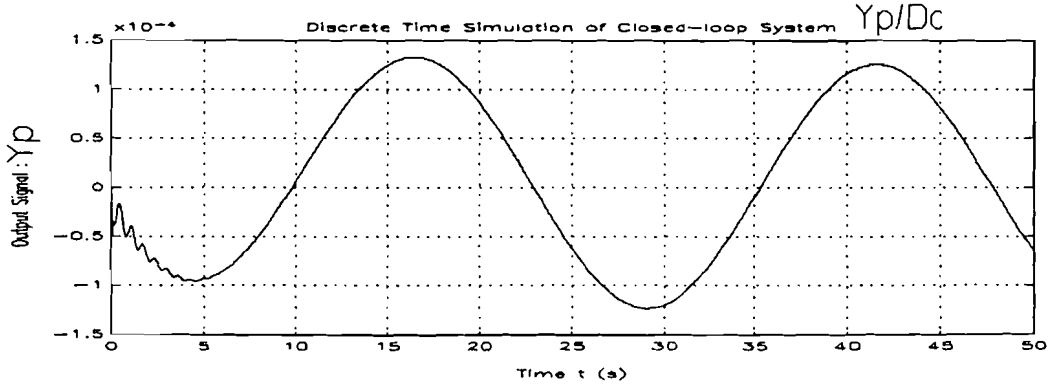

figure 7.10: time simulation crane disturbances on Y

As can be seen in figure 7.10, the oscillations have become much smaller. As a consequence, the variations in the steady state are grown, but they are still very small.
Finally, the magnitude of the modelling error is increased as much as possible and a suitable controller for the rotation around the negative y-axis is designed also.
For the rotation around the positive x-axis, the same results can be derived.
For all of the three subprocesses, the controllers have been designed. The bode-plots of the closed loop transfer functions and controllers are given in appendix 11. The transfer functions of the derived shaping filters are given in appendix 12.

8: Simulation results.

8.1: Introduction.

In chapter seven, the controllers for the three subprocesses average height, rotation around the negative y-axis, and rotation around the positive x-axis are designed. Now the controllers will be analyzed with the simulation model which is described in chapter 7 also. There are a couple of interesting facts which have to be analyzed. Of course a stable result will be the most important issue. Besides this stability, the servo voltage has to be smaller than 5 Volt. Only if these requirements are fulfilled, the controller can be used, otherwise the designing process has to be restarted. The simulations will last 50 seconds. At t=0, the crane starts rotating and at t=5 the load will be picked up.

8.2: Simulations without a controller.

Based on the simulation model derived in chapter 7, the simulink model has been modified. The two feed-forward and the feedback controlers are added to the simulation model. To make the comparison between the platform with and without the controllers more easily, the effects of the crane disturbances on the platform without a controller are plotted again. In this case, the movements of the floats in the water are relatvely large. Therefore the lower bound of the input signal of the convolution sum has to be increased to 5mm/sec to arrive at stable results. For the simulations with the controllers, this boundery is made 2.5mm/sec.

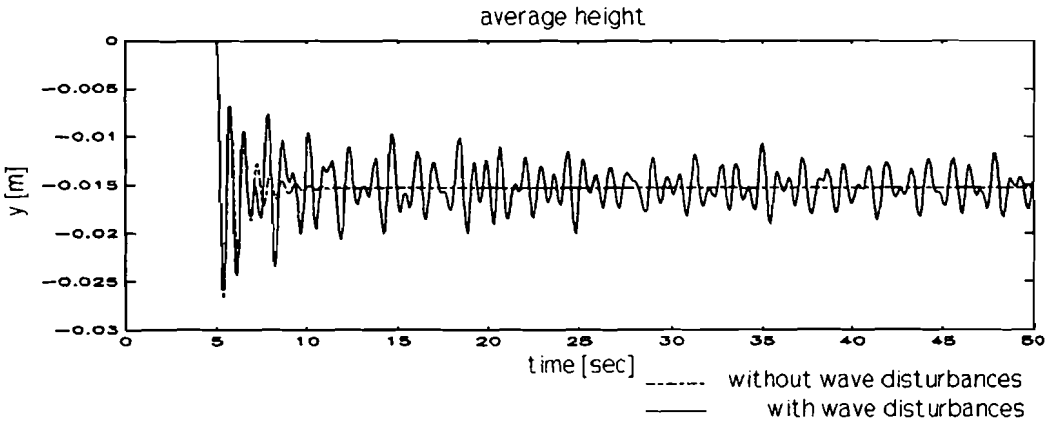

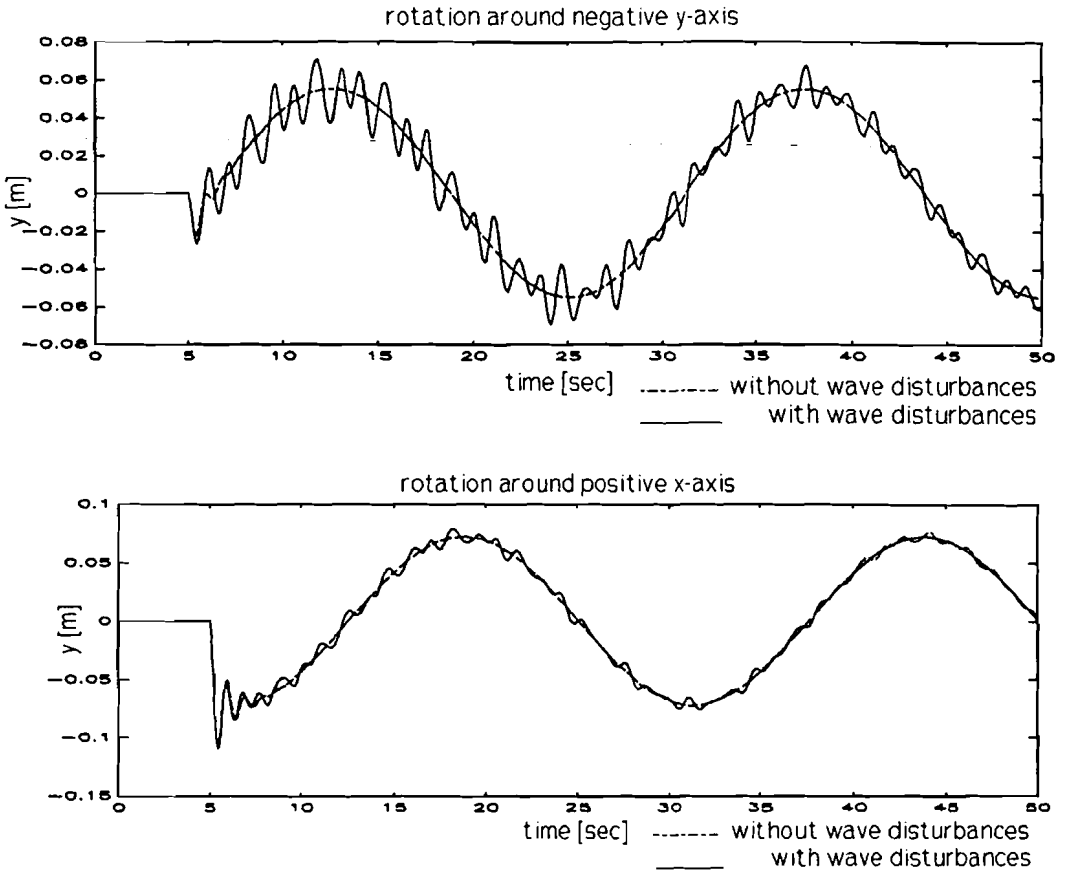

figure 8.1: simulations without a controller.

8.3: Simulations with a controller.

With the simulation model it is possible to make simulations for different output signals. First the output of the average height, rotation around the negative y-axis, and the rotation around the positive x-axis will be simulated. The results are plotted in figure 8.2.

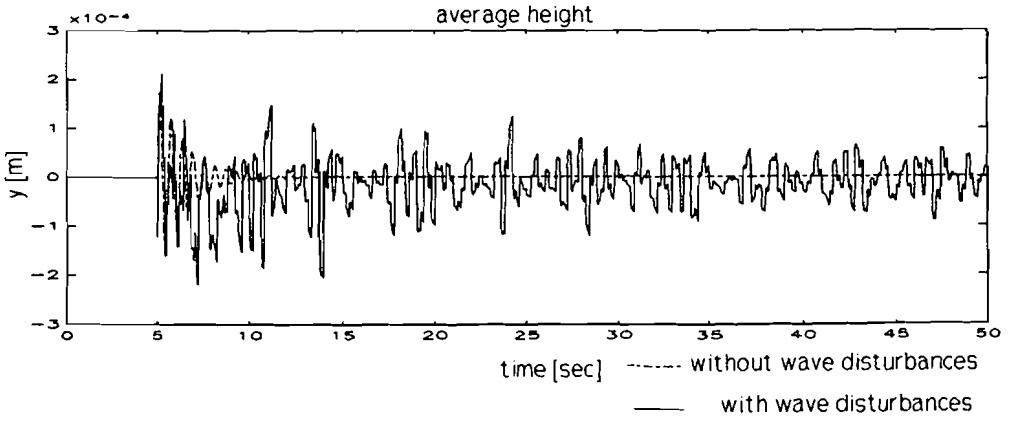

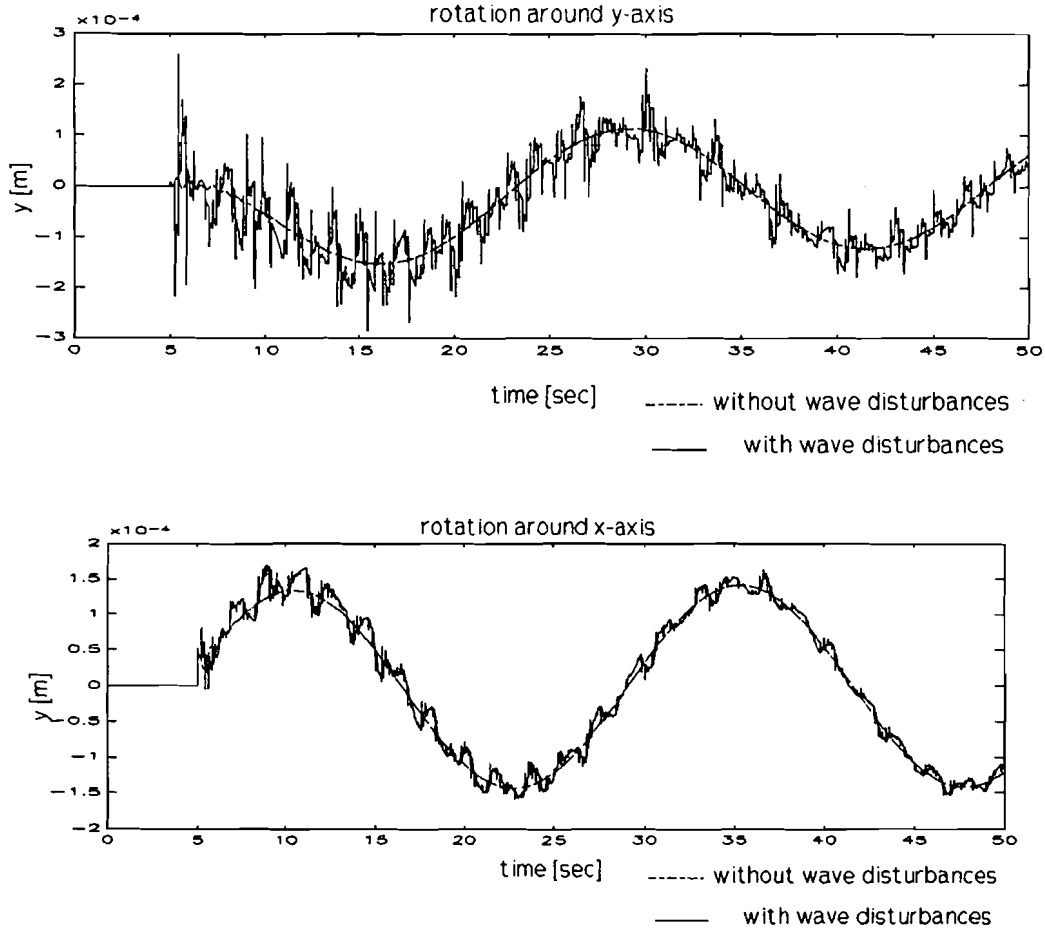

figure 8.2: simulations platform with controllers.

As can be seen in figure 8.2, the simulations show some stable results. For all the three subprocesses, the wave disturbances are decreasing in the course of time. Since the crane keeps rotating, there will always be some wave disturbances left. Comparing figure 8.1 with 8.2, it can be concluded that the controller is able to reduce the crane disturbances by a factor 100. Especially in the plot of the rotation around the negative y-axis, the wave disturbances show some spikes. These spikes are caused by the simulation model itself. The spikes are caused by the fact that the convolution sum has a sampling frequency of 5 Hz. Because of this low sampling frequency, the output of the convolution sum will be a staircase signal in comparison with the 50 Hz of the platform. These 'steps' are high frequent and therefore of great influence on the differentiative character of the feed forward controller. To reduce these spikes, the simulink model contains a second order low-pass filter with a conner frequency of 2Hz. By an filter with an higher order, these spikes can be reduced more.

The stability in relation to the wave disturbances can de analyzed by examining these disturbances in the course of time.

These disturbances have to decrease after the load has been picked up. Since the crane keeps rotating, it may be clear that there will always be some disturbances left. With the aid of the simulink model, these disturbances are simulated and the results are plotted in figure 8.3.

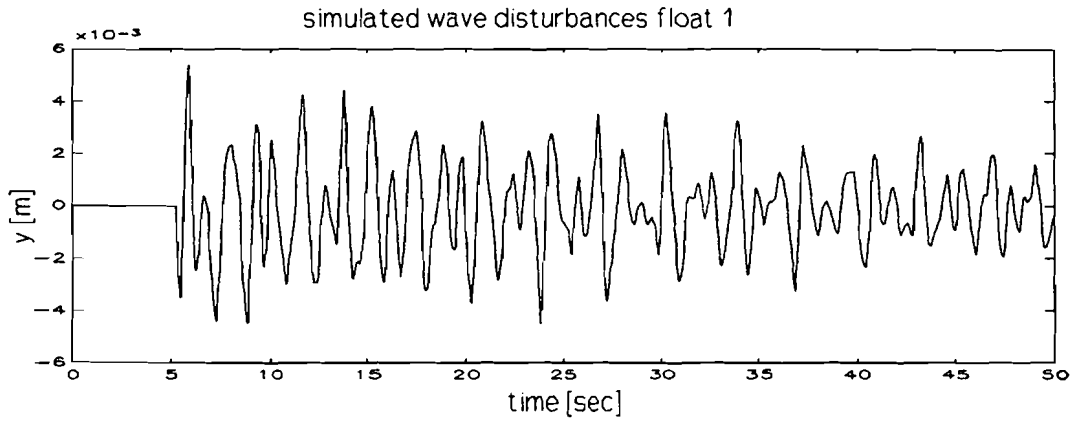

figure 8.3: wave disturbances in course of time.

As can be seen in figure 8.3, the wave disturbances are decreasing in the course of time. Therefore, it can be concluded that these disturbances are not of danger for the platform's stability.

Besides stability, the servo motor may not become saturated. With the simulink model, these voltages can be derived easily. The input voltage of servo 1 is plotted in figure 8.4

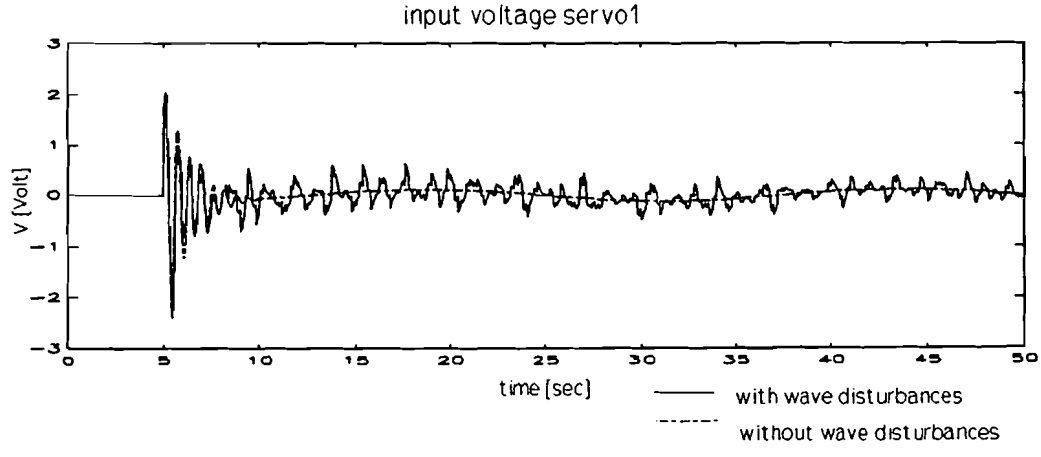

figure 8.4: input voltage servo 1

As can be seen in figure 8.4 the maximum input voltage is about 2 Volt. However, the load has been picked up at t=5 seconds. At this moment the arm of the crane is between two floats and therefore, the load's disturbances are divided among two floats.

If the load is picked up at t=0 second, the load's disturbances come on the account of one float only. In this case the servo voltage shows a spike of 5.5 Volt. At this moment the load is picked up in only one sample moment. This means within 0.02 second which causes a big jerk on the crane's arm. As a consequence, the controller has to react strong to compensate these disturbances. Therefore this spike can be reduced by picking up the load less coarse. As a result, the servo's input voltage will stay below 5 Volt.
In section 7.2 and 7.3, it was suggested that the damping of the transfer function of the crane disturbance reduction to the output U was probably to less if the disturbances would have the shape of a step. As mentioned above, there is a possibility of servo saturation. However, problems can be avoid by picking up the load less coarse.

Up until now, only the outputs of the three subprocesses have been investigated. The only outputs which can be seen in reality, are the variations in the distances H_i (see figure 2.3). With simulink these outputs can be derived easily also. Because of the fact that the variations in these outputs are almost equal, only the variations in H_1 will be plotted. The results are shown in figure 8.5.

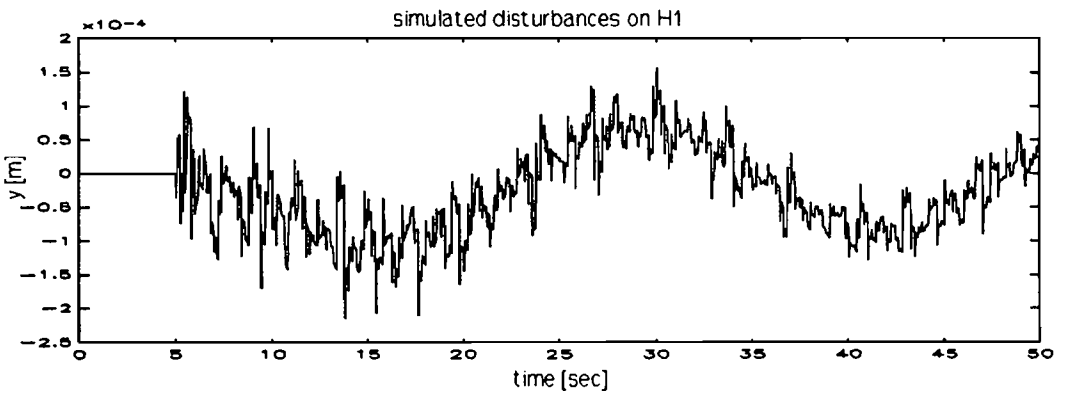

figure 8.5: variations in height H1.

Figure 8.5 shows that the disturbances caused by the crane and the waves are reduced to variations less than 1mm. This means that the crane disturbances are reduced a hundred times.

Finally a simulation without the second feed forward controller for the wave effects can be done. In first instance, it was expected that this would result in an unstable process. Very strong controllers are used, and as was found in [1], this can lead to instability very easily. The results are plotted in figure 8.6

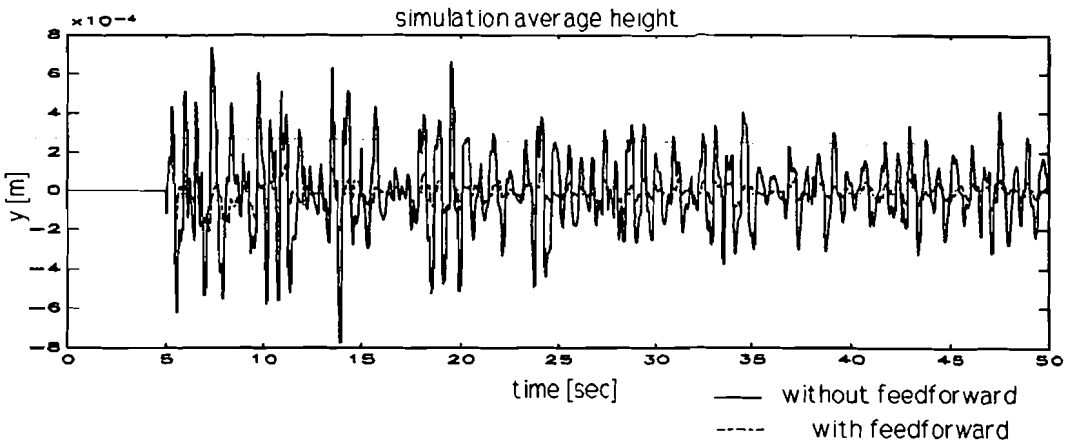

figure 8.6; simulation results with and without the second feed forward.

It is true that the disturbances without the second controller become much larger, but as can be seen in figure 8.6, the simulation without the feed forward controller doesn't show instability. This is contradictory with the results found in [1] which are plotted in figure 3.16. Is it possible to explain these results, or is the simulation model still insufficient to represent reality accurately. A possibly explanation can be found in the fact that the controller of figure 3.16 is designed under the restriction that the servo voltage has to stay below the 0.8 Volt. This restriction was made to increase the resolution of the computer's D/A converter. This was necessary because of the fact that the servo voltage is about 0.2 Volt in steady state. With the low resolution of the D/A converter, limit cycles will be the result.
As a consequence, the servo motors were not able to follow the wave disturbances and strong controllers may cause unstable systems. By taking away the penalty on higher servo voltages, the servo motors are able to follow these wave disturbances, and stronger controllers can be derived. In figure 8.6, it can be seen that in this case, the feed back controller is able to reduce the wave disturbances by a factor 10 and no instability seems to occur.

As can be seen in figure 8.4, the servo voltage necessary to account for the crane disturbances is still 0.2 Volt in steady state, and therefore there is a possibility of limit cycles again. However, the magnitude of the voltages used to reduce the wave disturbances is much larger than the voltages of these limit cycles. By heightening the penalty on the input voltage to come to an higher resolution of the A/D converter, the wave disturbances can't be reduced any more, and the result will be that the performance of the whole system will decrease a lot. Therefore, the penalty on the servo voltage will not be changed. The effects of this A/D conversion are not investigated yet.

9: Conclusions.

For the floating platform an adequate H_∞ controller especially for wave disturbances, has been designed. Because of the fact that the platform has been broken down, the new controller had to be designed with the aid of a simulation model which is derived first.The design is made with the use of the existing model of the floating platform. The model exists of three mathematical independent SISO (single input single output) models. The parameters of these models were identified before.

With the controller designed by J.P.H.M Bouwels, a disturbance reduction of a factor six could be reached. By using a stronger controller, the actual process became instable. This instability was caused by the unmodelled effects of the wave disturbances. These disturbances come into existence by the movements of the floats in the water.

To arrive at better results, there are two possibilities.

1) Modelling the wave disturbances also.
2) Adding extra input signals, in the shape of wave height measurements, to the model.

It is expected that the first option will give the best results. However besides the fact that the derived controller will only be useful for this tub, modelling the wave disturbances isn't very easy. Because of the small size of the tub, there are a lot of wave reflections which make modelling very complicated.

Therefore the second option has been chosen.

It can be derived that the wave disturbances can be seen as disturbances on the distance between a float and the platform. The wave disturbances are added to the already existing model descriptions. For the simulation model, the transfer of the movement of the floats to the height of the waves had to be used. As mentioned before this transfer function is hard to be derived. Therefore measured responses have been used. The wave disturbances have been calculated by making use of a convolution sum. Of course, the linearity of the wave disturbances had to be verified first. With this model it was possible to simulate the responses of the platform in combination with the wave effects. To verify the results of the simulations, some of the measurements described in [1] are repeated. It can be concluded that the simulations and the measurements coincide a lot. Both the two controllers described in [1] are used in the simulations, and what was seen in reality also, the strong controller caused an instable process.

The next step to be taken was to design a new H_∞ controller which uses the height of the waves as extra input signals. Because of the fact that the wave disturbances can be measured well, a second feed forward controller will be used.

For all of the three SISO subprocesses, these controllers had to be derived. For the platform, there are three disturbing input signals. Crane disturbances, wave disturbances, and disturbances caused by modelling errors and offset and drift on servo amplifiers).

On the other side, there are two output signals which to be controlled:

The variations in the height of the platform, and the input voltage of the servo motors. These requirements are transformed to requirements on the three SISO subprocesses. In first instance, a better controller could not be designed. The reduction of the wave disturbances was minimal. To find the origin of the problem, the model is simplified to a model which only contains the feed forward controller used to reduce the wave disturbances. For this controller, the results were disappointing also. However, the results in a time-continuous implementation were much better. The bad performance was caused by the fact that in the discrete time implementation, the controller has to be a predictor. Therefore there will always be a prediction error and better results can not be reached. To reduce this error, the sample frequency of the platform modes is increased to 50 Hz. At this frequency a wave disturbance reduction of 30 dB could be reached.

For the complete model the result became much better also. After some redesigns of the shaping filter good controllers could be derived. With these controller, the variations in the height of the platform become smaller than 1 mm while the servo voltage stays below 5 Volt. When these controllers are tested with the simulation model, the simulations show stable results.
By making use of these controllers, the performance of the platform becomes much better than when the controllers described in [1] are used. This is caused by the fact that the penalty on the servo voltage is decreased. By lowering this penalty, the controllers become able to follow the wave disturbances. As a consequence, limit cycles can come into existence when an A/D converter is used, but avoiding these limit cycles will results in a worse performance.

Recommendations

1) Further verifications of the simulation model on the basis of the newly built platform.
2) Adding the A/D effects to the simulation model. In this case the effects of the limit cycles can be investigated.
3) Try to reduce the sample frequency by modifying the servo transfer function in such a way that it can be inverted (by adding a zero for example).
4) The controller seems able to keep the variations of the height of the platform within a bound of 1 mm. Unfortunately such an accurate sensor is not present yet. Since the performance of the controller depends on the accuracy of the sensors, these sensors have to be designed first.

REFERENCES.

[1] **Bouwels, J.P.H.M.**
"Ontwikkeling en beproeving van verschillende regelaars (LQG, H_∞) voor de horizontale afregeling van een drijvend platform met een draaiende kraan als verstoring".
Afstudeerverslag,
Technische Universiteit Eindhoven, Faculteit der Elektrotechniek,
Vakgroep Meet en Regeltechniek, 1991.

[2] **Falkus, H.M.**
"H_∞ Robust Control Design for an Electromechanical Servo System"
Eindhoven University of Technology, The netherlands
Faculty of Electrical Enginering, Measurement and Control Group

[3] **Liebregts, W.R.H.M.**
"A new identification technique for H_∞ robust control design:
Identification of the water-vessel process"
Einhoven University of Thechnology, The Netherlands
Faculty of Electrical Enginering, Measurement and Control Group

[4] **Simulab User's Guide**
For use with the Microsoft Windows System
December 1991.

[5] **Glover, K. and Doyle, J.C.**
"State-space formulea for all stabilizing controllers that satisfy an H_∞-norm bound and relations to risk sensitivity"
System & Control Letters, Vol 11, 1988, page 167-172.

[6] **Klomstra, M., v.d. Boom, A.J.J., Damen, A.A.H.**
"A comparison of classical and modern controller design : A case study",EUT Report 90-E-244, Department of Electrical Engineering, Eindhoven University of Technology, The Netherlands, november 1990.

[7] **Glover, K. and MacFarlane, D.C.**
"Robust controller design using normalized coprime factor plant descriptions", Lecture notes in control information sciences, No.138, Springer, 1990.

[8] **Janssen, J.F.R.**
"Identificatie en regeling van een drijvend platform."
Afstudeerverslag,
Technische Universiteit Eindhoven, Faculteit der Elektrotechniek,
Vakgroep Meet en Regeltechniek, augustus 1990.

[9] **Falkus, H.M., Damen, A.A.H. and Bouwels, J.P.H.M.**
"General MIMO H_∞ Control Design Framework
31st IEEE CDC, Tuscon, Arizona, December 16-18 1992

[10] **Damen, A.A.H., Falkus, H.M., Bouwels, J.P.H.M.**
"Modeling and Control of a Floating Platform"
To be published.
Eindhoven University of Technology, The netherlands
Faculty of Electrical Enginering, Measurement and Control Group

[11] **Looman, R. and Mentink, R.**
"Het drijvend platform: Realistaie van en stabilisatieonderzoek aan een vereenvoudigd model"
Afstudeerverslag geschreven in opdracht van de Hogeschool Eindhoven en de Technische Universiteit Eindhoven, afdeling elektrotechniek, vakgroep Meet- & Regeltechniek, januari 1993

LIST OF SYMBOLS

SYMBOL	: DESCRIBTION	
A_f	: surface of the bottom of the float	[m]
A_t	: surface of the tub	[m]
A,B,C,D	: state-space matrices	
A_d,B_d,C_d,D_d	: state-space representation of V_d	
A_c,B_c,C_c,D_c	: state-space representation of V_c	
A_w,B_w,C_w,D_w	: state-space representation of V_w	
A_y,B_y,C_y,D_y	: state-space representation of W_y	
A_u,B_u,C_u,D_u	: state-space representation of W_u	
C_{ff1}	: feedforward controller crane disturbances	
C_{ff2}	: feedforward controller wave disturbances	
C_{fb}	: feedback controller	
D	: height of the float	[m]
D_d	: shaped genral disturbances	
D_c	: shaped crane disturbances	
D_w	: shaped wave disturbances	
F	: transformation matrix V_i (i={1,2,3}) to V_i (i={a,y,x})	
F^{-1}	: transformation matrix y_i (i={a,y,x}) to h_i (i={1,2,3})	
F_i	: crane disturbances on the sub-processes with i={a,x,y}	[N]
g	: gravity force	[m/s^2]
G	: transfer matrix augmented plant	
G_{ij}	: elements of transfer matrix augmented plant	
G_i	: transfer function of a subprocess with servo (i={a,y,x})	
H_a	: height of centre with regard to the ground	[m]
H_i	: height of beam i (i={1,2,3}) with regard to the ground	[m]
H_w	: transfer fuction wave disturbances	
h_i	: distance of beam i (i={1,2,3}) to equilibrium	[m]
H_s	: servo transfer function	
J_x	: inertia of the rotation around the positive x-axis	[kg(rad/s)^2
J_y	: inertia of the rotation around the negative y-axis	[kg(rad/s)^2
K_g	: Kalman gain	
K_{pi}	: constant used in transfer function subprocess (i={a,y,x})	
K_{1i}	: constant of the servo part of the subprocesses (i={a,y,x})	
K_{2i}	: constant of the platform part of the subprocess (i={a,y,x})	
K_y	: transformation constant for P_y	
K_x	: transformation constant for P_x	
K_∞	: Designed H_∞ controller.	
K_s	: constant of the servo transfer function	
L	: distance between centre and end of beam	[m]
M	: mass of the total platform	[kg]
m	: mass of the load	[kg]
M_k	: closed-loop transfer function augmented plant	
n_d	: general disturbance signal	
n_c	: crane disturbance signal	
n_w	: wave disturbance signal	

P_i	: platform transfer functions (i={a,y,x})	
R_i	: crane disturbance transfer function (i={a,y,x})	
u	: control input augmented plant	
u_i	: input of the three subprocesses (i={a,y,x})	
U_p	: servo input of the augmented plant of the platform	
V_d	: shaping filter general disturbances	
V_c	: shaping filter crane disturbances	
V_w	: shaping filter wave disturbances	
V_i	: input voltage servo (i={1,2,3})	[V]
V_i	: input voltage of the three subprocesses (i={a,y,x})	[V]
w	: exogenous inputs augmented plant	
W_y	: weighting filter output Y_p	
W_h	: water height with regard to the ground	[m]
W_z	: water height without a float	[m]
W_{h0}	: water height in stationary circumstances	[m]
w_{whi}	: wave disturbances around float i (i={1,2,3})	[m]
w_i	: wave disturbances on the three subprocesses (i={a,y,x})	[m]
W_t	: increase of water height caused by float	[m]
W_u	: weighting filter servo input U_p	
X_i	: distance between float i (i={1,2,3}) and the platform	[m]
x_i	: distance of X_i to equilibrium (i={1,2,3})	[m]
x_i	: input of the transfer function of the platform part (i={a,y,x})	
y_i	: output of the three subprocesses (i={a,y,x})	
y	: measured output augmented plant	
Y_p	: output of the augmenteed plant of the platform	
z	: output to be controled augmented plant	
γ	: H_∞ norm of M_k with the calculated controllers	
Δ_i	: depth of float i (i={1,2,3}) in the water	[m]
δ_i	: depth of float i (i={1,2,3}) to equilibrium	[m]
Θ_x	: rotation around the positive x-axis	[rad]
Θ_y	: rotation around the negative y-axis	[rad]
Φ	: angle between x-axis and the arm of the crane	[rad]

APPENDIX 1: Poles, zeros, and constants of the platform

	average height	rotation around the y-axis	rotation around the-axis
poles G(z) p_1, P_2 and p_s	0.6036+0.6960i 0.6036-0.6960i 1	0.6624+0.5654i 0.6624-0.5654i 1	0.7022+0.5392i 0.7022-0.5392i 1
zeros G(z) z_1 en z_2	0.4631+0.8230i 0.4631-0.8230i	0.5240+0.7676i 0.5240-0.7676i	0.5380+0.7124i 0.5380-0.7124i
constants G(z)	$3.7.10^{-3}$	$4.3.10^{-3}$	$4.4.10^{-3}$
constants R(z)	$5.04.10^{-4}$	$1.2.10^{-3}$	$1.4.10^{-3}$

The poles of R(z) are equal to the poles of G(z) with the exception of the servo's pole p_s

Sampling frequency: 10 Hz

APPENDIX 2: Constants of servo- and platform transfer functions

	average height	rotation around the y-axis	rotation around the x-axis
K	$3.7.10^{-3}$	$4.3.10^{-3}$	$4.4.10^{-3}$
K_1	$55.69.10^{-3}$	$80.89.10^{-3}$	$83.61.10^{-3}$
K_2	0.6644	0.5316	0.5262

Sampling frequency: 10 Hz

$$K_y = \frac{K_{1y}}{K_{1a}} = 1.4525$$

$$K_x = \frac{K_{1x}}{K_{1a}} = 1.5013$$

APPENDIX 3: Poles, zeros, and constants of the H_∞ controllers described in [1].

strong controller:

	gemiddelde hoogte	rotatie om de -y-as	rotatie om de x-as
polen	0.0000[1)] 0.9000[2)] 0.9990[2)] 0.2395 -0.7583 -0.0510 0.4749 + 0.7710.i 0.4749 − 0.7710.i	0.0000[1)] 0.9990[2)] 0.9997[1)] 0.5239 + 0.6784.i 0.5239 − 0.6784.i -0.9815 0.1196 + 0.1994.i 0.1196 − 0.1994.i	-0.9853 -0.5245 0.5164 + 0.6067.i 0.5164 − 0.6067.i 0.9900[2)] 0.9900[2)] 0.4186 0.0000[1)] 0.2001[1)]
nulpunten van C_{fb}	0.0000[1)] -1.0000 -0.5000 -0.5000 0.6038 + 0.6960.i 0.6038 − 0.6960.i 0.9583 0.8735	0.0000[1)] 0.9997[1)] -0.9900 -0.9900 -1.0000 0.8764 0.6651 + 0.5655.i 0.6651 − 0.5655.i	-0.9000 -1.0000 0.7022 + 0.5392.i 0.7022 − 0.5392.i 0.5000 0.0000[1)] 0.9067 + 0.0765.i 0.9067 − 0.0765.i 0.2001[1)]
nulpunten van C_{ff}	-1.0000 -0.5000 -0.5000 -0.1637 0.4026 1.0701 0.9000[2)] 0.9990[2)]	-1.0000 -0.9900 -0.9900 0.2629 -0.0050 1.0439 0.9689 0.9990[2)]	-1.0000 -0.9000 -0.4299 0.4817 + 0.4624.i 0.4817 − 0.4624.i 0.5000 0.9900[2)] 0.9900[2)] 1.0010
versterking C_{fb} versterking C_{ff}	-19.3591 -0.0188	-12.3565 -0.0393	-62.5425 -0.5675

tame controller

	gemiddelde hoogte	rotatie om de -y-as	rotatie om de x-as
polen	0.0000[1)] 0.9990 + 0.0010.i[2)] 0.9990 − 0.0010.i[2)] -0.7266 0.4773 + 0.7602.i 0.4773 − 0.7602.i -0.0891 0.7364	0.0000[1)] 0.0020 0.9997[1)] 0.9990 + 0.0010.i[2)] 0.9990 − 0.0010.i[2)] -0.7571 0.5045 + 0.6459.i 0.5045 − 0.6459.i 0.8269	-0.8539 -0.4166 0.5745 + 0.5745.i 0.5745 − 0.5745.i 0.8399 0.9990 + 0.0010.i[2)] 0.9990 − 0.0010.i[2)] 0.0000[1)] 0.2001[1)]
nulpunten van C_{fb}	0.0000[1)] -1.0000 -0.9000 -0.9000 0.6036 + 0.6960.i 0.6036 − 0.6960.i 0.9789 + 0.0192.i 0.9789 − 0.0192.i	0.0000[1)] 0.9997[1)] -0.9000 -0.9000 0.6624 + 0.5654.i 0.6624 − 0.5654.i -1.0000 0.9764 + 0.0216.i 0.9764 − 0.0216.i	-0.9000 -0.9000 -1.0000 0.7022 + 0.5392.i 0.7022 − 0.5392.i 0.0000[1)] 0.9767 + 0.0215.i 0.9767 − 0.0215.i 0.2001[1)]
nulpunten van C_{ff}	-1.0000 -0.9000 -0.9000 -0.1694 0.3672 1.1716 0.9990 + 0.0010.i[2)] 0.9990 − 0.0010.i[2)]	-1.0000 -0.9000 -0.9000 0.2667 -0.0050 1.1497 0.9529 0.9990 + 0.0010.i[2)] 0.9990 − 0.0010.i[2)]	-1.0000 -0.9000 -0.9000 -0.4199 0.5523 + 0.5443.i 0.5523 − 0.5443.i 0.9990 + 0.0010.i[2)] 0.9990 − 0.0010.i[2)] 1.0041
versterking C_{fb} versterking C_{ff}	-1.5023 -0.0014	-0.6394 -0.0020	-0.7406 -0.0285

APPENDIX 4: Manual simulation programs

The simulations described in the report are made with the aid of the *MATLAB* Toolbox *SIMULINK*. With this toolbox, M-files can be built by drawing block diagrams. The results of a simulation can be evaluated in *MATLAB* easily.
The files used for the simulations can be found in the directory *PLATFORM*.
This directory contents:

1) platform.m
2) golfplat.m
3) golfregl.m
4) golfregh.m
5) respons.m
6) platgeg.mat
7) regelaar.mat

The files five six, and seven are necessary for the simulation models (1 to 4) and will be described first.

1) respons.m:
   In the toolboxes of SIMULINK, a block describing a convolution sum, can't be found. For this reason a M-file has been written. This file is represented in appendix 5. The input matrices of this file can be found in the file platgeg.mat. Before starting a simulation, this variables have to be made global. This is described in the next section.

2) platgeg.mat
   This file contents:
   - A input matrix A. This matrix contents the input signals for the servos. The first column of this matrix contains time points, the second one contains the input value for the servos at that moment. Every simulation programme contains a block *INPUT* in which the values of this matrix are divided to the three signals for the servos. Up until now, the second column describes a unity step. Of course, it is possible to change the shape of this signal.
   - A matrix *STAPRES*. This matrix is used in the M-file RESPONS and contains the two measured step responses, the responses are multiplied by the factor 1.2 which is derived in chapter 3. In chapter 3 of the report, it is mentioned that a sample frequency of 10 Hz is used. In order to reduce the calculation time, a sample frequency of 5 Hz is used during the simulations. In spite of this lower sample frequency, the results are almost equal. Only for the simulation model golfregh some adaptions have to be made. Besides the calculation of the convolution sum.

The whole model *GOLFREGH* has a sample frequency of 50 Hz. The wave disturbances are calculated with a frequency of 5 Hz. In the mean time, the output of the convolution sum stays unchanged. In other words, the output becomes a sort of staircase signal. This signal causes a lot of disturbances. Therefore the wave disturbances have to be made smooth by placing a low-pass filter after the output of the convolution sum.

- A input matrix *INGANG*. This matrix contains the inputs necessary for the convolution sum. When the simulation is started, this matrix contents only zeros.

  As mentioned in section 3.3, there is a lower bound for the input signals. Input signals below this bound are made zero. A good bound for acceptable simulation results is 0.0025 m/sec. Of course it dempends on the magnitude of the float's movement. Therefore, it is necassary to check if no instability occurs when a simulation without a controller is done. In case of instablity, this lower bound has to be raised.
- A matrix *NEWSAM*. The variables in this matrix are used to give information of new sample moments.
- A matrix *Y*. This matrix contains the calculated output signals of the convolution sum.

Before starting up a simulation. The variables *STAPRES INGANG NEWSAM* and Y have to be made global. This can be done by typing: 'global stapres ingang newsam y;'in the *MATLAB COMMAND WINDOW*.

3) regelaar.
   This file contains the controller matrices used in the simulation model *Golfregh*. If this simulation model is used, this file has to be loaded in the *MATLAB COMMAND WINDOW*.

A short survey of the four simulation models is given below.

1) Platform.
   This is a simple model of the platform. Only the disturbances caused by the crane are modelled. This model is used to verify the plots shown in [1].

2) Golfplat
   This model is an enlargement of the model mentioned before. In this model the effects of the wave disturbances are modelled also. By interrupting the feedback, the model will give the same results as the model Platform. The diagram of this model is given in figure 3.7.

3) Golfregl.

This model is an enlargement of the models mentioned above also. This model contains a feedforward and a feedback controller as mentioned in figure 3.14. In [1], two set of controllers are described. For both sets of controllers, a simulink block is made. By exchanging these blocks, the performance of both controllers can be analyzed. The blocks which are not used, are placed right under in the simulink diagram.

4) Golfregh.

This model is based on figure 3.14 also. Besides the feed forward and the feedback controllers, a second feedforward controller is placed. The diagram is given in figure 7.1.

Because of the reasons given in chapter four, all blocks in the simulink diagram have a sample frequency of 50 Hz. An exception is made for the convolution sum. This block still has a sample frequency of 5 Hz.

In contrast with the model Golfregl, the controller is given in a State Space equation. The matrices of the controllers are given in the file regelaar.mat. Before starting the simulation, this file has to be loaded in the *MATLAB COMMAND WINDOW* first. New controllers designed with the aid of MHC can be evaluated easily by changing the matrices in regelaar.mat.

APPENDIX 5: THE M-FILE RESPONS.M

% M-file used for the calculation of the convolution sum. For flag definitions, see the manuel of simulink [4]. The convolution sum is calculed by multiplying the marix *INGANG* by the matrix *STAPRES*. The matrix ingang contains all the sample moments of the input. Every time a new sample is taken, all the elements of the matrix INGANG are placed one step backward. The last element is left away. The new sample becomes the first element of the matrix.

```
function [sys, x0]= simom(t,x,u,flag)
ts=0.2;                                  % sample freqency
sam=fix(t/ts);                           % determine sample moment
newsam(2)=sam;

if abs(flag)==1
  sys = [];
elseif flag==3
    if newsam(1)~ =newsam(2)
      % in this case a new sample output has to be calculated.
      % All element of the matrix INGANG are shifted backward.
      % The new input sample becomes the first element of this matrix
       for k=1:599
          ingang(601-k,:)=ingang(600-k,:);
       end
      % Input values below the threshold are made zero.
       if abs( u(1))>2.5e-3 ingang(1,1)=u(1);
          else ingang(1,1)=0;
       end
       if abs(u(2))>2.5e-3 ingang(1,2)=u(2);
         else ingang(1,2)=0;
       end
       if abs(u(3))>2.5e-3 ingang(1,3)=u(3);
         else ingang(1,3)=0;
       end
       uit=stapres*ingang;
      % The wave disturbances on every float are the sum of
      % disturbances caused by the float itself, and the
      % disturbances caused by the two other floats.
       uit1=uit(1,1)+uit(2,2)+uit(2,3);
       uit2=uit(1,2)+uit(2,1)+uit(2,3);
```

```
        uit3=uit(1,3)+uit(2,1)+uit(2,2);
        y=[uit1 uit2 uit3];
        newsam(1)=newsam(2);
          sys = y;
    else sys=y;
    end

elseif flag==0
%       the simulation is just started and the matrices INGANG and Y have to contain
        zeros only
  sys = [0, 0, 3, 3 ,0,1];
  ingang=zeros(600,3);
  newsam=[-1 0];
  y=[0 0 0];
else
  sys = [];
end
```

APPENDIX 6: Deriviation of M_k

The transfer matrix G of the augmented plant of figure 5.1, can be decribed as

$$\begin{bmatrix} z \\ y \end{bmatrix} = \begin{bmatrix} \tilde{Y} \\ \tilde{U} \\ \hline Y_p \\ D_c \\ D_w \end{bmatrix} = \left[\begin{array}{cccc} W_y V_m & W_y R V_c & W_y P V_w - & W_y P H \\ 0 & 0 & 0 & W_u \\ \hline V_d & R V_c & P V_w & P H_s V_c \; 0 \quad 0 \\ 0 & 0 & V_w & 0 \end{array}\right] = \begin{bmatrix} n_m \\ n_c \\ n_w \\ \hline U_p \end{bmatrix} \tag{B6.1}$$

$$= \begin{bmatrix} G_{11} & G_{12} \\ G_{21} & G_{22} \end{bmatrix} \begin{bmatrix} W \\ U \end{bmatrix} = G \begin{bmatrix} w \\ u \end{bmatrix}$$

For the controller the next equation can be derived.

$$U = U_p = \begin{bmatrix} C_{fb} & C_{ff1} & C_{ff2} \end{bmatrix} \begin{bmatrix} Y_p \\ D_c \\ D_w \end{bmatrix} = K_c Y \tag{B6.2}$$

The closed-loop transfer function of w to z can be described as follows:

$$M_k = G_{11} + G_{12} K_c (I - G_{22} K_c)^{-1} G_{21} \tag{B6.3}$$

Filling up G_{11}, G_{12}, G_{21} and G_{22} of equation B6.1 in equation B6.3 gives:

$$M_k = \begin{bmatrix} W_y V_d & W_y R V_c & W_y P V_w \\ 0 & 0 & 0 \end{bmatrix} + \begin{bmatrix} W_y P H_s \\ W_u \end{bmatrix} \begin{bmatrix} C_{fb} & C_{ff1} & c_{ff2} \end{bmatrix} \left[I_3 - \begin{bmatrix} P H_s \\ 0 \\ 0 \end{bmatrix} \begin{bmatrix} C_{fb} & C_{ff1} & C_{ff2} \end{bmatrix} \right]^{-1} \begin{bmatrix} V_d & R V_c & P V_w \\ 0 & V_c & 0 \\ 0 & 0 & V_w \end{bmatrix}$$

$$= G_{11} + \begin{bmatrix} W_y P H_s C_{fb} & W_y P H_s C_{ff1} & W_y P H_s C_{ff2} \\ W_v C_{fb} & W_v C_{ff1} & W_v C_{ff2} \end{bmatrix} \frac{1}{I - P H_s C_{fb}} \begin{bmatrix} 1 & -P H_s C_{ff1} & -P H_s C_{ff2} \\ 0 & 1 - P H C_{fb} & 0 \\ 0 & 0 & 1 - P H C_{fb} \end{bmatrix} \begin{bmatrix} V_d & R V_c & P V_w \\ 0 & V_c & 0 \\ 0 & 0 & V_w \end{bmatrix}$$

$$= G_{11} + \frac{1}{1 - P H_s C_{fb}} \begin{bmatrix} W_y P H_s C_{fb} & W_y P H_s C_{ff1} & W_y P H_s C_{ff2} \\ W_v C_{fb} & W_v C_{ff1} & W_v C_{ff2} \end{bmatrix} \begin{bmatrix} V_d & R V_c - P H_s C_{ff1} V_c & P V_w - P H_s C_{ff2} V_w \\ 0 & (I - P H_s C_{fb}) V_c & 0 \\ 0 & 0 & (1 - P H_s C_{fb}) V_w \end{bmatrix} \tag{B6.4}$$

$$= G_{11} + \frac{1}{I - P H_s C_{fb}} \begin{bmatrix} W_y P H_s C_{fb} V_d & W_y P H (C_{fb} R + C_{ff1}) V_c & W_y P H_s (C_{fb} P + C_{ff2}) V_w \\ W_u C_{fb} V_d & W_u (C_{fb} R + C_{ff1}) V_c & W_u (C_{fb} P + C_{ff2}) V_w \end{bmatrix}$$

$$= \frac{1}{I - P H_s C_{fb}} \begin{bmatrix} W_y V_d & W_y (P H_s C_{ff1} + R) V_c & W_y (P H_s C_{ff2} + P) V_w \\ W_u C_{fb} V_d & W_u (C_{fb} R + C_{ff1}) V_c & W_u (C_{fb} P + C_{ff2}) V_w \end{bmatrix}$$

Appendix 7: State-space matrix augmented plant.

The state space describtion of the augmented plant can be described in a following way (see chapter 4):

$$\left[\begin{array}{c|cc} A & B_1 & B_2 \\ \hline C_1 & D_{11} & D_{12} \\ C_2 & D_{21} & D_{22} \end{array}\right]$$

For the augmented plant of figure 5.1, the state space matrix becomes:

$$\left[\begin{array}{cccccccc|cccc} A_{p1} & 0 & 0 & 0 & 0 & 0 & 0 & 0 & 0 & 0 & 0 & B_{p1} \\ 0 & A_{p2} & 0 & 0 & 0 & B_{p2}C_w & 0 & 0 & 0 & 0 & B_{p2}D_w & 0 \\ 0 & 0 & A_r & 0 & B_rC_c & 0 & 0 & 0 & 0 & B_rD_c & 0 & 0 \\ 0 & 0 & 0 & A_d & 0 & 0 & 0 & 0 & B_d & 0 & 0 & 0 \\ 0 & 0 & 0 & 0 & A_c & 0 & 0 & 0 & 0 & B_c & 0 & 0 \\ 0 & 0 & 0 & 0 & 0 & A_w & 0 & 0 & 0 & 0 & B_w & 0 \\ B_yC_{p1} & B_yC_{p2} & B_yC_r & B_yC_d & B_yD_rC_c & B_yD_{p2}C_w & A_y & 0 & B_yD_d & B_yD_rC_c & B_yD_{p2}D_w & B_yD_{p1} \\ 0 & 0 & 0 & 0 & 0 & 0 & 0 & A_u & 0 & 0 & 0 & B_u \\ \hline D_yC_{p1} & D_yC_{p2} & D_yC_r & D_yC_d & D_yD_rC_c & D_yD_{p2}C_w & C_y & 0 & D_yD_d & D_yD_rC_c & D_yD_{p2}D_w & D_yD_{p1} \\ 0 & 0 & 0 & 0 & 0 & 0 & 0 & C_u & 0 & 0 & 0 & D_u \\ \hline C_{p1} & C_{p2} & C_r & C_d & D_rC_c & D_{p2}C_w & 0 & 0 & D_d & D_rD_c & D_{p2}D_w & 0 \\ 0 & 0 & 0 & 0 & C_c & 0 & 0 & 0 & 0 & D_c & 0 & 0 \\ 0 & 0 & 0 & 0 & 0 & C_w & 0 & 0 & 0 & 0 & D_w & 0 \end{array}\right]$$

The poles of the shaping filter V_d and the transfer function P_1 are similar. In the same time, the MATLAB toolbox MHC will make the matrices A_r and A_{p1} equal to the matrices A_{p2} and A_d. This means $A_{p1}=A_{p2}=A_r=A_d$ and $C_{p1}=C_{p2}=C_r=C_d$.

It follows that for the state-space matrix mentioned above, the columns 2,3 and 4 can be cancelled. In this case, the rows 2,3 and 4 have to be added to row 1.
The transfer functions P_1 and R have more poles than zeros. This means there is no direct feedthrough and D matrices of these transfer functions are zero.

Carrying out the two remarks mentioned on the previous page, the state-space matrix can be simplified to the following matrix.

$$\left[\begin{array}{c|cc} A & B_1 & B_2 \\ \hline C_1 & D_{11} & D_{12} \\ C_2 & D_{21} & D_{22} \end{array}\right] =$$

$$\left[\begin{array}{ccccc|ccc|c} A_{pl} & B_r C_c & B_{p2} C_w & 0 & 0 & B_d & B_r D_c & B_{p2} D_w & B_{pl} \\ 0 & A_c & 0 & 0 & 0 & 0 & B_c & 0 & 0 \\ 0 & 0 & A_w & 0 & 0 & 0 & 0 & B_w & 0 \\ B_y C_{pl} & 0 & B_y D_{p2} C_w & A_y & 0 & D_y D_D & 0 & B_y D_{p2} D_w & 0 \\ 0 & 0 & 0 & 0 & A_u & 0 & 0 & 0 & B_u \\ \hline D_y C_{pl} & 0 & D_y D_{p2} C_w & C_y & 0 & D_y D_m & 0 & D_y D_{p2} D_w & 0 \\ 0 & 0 & 0 & 0 & C_u & 0 & 0 & 0 & D_u \\ \hline C_{pl} & 0 & D_{p2} C_w & 0 & 0 & D_D & 0 & D_{p2} D_w & 0 \\ 0 & C_c & 0 & 0 & 0 & 0 & D_c & 0 & 0 \\ 0 & 0 & C_w & 0 & 0 & 0 & 0 & D_w & 0 \end{array}\right]$$

APPENDIX 8: Poles zeros and constants of the platform in the S domain.

AVERAGE HEIGHT:

poles -0.8200+8.5638*i
-0.8200-8.5638*i
0

zeros -0.6007+10.5056*i
-0.6007-10.5056*i

K $3.7.10^{-2}$

ROTATION AROUND THE NEGATIVE Y-AXIS

poles -1.3824+7.0656*i
-1.3824-7.0656*i
0

zeros -0.7073+9.9086*i
-0.7073-9.9086*i

K 0.0425

ROTATION AROUND THE POSITIVE X-AXIS

poles -1.2179+6.5484*i
-1.2179-6.5484*i
0

zeros -1.1668+9.6782*i
-1.1668-9.6782*i

K 0.0371

APPENDIX 9: Poles, zeros, and constants by a sampling frequency of 50 Hz

	average height	rotation around the y-axis	rotation around the-axis
poles G(z) p_1, P_2 and P_s	0.9693+0.1677i 0.9693-0.1677i 1	0.9630+0.1370i 0.9630-0.1370i 1	0.9676+0.1275i 0.9676-0.1275i 1
zeros G(z) z_1 and z_2	0.9664+0.2060i 0.9664-0.2060i	0.9667+0.1940i 0.9667-0.1940i	0.9588+0.1878*i 0.9588-0.1878*i
constants G(z)	$7.4.10^{-3}$	$8.4.10^{-4}$	$7.4.10^{-4}$
constants R(z)	$2.2.10^{-5}$	$5.6.10^{-5}$	$6.3.10^{-5}$

The poles of R(z) are equal to the poles of G(z) with exceptance of the servo's pole p_s.

Sample frequency: 50 Hz

APPENDIX 10: Constants of servo- and platform transfer functions

	average height	rotation around the y-axis	rotation around the x-axis
K_p	$7.4.10^{-4}$	$8.4.10^{-4}$	$7.4.10^{-4}$
K_1	$55.45.10^{-3}$	$80.80.10^{-3}$	$79.32.10^{-3}$
K_2	0.6671	0.5198	0.4681

$$K_y = \frac{K_{1y}}{K_{1a}} = 1.4571$$

$$K_x = \frac{K_{1x}}{K_{1a}} = 1.4304$$

APPENDIX 11: Bode-plots of the closed loop transferfunctions and controllers

For the three subprocesses average height, rotation around the negative y-axis and rotation around the positive x-axis, the bode-plots of the six closed-loop transfer functions and the three controllers can be derived. For all of the three subprocesse, the following definiyions have to be made.

$C_{11}=C_{feedback}$
$C_{12}=C_{feedforward}$:controller for crane disturbances
$C_{13}=C_{feedforward}$:controlller for wave disturbances. are shown in the next plots. For all of

$P_{11}=Y_{pi}/D_{ci}$ with $i=\{a,y,x\}$
$P_{21}=U_{pi}/D_{ci}$
$P_{12}=Y_{pi}/D_{di}$
$P_{22}=U_{pi}/D_{di}$
$P_{13}=Y_{pi}/D_{wi}$
$P_{23}=U_{pi}/D_{wi}$

The augmented plants are imported in the MATLAB toolbox MHC. The file names are:
average height : gemhr32hs.mat
rotation around the negative y-axis : rotyr32hs.mat
rotation around the positive x-axis : rotxr32hs.mat

AVERAGE HEIGHT Ypa/D_{ca}, Y_{pa}/D_{da} and Y_{pa}/D_{wa}

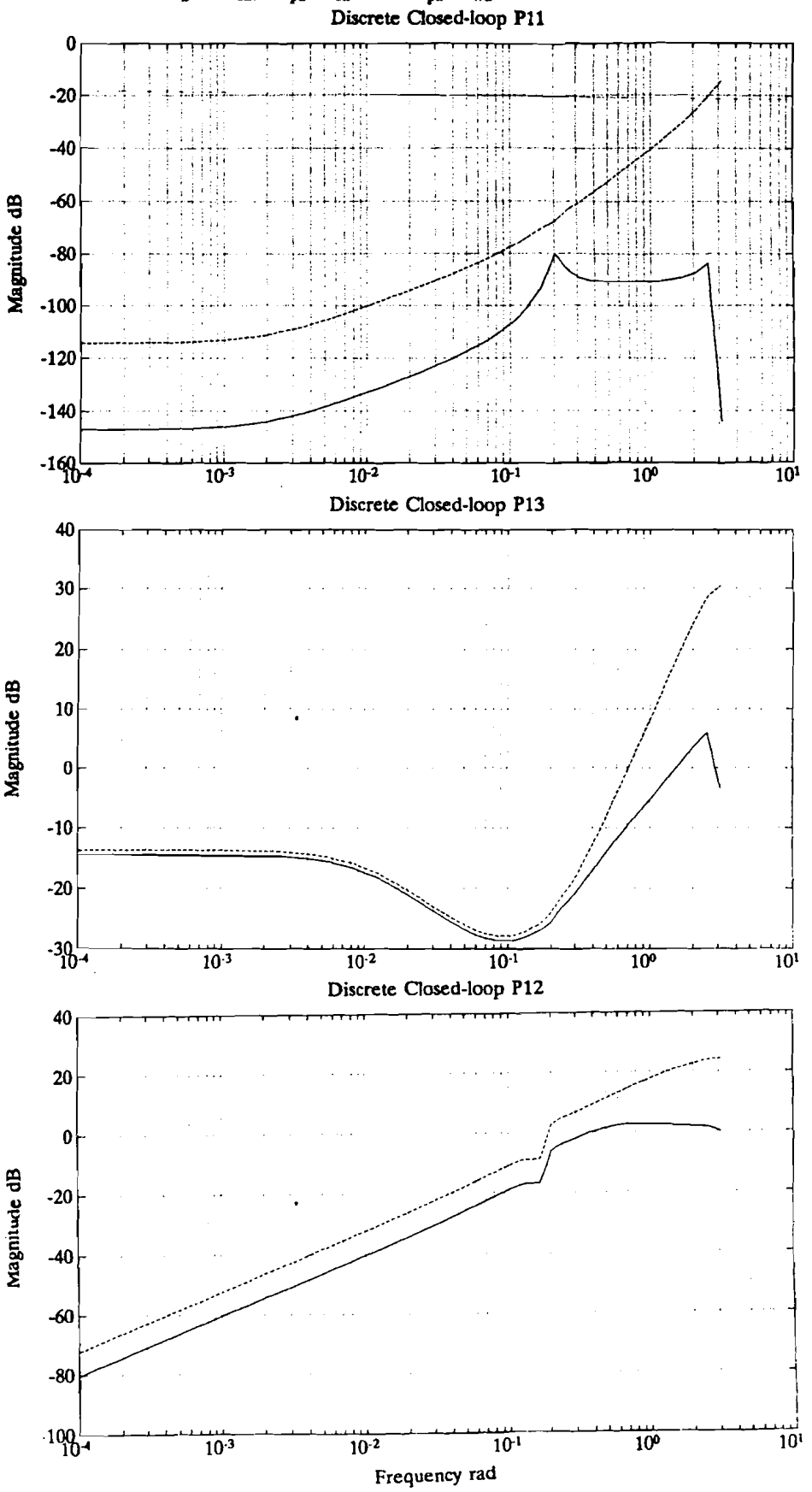

AVERAGE HEIGHT Upa/D_{ca}, U_{pa}/D_{da} and U_{pa}/D_{wa}

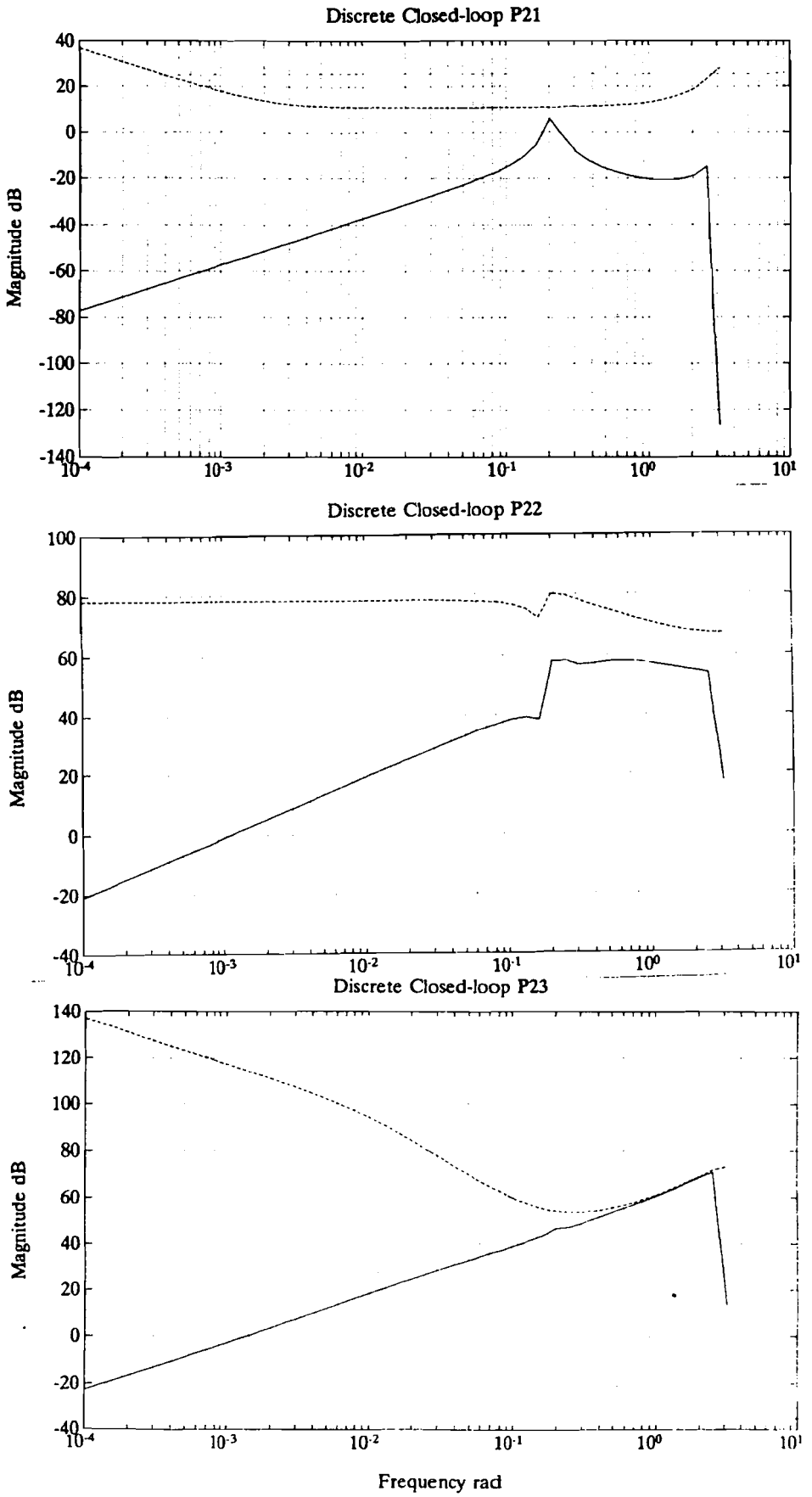

AVERAGE HEIGHT CONTROLLERS C_{fb}, C_{ff1}, C_{ff2}

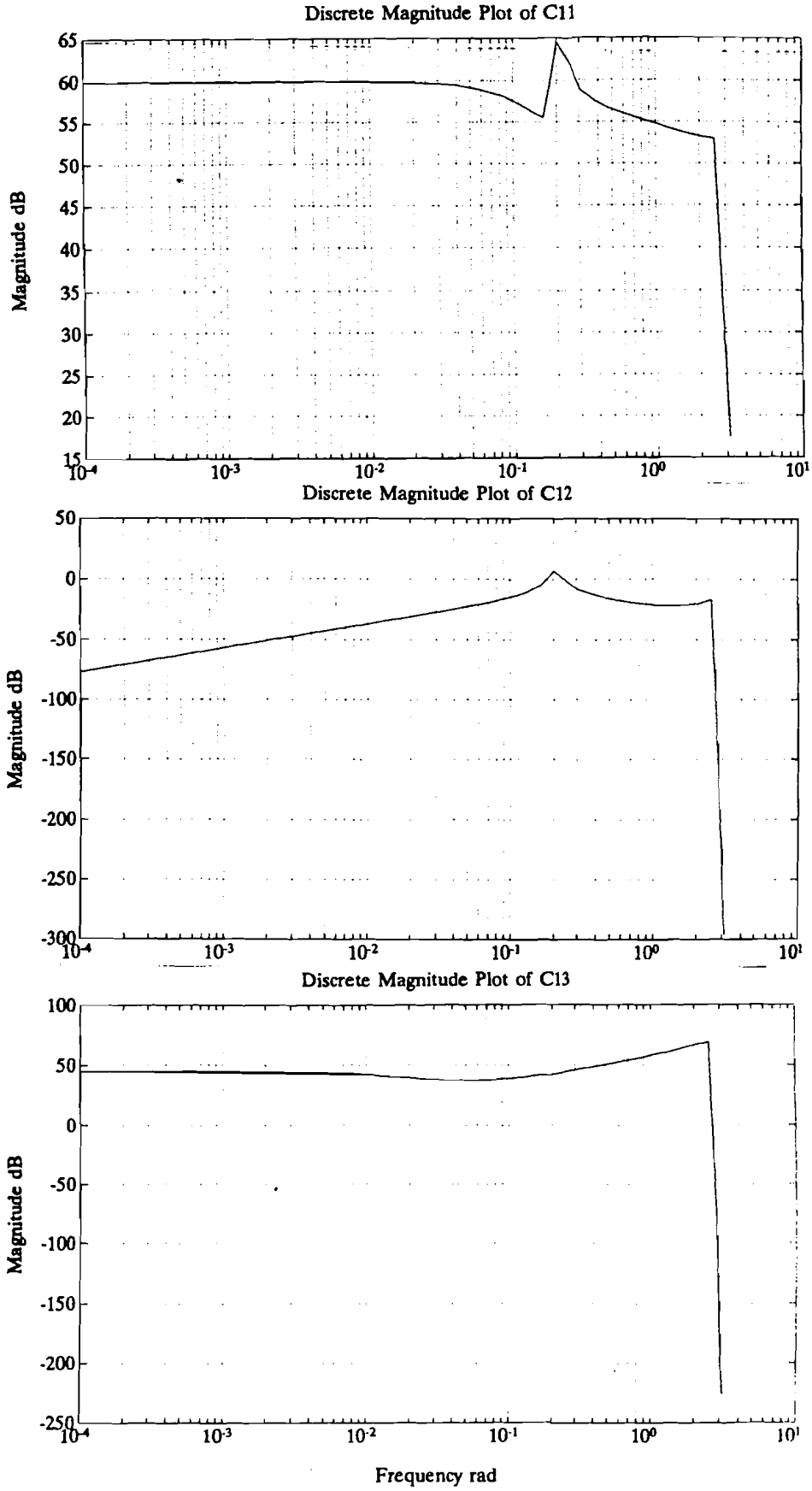

ROTATION AROUND THE NEGATIVE Y-AXIS: Ypy/D_{cy}, Y_{py}/D_{dy} and Y_{py}/D_{wy}

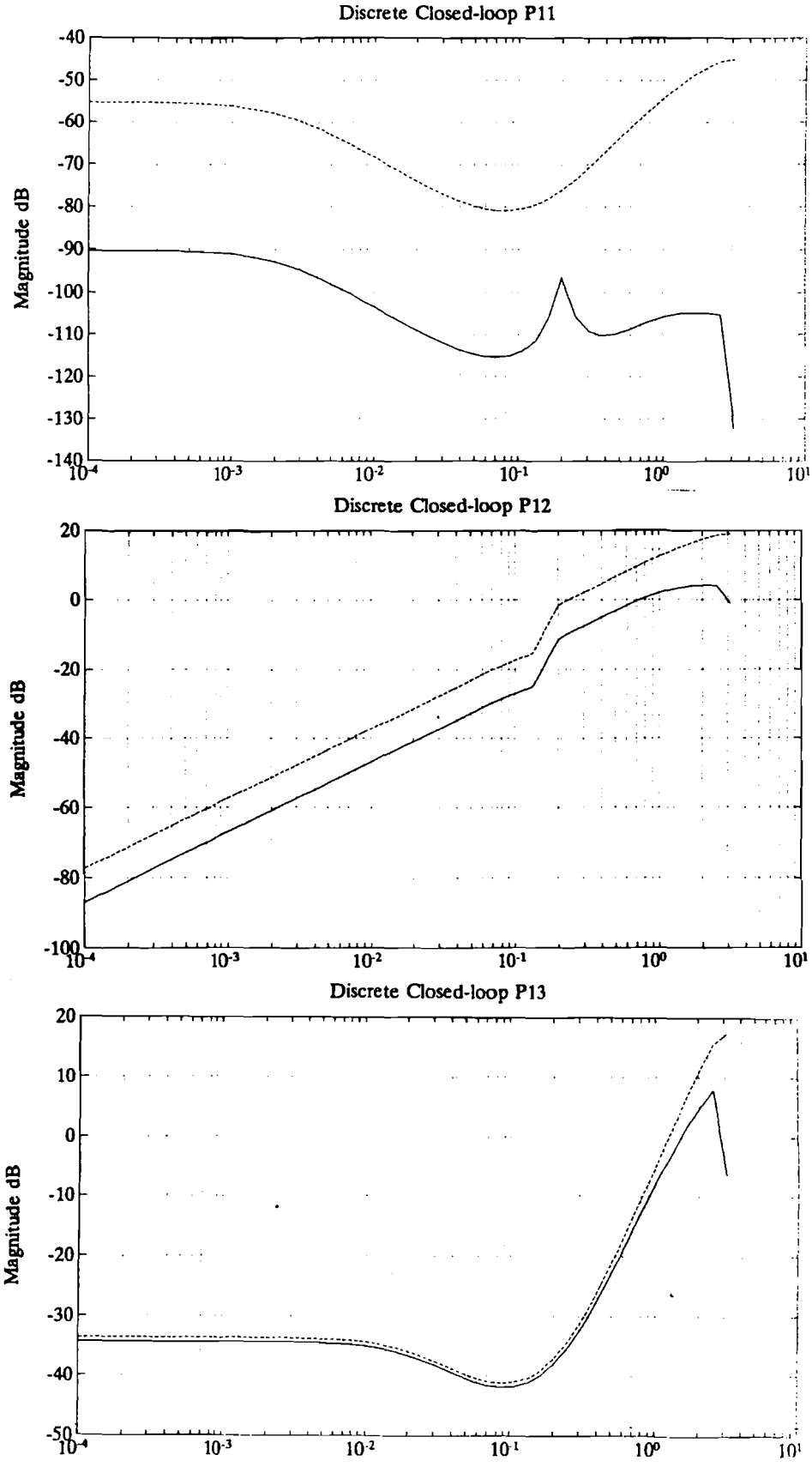

ROTATION AROUND THE NEGATIVE Y-AXIS: Upy/D_{cy}, U_{py}/D_{dy} and U_{py}/D_{wy}

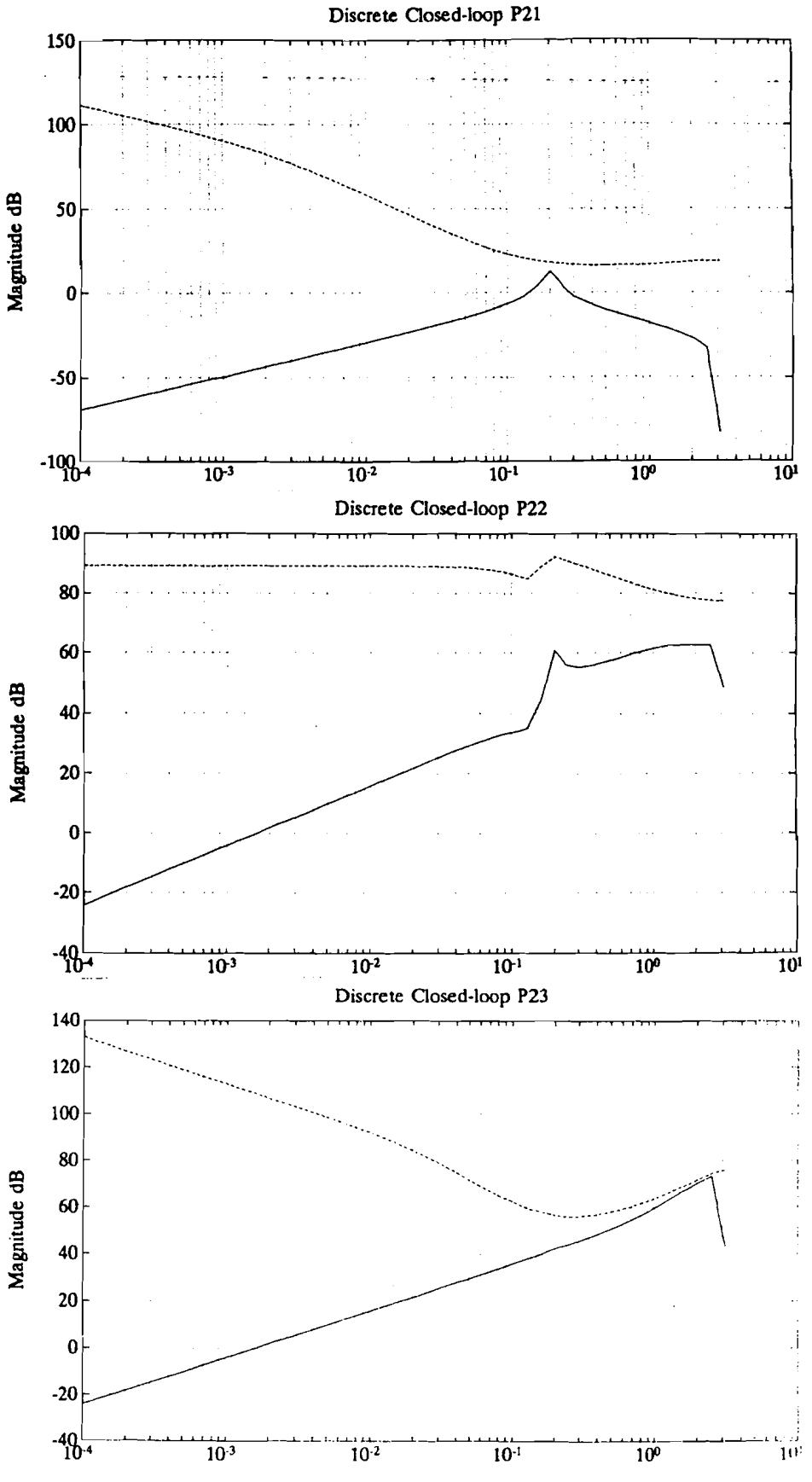

CONTROLLERS ROTATION AROUND THE NEAGTIVE Y-AXIS C_{fb}, C_{ff1}, C_{ff2}

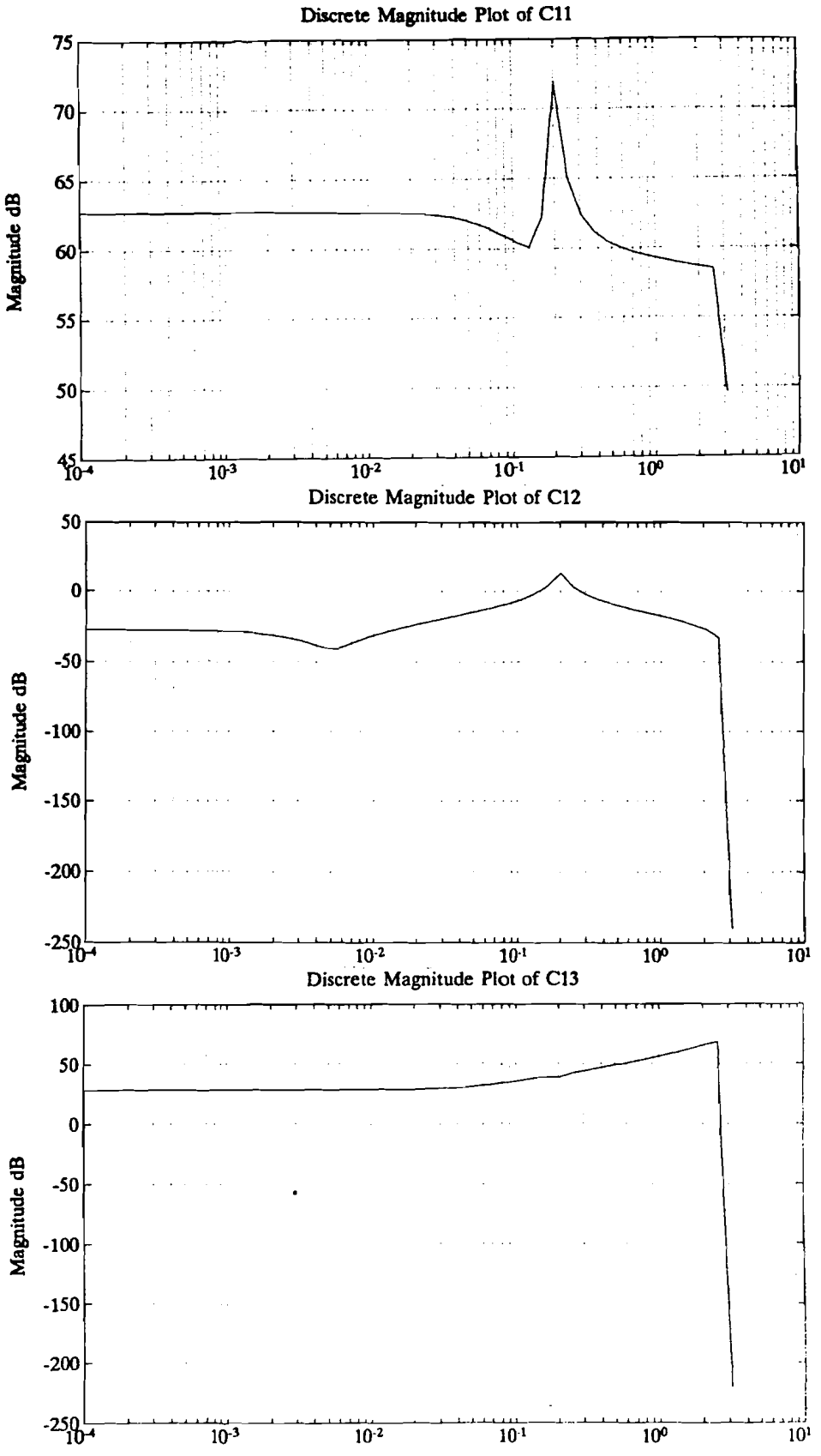

ROTATION AROUND THE POSITIVE X-AXIS: Y_{px}/D_{cx}, Y_{px}/D_{dx} and Y_{px}/D_{wx}

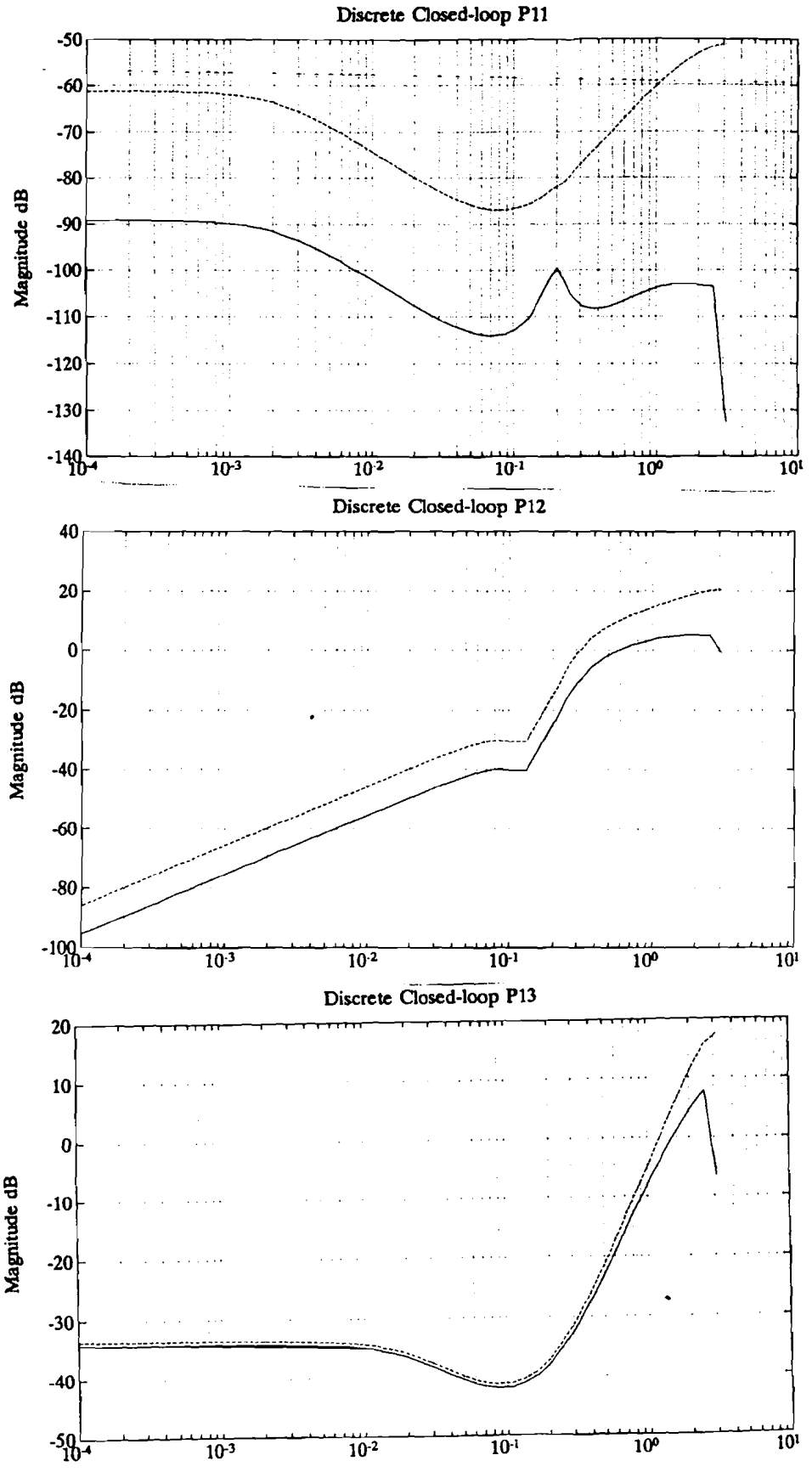

ROTATION AROUND THE POSITIVE X-AXIS: U_{px}/D_{cx}, U_{px}/D_{dx} and U_{px}/D_{wx}

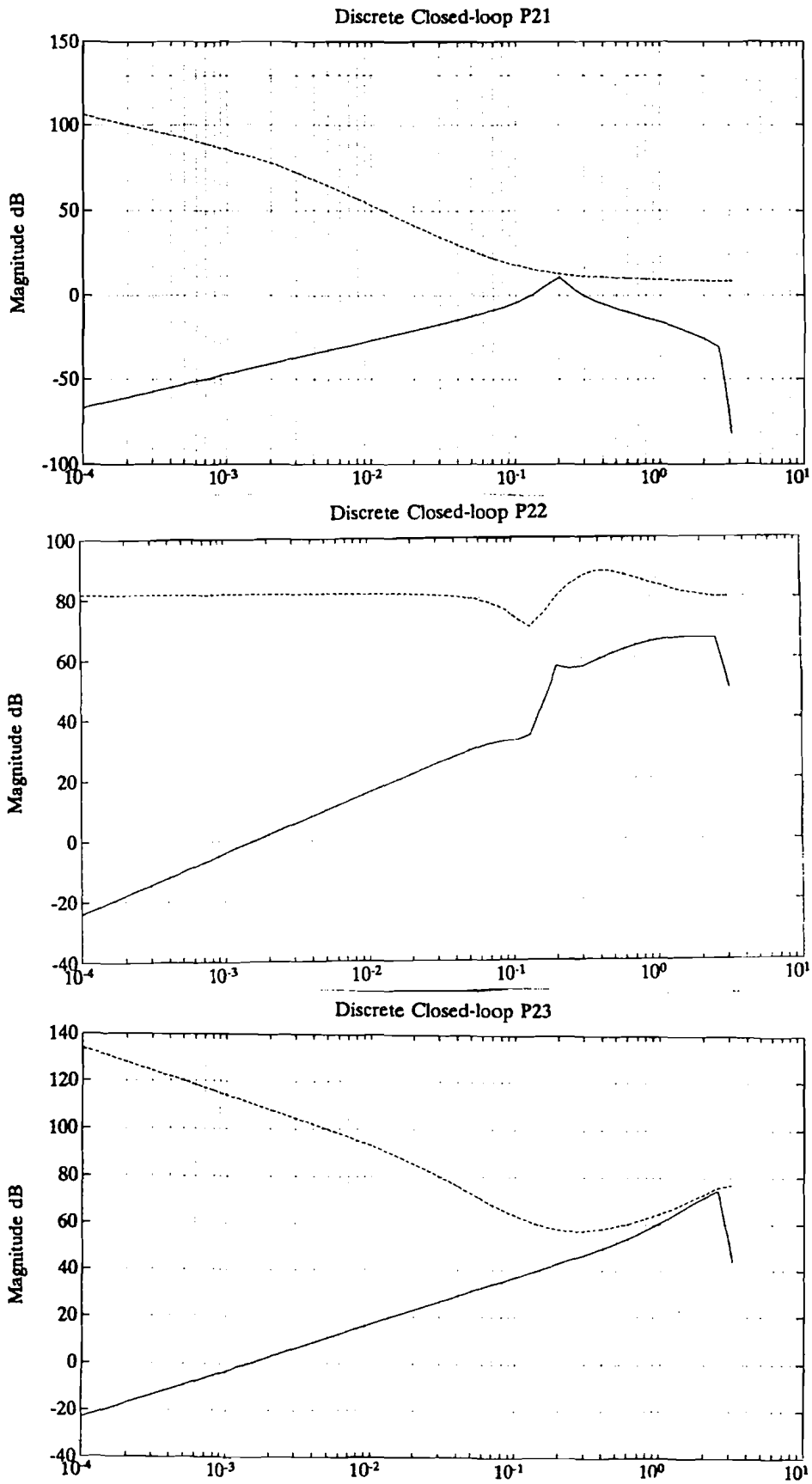

CONTROLLERS ROTATION AROUND THE NEAGTIVE Y-AXIS C_{fb}, C_{ff1}, C_{ff2}

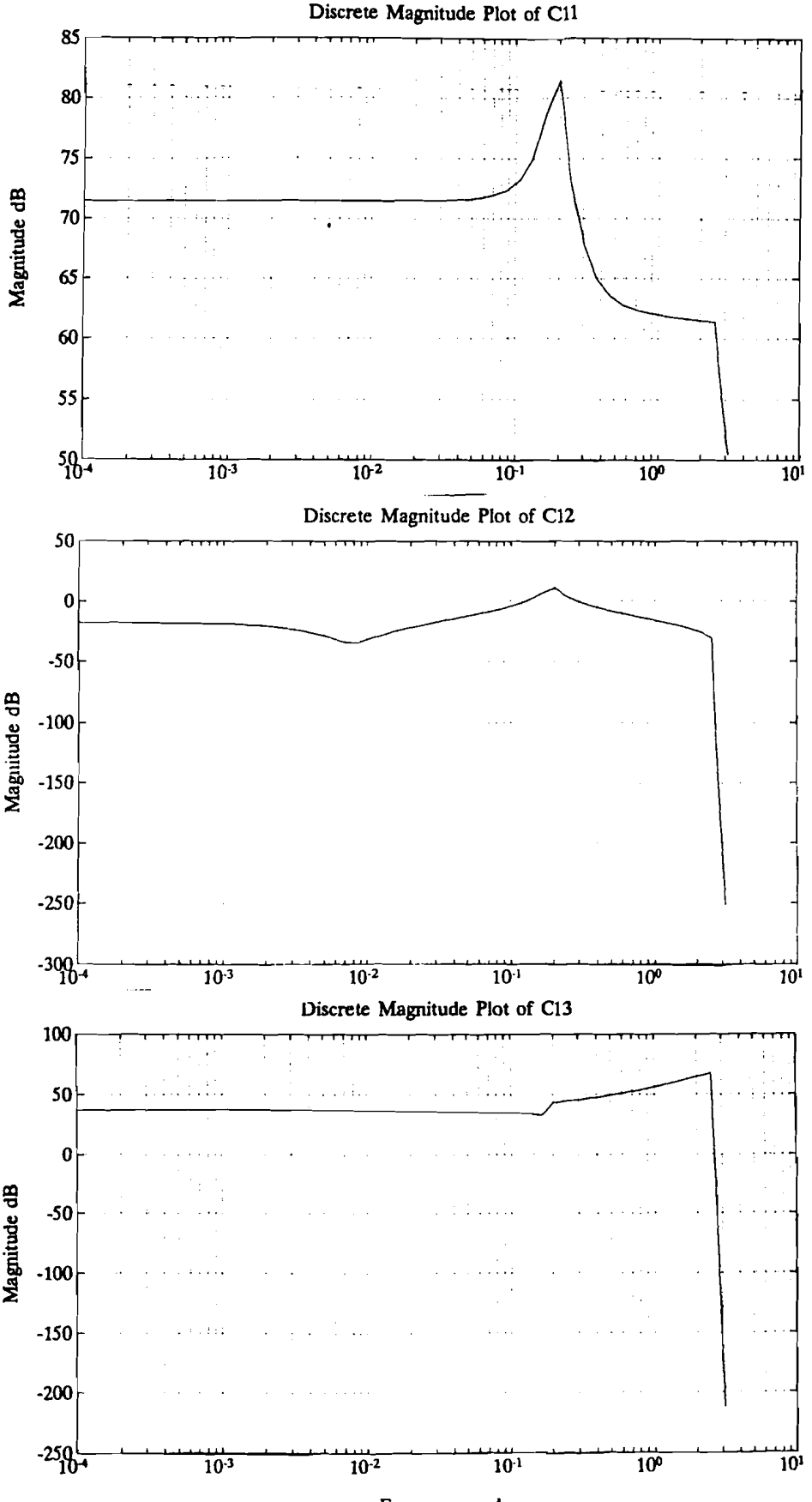

APPENDIX 12: Transfer functions of the shaping and weighting filters.

The controllers of the subprocesses average height, rotation around the negative y-axis and rotation around the positive x-axis are derived with the following shaping and weighting filters.

AVERAGE HEIGHT:

$$V_d = \frac{z^3 - 2.666z^2 - 2.39z - 0.715}{z^3 - 2.939z^2 + 2.906z - 0.968}$$

$$V_c = -320 \times \frac{z + 1.498}{z - 0.998}$$

$$V_w = 0.4598 \times \frac{z^3 + 3.331z^2 - 4.922z + 0.636}{z^3 - 2.456z^2 - 2.011z - 0.549}$$

$$W_y = 0.13 \times \frac{1}{z - 0.9}$$

$$W_u = 2.9.10^{-4} \times \frac{z - 1}{z - 0.2}$$

ROTATION AROUND NEGATIVE Y-AXIS

$$V_d = 0.2 \times \frac{z^3 - 2.689z^2 + 2.430z - 0.7345}{z^3 - 2.926z^2 + 2.872z^1 - 0.9461}$$

$$V_c = 120 \times \frac{z^2 - 4.212z + 3.207}{z^2 - 1.774z + 0.786}$$

$$V_w = 0.2044 \times \frac{z^3 + 3.377z^2 - 4.912z + 0.635}{z^3 - 2.456z^2 + 2.011z - 0.5488}$$

$$W_y = 1.2 \times \frac{1}{z - 0.9}$$

$$W_u = 4.5.10^{-4} \times \frac{z - 1}{z - 0.2}$$

ROTATION AROUND POSITIVE X-AXIS

$$V_d = 0.1667 \times \frac{z^3 - 2.687z^2 + 2.422z - 0.751}{z^3 - 2.935z^2 + 2.888z - 0.9525}$$

$$V_c = 240 \times \frac{z^2 - 4.213z + 3.206}{z^2 - 1.774z + 0.7866}$$

$$V_w = 0.2022 \times \frac{z^3 + 3.376z^2 - 4.906z + 0.634}{z^3 - 2.456z^2 + 2.011z - 0.5488}$$

$$W_y = 1.2 \times \frac{1}{z - 0.9}$$

$$W_u = 4.10^{-4} \times \frac{z - 1}{z - 0.2}$$

APPENDIX 13:

The water level is measured with the sensors used in the water vessel test array [3]. The test array is shown in figure 13.1.

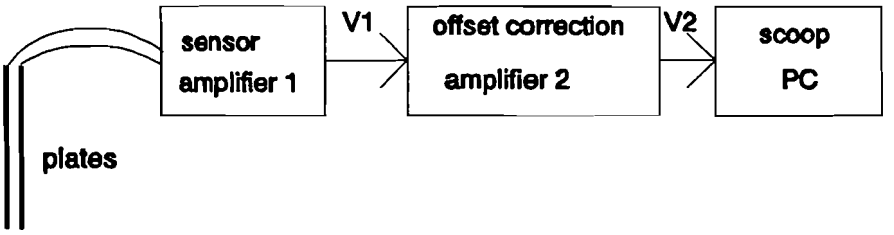

figure 13.1: test array water level sensor.

The block 'sensor' contains the water level sensor which is used for the water-vessel process [3]. The circuit is modified a little to reduce the time constant. The modifications are described in [11]. The output of this sensor is proportional with the water level between the two plates. Because of the fact that the wave heights are of more intrest, the DC component has to be removed. This DC component is removed in the second block of figure 13.1. The range of the A/D converter of the computer is between 0 and 5 Volt. Therefore the average output voltage V_2 has to be about 2.5 Volt. The circuit of the second block of figure 13.1 is shown in 13.2.

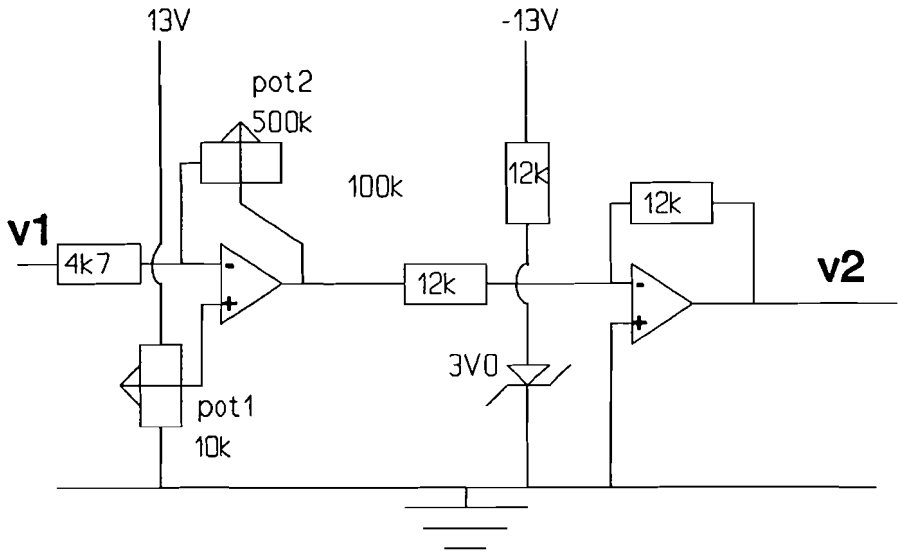

figure 13.2: circuit used for offset correction.

In figure 13.2:

pot1 is used for offset correction
pot2 is used to adjust the amplification.
opamp2 is used to adjust an average output voltage of 3 Volt.

The offset correction will be optimal by a strong amplification of the first block in figure 13.1 and a small amplification of the second. However, if the amplification of the first block is to large, the output Voltage V_1 will not be linear.